

Electronic Supplementary Information

Bimetallic nickel-lutetium complexes: Tuning the properties and catalytic hydrogenation activity of the Ni site by varying the Lu coordination environment

Bianca L. Ramirez[†], Prachi Sharma^{†,‡}; Reed J. Eisenhart[†]; Laura Gagliardi^{†,‡}; Connie C. Lu^{†,*}

[†]Department of Chemistry and [‡]Minnesota Supercomputing Institute & Chemical Theory Center, University of Minnesota, Minneapolis, Minnesota 55455-0431, United States

Page	SI Table of Contents
S4	Experimental Section
S8	X-ray Structure and Refinement Data
S9	Table S1. Crystallographic Details for 1 , 2 , 3 , 3 -THF, 4
S10	Table S2. Selected Literature Heterobimetallic d-f Complexes with Short Intermetal Distances
	NMR Spectroscopy
S11	Figure S1. ¹ H NMR spectrum of ¹ Pr ₂ PCH ₂ NHPh
S11	Figure S2. ¹³ C NMR spectrum of ¹ Pr ₂ PCH ₂ NHPh
S12	Figure S3. ¹ H NMR spectrum of (¹ Pr ₂ PCH ₂ NHPhAr) ₃ tacn
S12	Figure S4. ¹³ C NMR spectrum of (¹ Pr ₂ PCH ₂ NHPhAr) ₃ tacn
S13	Figure S5. ¹ H{ ³¹ P} NMR spectrum of ¹ Pr ₂ PCH ₂ NKPh
S13	Figure S6. ³¹ P NMR spectra overlay of all reported complexes: 1 , 2 , 3 , 4 (in C ₆ D ₆), and 3 -THF
S14	Figure S7. ¹ H{ ³¹ P} NMR spectrum of 1
S14	Figure S8. ¹ H{ ³¹ P} NMR spectrum of 2
S15	Figure S9. ¹ H{ ³¹ P} NMR spectrum of 3
S15	Figure S10. ¹ H{ ³¹ P} NMR spectrum of 3 -THF
S16	Figure S11. ¹ H{ ³¹ P} NMR spectrum of 4
S16	Figure S12. ¹ H{ ³¹ P} NMR spectrum of 3 titrated with varying equivalents of THF.
S17	Figure S13. ³¹ P NMR spectrum of 3 titrated with varying equivalents of THF and solvent binding isotherm data
S17	Figure S14. Fitted solvent binding isotherm data for the titration of plot of 3 with THF
S18	Figure S15. A Scatchard plot of the Δδ versus Δδ/[THF] ₀ ,
S18	Figure S16. ¹ H{ ³¹ P} NMR spectrum of 3 under 1 atm and 4 atm H ₂ at room temperature
S19	Figure S17. ¹ H{ ³¹ P} NMR spectrum of 3 -THF under 1 atm and 4 atm H ₂ at room temperature
S19	Figure S18. ¹ H{ ³¹ P} NMR spectrum of 3 + 15 eq THF under 4 atm H ₂ at room temperature
S20	Figure S19. ¹ H{ ³¹ P} NMR spectrum of 4 under 4 atm H ₂ at room temperature in THF- <i>d</i> ₈ and toluene- <i>d</i> ₈
S20	Figure S20. ³¹ P NMR overlay of 3 under Ar, 1 atm H ₂ and 4 atm H ₂ at 298 K
S21	Figure S21. ³¹ P NMR overlay of 3 -THF (3 + 15 eq THF- <i>d</i> ₈) under Ar, 1 atm H ₂ and 4 atm H ₂ at 298 K
S21	Figure S22. ³¹ P NMR overlay of 3 -THF under Ar, 1 atm H ₂ and 4 atm H ₂ at 298 K

S22	Figure S23. ^{31}P NMR overlay of 4 under Ar, 1 atm H_2 and 4 atm H_2 at 298 K
S22	Figure S24. ^{31}P NMR overlay of 3 under Ar, 1 atm H_2 , and 4 atm H_2 (at rt) cooled to 190 K
S23	Figure S25. Variable temperature ^{31}P NMR of 3 under 4 atm H_2 at rt $^1\text{H}\{^{31}\text{P}\}$ NMR overlay of 3 under Ar, 1 atm H_2 , and 4 atm H_2 (at rt) cooled to 190 K
S23	Figure S26. $^1\text{H}\{^{31}\text{P}\}$ NMR overlay of 3 under Ar, 1 atm H_2 , and 4 atm H_2 (at rt) cooled to 190 K
S24	Figure S27. Variable temperature proton NMR of 3 under 4 atm H_2 at rt
S24	Figure S28. ^{31}P NMR overlay of 3 -THF (3 + 15 eq THF- d_8) under Ar, 1 atm H_2 , and 4 atm H_2 cooled to 190 K
S25	Figure S29. ^{31}P NMR overlay of 3 -THF under Ar, 1 atm H_2 , and 4 atm H_2 cooled to 190 K
S25	Figure S30. Variable temperature ^{31}P NMR of 3 -THF under 4 atm H_2 at rt
S26	Figure S31. Proton $^1\text{H}\{^{31}\text{P}\}$ NMR spectrum of 3 -THF under 4 atm H_2 (at rt) cooled to 190 K
S26	Figure S32. Variable temperature proton NMR of 3 -(H_2)THF
S27	Figure S33. Plot of T_1 relaxation time of bound H_2 resonances of 3 -(H_2)THF at various temperatures from 243 K to 210 K
S27	Figure S34. ^{31}P NMR overlay of 4 under Ar and 4 atm H_2 (at rt) cooled to 190 K
S28	Figure S35. Proton $^1\text{H}\{^{31}\text{P}\}$ NMR spectrum of 4 under 4 atm H_2 (at rt) cooled to 190 K
S28	Figure S36. ^{31}P NMR overlay of 4 under Ar, 1 atm H_2 and 4 atm H_2 (at rt) cooled to 190 K
S29	Figure S37. Proton $^1\text{H}\{^{31}\text{P}\}$ NMR spectrum of 4 under 4 atm H_2 (at rt) cooled to 190 K
S29	Figure S38. ^{31}P NMR overlay of $\text{Ni}(\text{N}(o\text{-}(\text{NHCH}_2\text{P}^i\text{Pr}_2)\text{C}_6\text{H}_4)_3)$ under Ar and 4 atm H_2 (at rt) cooled to 190 K
S30	Figure S39. Proton $^1\text{H}\{^{31}\text{P}\}$ NMR spectrum of $\text{Ni}(\text{N}(o\text{-}(\text{NHCH}_2\text{P}^i\text{Pr}_2)\text{C}_6\text{H}_4)_3)$ under 4 atm H_2 at rt and cooled to 190 K
S30	Figure S40. ^{31}P NMR overlay of 3 in presence of 0.37 M styrene and 0.37 M styrene and 4 atm H_2 (at rt) cooled to 190 K
S31	Figure S41. ^{31}P NMR overlay of 3 -THF in presence of 0.37 M styrene and 0.37 M styrene and 4 atm H_2 (at rt) cooled to 190 K
	Electrochemical Studies
S32	Figure S42. Stacked cyclic voltammograms of the <i>in situ</i> generation of 3 -THF
S32	Figure S43. Overlay of cyclic voltammograms of 3 under varying electrolyte conditions
S33	Figure 44. Stacked CVs of 3 in 0.1 M $[\text{N}^n\text{Pr}_4][\text{BAR}^{\text{F}}_4]$ in DFB with FeCp_2 as an internal reference
S33	Figure S45. Overlay of cyclic voltammograms of 4 under varying electrolyte conditions
S34	Figure S46. Cyclic voltammogram of $\text{Ni}\{\text{N}(o\text{-}(\text{NCH}_2\text{P}^i\text{Pr}_2)\text{C}_6\text{H}_4)_3\}$
S34	Figure S47. Comparative cyclic voltammograms of 3 -THF and 4 with 0.1 M $[\text{P}^n\text{Bu}_4\text{N}][\text{PF}_6]$ electrolyte in THF
S35	Figure S48. Scan rate study of Ni 0/1 oxidation event of 3 -THF
S35	Figure S49. Scan rate study of Ni reduction event of 3 -THF
S36	Figure S50 and S51. Cyclic voltammograms of $^i\text{Pr}_2\text{PCH}_2\text{NKPh}$ and 1

S37	Figure S52. Cyclic voltammogram of difluorobenzene solvent window
	UV-Visible Spectroscopy
S38	Figure S48. Expanded UV-Vis spectra of complexes 3 and 4 in DFB and 3 -THF
S38	Figure S49. UV-Visible spectra of 4 in DFB and in THF
S39	Table S3. UV-Vis Model Parameters
S39	Figure S50. Modeled UV-Visible spectrum of 3 -THF (0.025mM in THF)
S40	Figure S51. Modeled UV-Visible spectrum of 3 -THF (0.103 mM in THF)
	Catalysis Tables
S40	Table S4. Hydrogenation of Styrene to Ethylbenzene Mediated by 1-4^a
S41	Table S5. Substrate Scope for Olefin Hydrogenation for 3
S41	Table S6. Optimization Conditions for Olefin hydrogenation
	Computational Details
S42	Table S7. Comparison of metrics of DFT vs. X-ray structure for 4
S42	Table S8. Calculated charges at the metal centers of the ground spin state
S43	Figure S52. Natural orbitals for 3 from CASSCF calculations
S43	Figure S53. Natural orbitals for 3 -THF from CASSCF calculations
S44	Figure S54. Natural orbitals for 4 from CASSCF calculations
S44	Table S9. Percentage of Metal Character (% Lu and %Ni) in Ni-Lu Bonding Orbitals From CASSCF Calculations
S45	Figure S55. 3d orbital splitting (Ni) for 3 as predicted by DFT calculations.
S45	Table S10. Frontier molecular orbitals and the orbital energies for 3 calculated using DFT calculations
S46	Figure S56. 3d orbital splitting of Ni for 3 -THF as predicted by DFT calculations
S46	Table S11. Frontier molecular orbitals and the orbital energies for 3 -THF calculated using DFT calculations
S47	Figure S57. 3d orbital splitting of Ni for 4 as predicted by DFT calculations
S47	Table S12. Frontier molecular orbitals and the orbital energies for 4 calculated using DFT calculations.
S47	Table S13. Compositions of LUMO from the DFT calculations
S48	Table S14. Absolute DFT and CASSCF energies in atomic units
S48	XYZ coordinates for DFT geometry-optimized 3
S49	XYZ coordinates for DFT geometry-optimized 3 -THF
S50	XYZ coordinates for DFT geometry-optimized 4
S51	References

Note: RasOrb files, which are editable files produced by the rasscf program of *Molcas* to allow the possibility to read the orbitals in a later run, are available as separate TXT files.

Experimental Section

General Considerations. Unless otherwise stated, all manipulations were performed under an inert atmosphere in a glovebox or using standard Schlenk techniques. Standard solvents were deoxygenated by sparging with inert gas and dried by passing through activated alumina columns of a SG Water solvent purification system. Deuterated solvents were purchased from Cambridge Isotope Laboratories, Inc. or Sigma–Aldrich, degassed via freeze–pump–thaw cycles and stored over activated 4 Å molecular sieves. Elemental analyses were performed by Robertson Microlit Laboratories, Inc. (Ledgewood, NJ). ^1H and ^{31}P NMR spectra were recorded on Varian 500 MHz, Bruker 500 MHz, or Bruker 400 MHz spectrometers at ambient temperature unless otherwise stated. All ^1H and ^{13}C NMR spectra were referenced internally to the residue solvent and ^{31}P NMR were referenced to an external 85% H_3PO_4 standard. The temperature of the probe during the variable-temperature NMR experiments was calibrated against an external methanol standard at temperatures below 25 °C. NMR titration data was modeled using *bindfit* fitting software, available through supramolecular.org,¹ using a simple 1:1 binding model and a Nelder–Mead fit method.^{2,3} UV–Visible spectra were collected at room temperature on a Cary 300 Bio UV-Visible spectrophotometer and simulated using the program *BF* written by Eckhard Bill.⁴ Cyclic voltammetry was performed with a CH Instruments 600 electrochemical analyzer with a one–cell setup, comprising a glassy carbon working electrode, a platinum wire counter electrode, and Ag/AgNO₃ reference electrode in acetonitrile. Analytes were measured in 0.1M [*n*-Bu₄N]PF₆ in THF, 0.1M [*n*-Pr₄N][BAR^F₄] (BAR^F₄ = tetrakis(3,5-bis(trifluoromethyl)phenyl)borate) in THF, or 0.1M [*n*-Pr₄N][BAR^F₄] in difluorobenzene solutions and internally referenced to the FeCp₂/FeCp₂⁺ redox couple.

The reagents Ni(COD)₂, LuCl₃, and diisopropylphosphine were purchased from Strem Chemicals and used without further purification. Aniline was purchased from Sigma–Aldrich and purified by vacuum distillation before use. 1,4,7–tris(2′–aminophenyl)–1,4,7–triazacyclononane⁵, diisopropylphosphinomethanol⁶, Ni(N(*o*–(NHCH₂PⁱPr₂)C₆H₄)₃)⁷, and [^{*n*}Pr₄N][BAR^F₄]⁸ were synthesized according to literature procedures.

Synthesis of ⁱPr₂PCH₂NHPh. A tube–shaped Schlenk reaction flask with an adjustable large–bore Teflon valve was charged with a magnetic stir bar, diisopropylphosphinomethanol (2.31 g, 2.50 mL, 16 mmol) and aniline (1.45 g, 1.42 mL, 16 mmol). The sides of the flask were rinsed with THF (~3 mL) to ensure full transfer. The solution was stirred at 65 °C for 13 h, and then the solvent removed in vacuo to afford a clear oil. The oil was extracted into hexane and filtered through a Celite pad and dried in vacuo. The product was used as is without further purification (3.22 g, 90 %). ^1H NMR (400 MHz, C₆D₆, δ): 7.17 (t, $^3J = 6.9$ Hz, 2H, aryl CH), 6.76 (td, $^{3,4}J = 7.3$ & 1.2 Hz, 2H, aryl CH), 6.50 (d, $^3J = 8.7$ Hz, 1H, aryl CH), 3.50 (br, 1H, NH), 3.03 (d, $^2J_{\text{HP}} = 5.2$ Hz, 2H, CH₂PⁱPr₂), 1.55 (m, 2H, CHMe₂), 0.96 (m, 12H, CH₃). ^{31}P NMR (282 MHz, C₆D₆, δ): 4.2. ^{13}C NMR (126 MHz, C₆D₆, δ): 149.1 (d, $J = 9.3$ Hz), 129.1, 117.4, 112.9, 38.6 (d, $J = 14.5$ Hz), 22.9 (d, $J = 13.0$ Hz), 19.9 (d, $J = 16.5$ Hz), 18.7 (d, $J = 9.5$ Hz). ESI-MS-TOF m/z : [M+Na]⁺ calcd for C₁₃H₂₂NPNa 246.1392; found: 246.1418.

Synthesis of ⁱPr₂PCH₂NKPh. In a 20–mL scintillation vial, KN(TMS)₂ (0.447 g, 2.24 mmol) was dissolved in 5 mL of toluene and then added to a stirring solution of ⁱPr₂PCH₂NHPh (0.500 g, 2.24 mmol) in toluene (~5 mL) at room temperature. Within 15 min, a yellow precipitate was formed. After stirring for an additional 45 min, the yellow solids were isolated via filtration, washed with toluene (3 x 2 mL), and dried in vacuo to give the desired product as a bright yellow powder (503

mg, 86 %). $^1\text{H}\{^{31}\text{P}\}$ NMR (400 MHz, THF- d_8 , δ): 6.64 (br, 2H, aryl CH), 5.98 (br, 2H, aryl CH), 5.59 (t, $^3J = 6.9$ Hz, 1H, aryl CH), 3.14 (s, 2H, $\text{CH}_2\text{P}^i\text{Pr}_2$), 1.81 (septet of d, $J = 7.2$ & 3.6 Hz, 2H, CHMe_2), 1.16–1.09 (m, 12H, CH_3). ^{31}P (282 MHz, THF- d_8 , δ): 1.3. ^{13}C NMR (126 MHz, THF- d_8 , δ): 163.3, 130.0, 104.5, 48.0, 24.4, 20.7, 20.5, 6.9.

Synthesis of $(^i\text{Pr}_2\text{PCH}_2\text{NHPAr})_3\text{tacn}$. A tube-shaped Schlenk reaction flask with an adjustable large-bore Teflon valve was charged with a magnetic stir bar, diisopropylphosphinomethanol (1.00 g, 1.07 mL, 6.7 mmol) and 1,4,7-tris(2'-aminophenyl)-1,4,7-triazacyclononane (1.00 g, 2.28 mmol). The sides of the flask were rinsed with THF (~3 mL) to ensure full transfer. The solution was stirred at 65 °C for 13 h, and then the solvent removed in vacuo to afford a clear oil. The oil was extracted into hexane and filtered through a Celite pad and dried in vacuo. The crude product was dissolved in 10 mL hexane, filtered, and purified by eluting through a short silica plug with hexane (60 mL). Evaporation of the eluate in vacuo yielded a colorless oil (1.10 g, 60%). ^1H NMR (400 MHz, C_6D_6 , δ): 7.18 (d, $^3J = 8.0$ Hz, 3H, aryl CH), 7.12 (t, $^3J = 7.7$ Hz, 3H, aryl CH), 6.80 (d, $^3J = 8.0$ Hz, 3H, aryl CH), 6.75 (t, $^3J = 7.6$ Hz, 3H, aryl CH), 5.22 (br, 3H, NH), 3.54 (br, 12H, tacn CH_2), 3.25 (d, $^2J_{\text{HP}} = 5.1$ Hz, 6H, CH_2^iPr_2), 1.72 (sept of d, $J = 7.0$ & 2.5 Hz, 6H, CHMe_2), 1.12–1.00 (m, 36H, CH_3). ^{31}P NMR (126 MHz, C_6D_6 , 121 MHz): δ 3.3. ^{13}C NMR (126 MHz, C_6D_6 , δ): 144.5 (d, $J = 8.4$ Hz), 142.1, 125.2, 122.8, 117.1, 110.8, 57.2, 38.9 (d, $J = 14.4$ Hz), 23.2 (d, $J = 13.5$ Hz), 19.9 (d, $J = 16.0$ Hz), 18.9 (d, $J = 9.9$ Hz). ESI-MS-TOF m/z : $[\text{M}+\text{Na}]^+$ calcd for $\text{C}_{45}\text{H}_{75}\text{N}_6\text{P}_3\text{Na}$ 815.5192; found, 815.5313.

Synthesis of $\text{Lu}(^i\text{Pr}_2\text{PCH}_2\text{NPh})_3$ (1**).** In a 20-mL scintillation vial, a solution of $^i\text{Pr}_2\text{PCH}_2\text{NHPH}$ (0.300g, 1.34 mmol) in Et_2O (~4 mL) was frozen in a LN_2 coldwell and then layered with $^n\text{BuLi}$ (0.537 mL, 1.34 mmol). The mixture was stirred for 1 h at room temperature and then dried in vacuo. The resulting solid was dissolved in THF (~4 mL) and frozen in a LN_2 coldwell. The thawing solution was layered on top of a frozen solution of LuCl_3 (0.126 g, 0.447 mmol) in THF (~8 mL). The solution was allowed to warm to rt and then stirred overnight. After drying the solution in vacuo, the resulting crude solid was washed with hexanes (8 mL) and then dissolved in benzene. After filtering through a Celite pad and drying in vacuo, the product was obtained as a white powder (0.376 g, 85%). Single crystals were grown by layering a concentrated toluene solution of **1** with hexane at -30 °C. $^1\text{H}\{^{31}\text{P}\}$ NMR (400 MHz, C_6D_6 , δ): 7.28 (t, $^3J = 7.7$ Hz, 6H, aryl CH), 7.07 (d, $^3J = 8.1$ Hz, 6H, aryl CH), 6.72 (t, $^3J = 7.2$ Hz, 3H, aryl CH), 3.53 (s, 6H, $\text{CH}_2\text{P}^i\text{Pr}_2$), 1.80 (br, 6H, CHMe_2), 1.11–0.84 (m, 36H, CH_3). ^{31}P NMR (282 MHz, C_6D_6 , δ): -9.4. ^{13}C NMR (126 MHz, C_6D_6 , δ): 157.0, 129.4, 115.9, 114.7, 43.0, 24.0, 20.7, 19.3, 18.8. Multiple EA attempts consistently showed incorporation of water. Anal. Calcd. for **1**(H_2O), $\text{C}_{39}\text{H}_{65}\text{N}_3\text{OP}_3\text{Lu}$: 54.48 C, 7.62 H, 4.89 N. Found: 54.50 C, 7.87 H, 4.83 N.

Alternative synthesis of **1.** To a stirring THF (~8 mL) solution of LuCl_3 (0.054 g, 0.191 mmol) in a 20-mL scintillation vial at room temperature, a THF solution (~4 mL) of $^i\text{Pr}_2\text{PCH}_2\text{NKPh}$ (0.150 g, 0.574 mmol) was added. The reaction was stirred overnight and then dried in vacuo. The crude was washed with hexanes (~8 mL) and dissolved in benzene. After filtering through a Celite pad, the solution was dried in vacuo to yield a white powder (0.129 g, 80%).

Synthesis of $\text{Lu}\{(^i\text{Pr}_2\text{PCH}_2\text{NAr})_3\text{tacn}\}$ (2**).** In a 20-mL scintillation vial, an Et_2O (~4 mL) solution of $(^i\text{Pr}_2\text{PCH}_2\text{NHPAr})_3\text{tacn}$ (0.337g, 1.51 mmol) was frozen in a LN_2 coldwell, and then layered with $^n\text{BuLi}$ (0.604 mL, 1.51 mmol). The mixture was stirred for 1 h at room temperature and then dried in vacuo. The resulting solid was dissolved in THF (~4 mL) and frozen in a LN_2 coldwell. The thawing solution was layered on top of a frozen solution of LuCl_3 (141.6 g, 0.50

mmol) in THF (~8 mL). The reaction was allowed to warm to rt and then stirred overnight. After drying the solution in vacuo, the resulting crude solid was washed with cold hexanes (8 mL) and then dissolved in benzene. After filtering through a Celite pad and drying in vacuo, the product was obtained as a white powder (0.280 g, 66%). Single crystals were grown by layering a concentrated toluene solution of **2** with hexane at $-30\text{ }^{\circ}\text{C}$. $^1\text{H}\{^{31}\text{P}\}$ NMR (400 MHz, C_6D_6 , δ): 7.26 (td, $^3J = 7.7$ & 1.5 Hz, 3H, aryl CH), 6.88 (d, $^3J = 7.6$ Hz, 3H, aryl CH), 6.70 (dd, $^3J = 7.8$ & 1.6 Hz, 3H, aryl CH), 6.55 (td, $^3J = 7.5$ & 1.3 Hz, 3H, aryl CH), 3.70 (d, $^2J = 13.2$ Hz, 3H, CHH'P'Pr₂), 3.45 (d, $^2J = 13.2$ Hz, 3H, CHH'P'Pr₂), 3.36 (m, 3H, NCHH'), 2.64 (m, 3H, N'CHH'), 2.52 (m, 6H, NC'HH'), 1.80 (sept, $^3J = 6.9$ Hz, CHMe₂, 3H), 1.44 (sept, $^3J = 7.2$ Hz, C'HMe₂, 3H), 1.16 – 1.03 (m, 36H, CH₃). ^{31}P NMR (282 MHz, C_6D_6 , δ): -7.1 . ^{13}C NMR (126 MHz, C_6D_6 , δ): 155.6 (d, $J = 9.1$ Hz), 141.6, 121.5, 114.0 (d, $J = 6.5$ Hz), 112.8, 57.7, 56.3, 46.7, 24.9 (d, $J = 15.3$ Hz), 23.6 (d, $J = 15.3$ Hz), 22.1 (d, $J = 19.1$ Hz), 21.1 (d, $J = 15.9$ Hz), 19.5 (d, $J = 12.2$ Hz), 18.5 (d, $J = 2.3$ Hz). Multiple EA attempts consistently showed incorporation of water. Anal. Calcd. for **2**(H₂O), C₄₅H₇₄N₆OP₃Lu: 54.98 C, 7.59 H, 8.55 N. Found: 55.01 C, 7.63 H, 8.52 N.

Synthesis of NiLu(ⁱPr₂PCH₂NPh)₃ (3**) and **3**-THF.** A solution of **1** (0.150 g, 0.180 mmol) in THF (~4 mL) was added to solid Ni(COD)₂ (0.049 g, 0.180 mmol), resulting in a red-orange color. The reaction was stirred for 16 h and then dried in vacuo. The crude was washed with cold hexanes (6 mL) and toluene (6 mL). The product was extracted into hot toluene and then filtered through a Celite pad. After drying in vacuo, a red powder was obtained (0.145 g, 90% yield). Alternatively, **3** can be synthesized by heating a solution of **1** and Ni(COD)₂ in toluene at $70\text{ }^{\circ}\text{C}$ for 16 h, during which red crystals of **3** precipitate. The crystals were collected and washed with cold. Single crystals were grown from a hot concentrated toluene solution of **3** cooled to room temperature and then placed in the freezer at $-28\text{ }^{\circ}\text{C}$. Single crystals of **3**-THF were grown by layering hexane on a concentrated THF solution at $-28\text{ }^{\circ}\text{C}$. $^1\text{H}\{^{31}\text{P}\}$ NMR (400 MHz, toluene-*d*₈, δ): 7.18 (t, $^3J = 7.7$ Hz, 6H, aryl CH), 6.65 (d, $^3J = 8.1$ Hz, 6H, aryl CH), 6.62 (t, $^3J = 7.2$ Hz, 3H, aryl CH), 3.96 (s, 6H, CH₂P'Pr₂), 2.23 (sept, $^3J = 7.2$ Hz, 6H, CHMe₂), 1.08 (d, $^3J = 7.1$ Hz, 18H, CH₃), 1.01 (d, $^3J = 7.1$ Hz, 18H, C'H₃). ^{31}P NMR (282 MHz, toluene-*d*₈, δ): -0.8 . UV-Vis (nm, in difluorobenzene): 366 (3900 M⁻¹ cm⁻¹), 405 (2650), 515 (660). Multiple EA attempts consistently showed incorporation of water. Anal. Calcd. for **3**(H₂O), C₃₉H₆₅N₃OP₃LuNi: 51.00 C, 7.13 H, 4.57 N. Found: 51.22 C, 6.61 H, 4.43 N.

Spectroscopic data for **3-THF:** $^1\text{H}\{^{31}\text{P}\}$ NMR (400 MHz, THF-*d*₈, δ): 6.94 (t, $^3J = 7.7$ Hz, 6H, aryl CH), 6.61 (d, $^3J = 8.0$ Hz, 6H, aryl CH), 6.34 (t, $^3J = 7.2$ Hz, 3H, aryl CH), 3.87 (s, 6H, CH₂P'Pr₂), 2.44 (sept, $^3J = 7.2$ Hz, 6H, CHMe₂), 1.30 (dd, $J = 7.3$ & 4.1 Hz, 36H, CH₃). ^{31}P NMR (282 MHz, THF-*d*₈, δ): 10.2. ^{13}C NMR (126 MHz, THF-*d*₈, δ): 159.5, 129.0, 116.8, 114.8, 54.82, 29.0, 21.8, 19.7. UV-Vis (nm, in THF): 407 (3312 M⁻¹ cm⁻¹), 451 (708), 548 sh (345).

Synthesis of NiLu(ⁱPr₂PCH₂NAr)₃tacn (4**).** A solution of **2** (0.404 g, 0.555 mmol) in THF (~12 mL) was added to solid Ni(COD)₂ (0.153 g, 0.555 mmol). The reaction was stirred for 16 h and then dried in vacuo. The crude was washed with cold pentane and then dissolved in toluene. After filtering through a Celite pad and drying in vacuo, a red-purple powder was obtained (0.316 g, 70% yield). Single crystals were grown by diffusion of hexane into a concentrated THF solution of **4**. $^1\text{H}\{^{31}\text{P}\}$ NMR (400 MHz, C_6D_6 , δ): 7.26 (td, $^3J = 8.6$ & 1.5 Hz, 3H, aryl CH), 6.75 (t, $^3J = 7.4$, 6H, aryl CH), 6.54 (td, $^3J = 7.4$ & 1.2 Hz, 3H, aryl CH), 3.66 (d, $^2J = 13.1$ Hz, 3H, CHH'P'Pr₂), 3.45 (d, $^2J = 13.2$ Hz, 3H, CHH'P'Pr₂), 3.41 (m, 3H, NCHH'), 2.60 (m, 6H, NC'HH'), 2.48 (dd, $J = 11.2$ & 3.1 Hz, 3H, NCHH'), 2.35 (sept, $^3J = 7.3$ Hz, 3H, CHMe₂), 1.89 (sept, $^3J = 7.2$ Hz, 3H, C'HMe₂), 1.36 (m, 18H, CH₃), 1.19 (m, 9H, C'H₃), 0.98 (m, 9H, C''H₃). ^{31}P NMR (282 MHz, C_6D_6 ,

δ): 15.0. ^{13}C NMR (126 MHz, C_6D_6 , δ): 157.1, 142.4, 128.9, 119.8, 111.6, 110.5, 59.8, 56.0, 49.4, 29.9, 26.4, 22.8, 21.5, 20.5, 19.75. UV–Vis (nm, in difluorobenzene): 504 ($4700\text{ M}^{-1}\text{cm}^{-1}$). Anal. Calcd. for $\text{C}_{45}\text{H}_{72}\text{N}_6\text{P}_3\text{LuNi}$: 52.80 C, 7.09 H, 8.21 N. Found: 53.03 C, 7.25 H, 8.03 N.

Catalytic hydrogenation of olefins by 3, 3–THF, and 4, NMR scale. A J. Young NMR tube was charged with 5.6 μmol of catalyst (**3** and **4**). A stock solution of olefin and ferrocene was prepared such 40 equivalents of olefin (0.37 M in 0.6 mL toluene- d_8 solution) and ferrocene (ca. 0.3M) as an internal integration standard was transferred into each sealed J. Young NMR tube. In the case of **3**–THF, the same procedure is carried out with THF as the solvent. One freeze–pump–thaw cycle was performed to evacuate the headspace, followed by cooling the NMR tube to LN_2 temperature and back–filling with H_2 (4 atm). In order to promote the mixing of H_2 into solution, the J. Young tube was inverted 3 x before being placed in an oil bath and heated to $100\text{ }^\circ\text{C}$. Olefin hydrogenation catalysis was monitored by ^1H NMR spectroscopy by quantitative integration of the vinylic protons of the olefin against those of the internal ferrocene standard (recycle delay = 20 s). Alkane product peaks were also integrated in cases where they did not overlap with NiLu peaks. All catalytic hydrogenation experiments were performed in triplicate unless otherwise indicated. Control experiments carried out under the same conditions in the presence of Hg (300 equiv) showed catalysis was uninhibited by the addition of mercury, with 94% conversion in the absence of mercury as compared to 91% conversion in the presence of mercury, consistent with a homogeneous catalytic process.

^1H NMR of Alkyl and Olefinic Peaks of Selected Hydrogenated and Isomerized Products (ppm, toluene- d_8):

ethyl benzene: 2.44 (q, $^2J = 8\text{ Hz}$, 2H, CH_2), 1.08 (t, $^2J = 8\text{ Hz}$, 3H, CH_3)

propylbenzene: 2.42 (t, $^2J = 7.5\text{ Hz}$, 2H, $\text{CH}_2\text{CH}_2\text{CH}_3$), 1.50 (sextet, $^2J = 7.5\text{ Hz}$, $\text{CH}_2\text{CH}_2\text{CH}_3$, 2H), 0.82 (t, $^2J = 7.5\text{ Hz}$, 3H, CH_3)

trans–2–octene: 5.43 (m, 2H, $\text{H}_3\text{CCHCH}(\text{CH}_2)_4\text{CH}_3$), 1.61 (d, $J = 5\text{ Hz}$, 3H $\text{H}_3\text{CCHCH}(\text{CH}_2)_4\text{CH}_3$)

octane: 1.21 (s, 12H)

trans-stilbene: 7.29 (d, $^2J = 6.9\text{ Hz}$, 4H, aryl CH), 6.93 (s, 2H)

bibenzyl: 2.71 (s, 4H)

Computational Methods.

DFT Calculations. Quantum-chemical studies were performed on the three bimetallic species **3**, **3**-THF, and **4**. Gas-phase geometry optimizations were initially screened for **4** with various DFT functionals, including PBE⁹, PBE-D3⁹⁻¹¹, PBE0¹², PBE0-D3¹⁰⁻¹², B3LYP-D3^{10, 11, 13-16}, B97-D3^{10, 11, 17}, M06-L¹⁸, B3P86¹⁹, and B3PW91¹³ implemented in the *Gaussian 09* program package (Table S7).²⁰ The Perdew–Burke–Ernzerhof exchange–correlation functional, PBE-D3, was found to have the best agreement with experimental data and, thus, used for all three bimetallic species. For C and H atoms, the double- ζ -quality basis set def-SV(P) was used, whereas the triple- ζ -quality basis set def-TZVP was employed for N, P, and Ni.²¹ The relativistic energy-consistent Stuttgart-Dresden effective core potential was used for Lu atom.²² The initial starting points for geometry optimizations were derived from experimentally determined X-ray structures.

CASSCF Calculations. These bimetallic species were further investigated with complete-active-space self-consistent-field (CASSCF)²³ method. CASSCF calculations, were performed with the MOLCAS 7.8 package on the DFT-optimized structures without symmetry constraints.²⁴ Relativistic all-electron ANO-RCC basis sets were used for all elements.^{25, 26} Double- ζ -quality (ANO-RCC-VDZP) basis sets were used for Lu, Ni, N and P and minimal basis sets (ANO-RCC-MB) were used for C and H atoms. Scalar relativistic effects were included by using the Douglas–Kroll–Hess Hamiltonian.²⁷ The two-electron integral evaluation was simplified by employing the Cholesky decomposition technique.²⁸ In the CASSCF calculations an active space of 10 electrons in 11 orbitals (10,11) was used for all species, which comprises the 3d, 4s and 4d orbitals of Ni and the 5d of Lu.

X-ray Crystallographic and Structure Refinement Details

A colorless plate of **1**, a colorless plate of **2**, red plate of **3**, red–orange plate of **3**-THF and a dark red block of **4** were mounted on a 200 μm MiTeGen microloop and placed on a Bruker APEX-II Platform diffractometer or a Bruker PHOTON-II CMOS diffractometer for data collection at 173(2) K or 123(2) K. The data collection was carried out using either Cu K α (**1**) or Mo K α (**2**, **3**, **3**-THF, **4**) radiation (graphite monochromator). The data intensity was corrected for absorption and decay (SADABS). Final cell constants were obtained from least-squares fits of all measured reflections. The structure was solved using SHELXT-97 and refined using SHELXL 97. A direct-methods solution was calculated which provided most non-hydrogen atoms from the E-map. Fullmatrix least-squares/difference Fourier cycles were performed to locate the remaining non-hydrogen atoms. All non-hydrogen atoms were refined with anisotropic displacement parameters. Hydrogen atoms were placed in ideal positions and refined as riding atoms with relative isotropic displacement parameters. A disordered toluene molecule in **3** resides on an inversion center and was modeled using SHELXTL SAME and SIMU restraints in addition to EADP constraints where appropriate. An isopropyl phosphine ligand arm in complex **4** was disordered over three positions and modeled using SIMU restraints in addition to EADP and EXYZ constraints where appropriate. A separate methyl group in **4** disordered over two positions was also modeled using SIMU restraints in addition to EADP and EXYZ constraints where appropriate.

Table S1. Crystallographic Details for Complexes **1**, **2**, **3**, **3**-THF, and **4**.

	1	2	3	3 -THF	4
chemical formula	C ₃₉ H ₆₃ N ₃ P ₃ Lu	C ₄₅ H ₇₂ N ₆ P ₃ Lu. [C ₆ H ₁₄] _{0.5}	C ₃₉ H ₆₃ N ₃ P ₃ LuNi. C ₇ H ₈	C ₃₉ H ₆₃ N ₃ P ₃ Lu. C ₄ H ₈ O	C ₄₅ H ₇₂ N ₆ P ₃ LuNi
Fw	841.80	1008.05	992.64	972.61	1023.67
cryst syst	triclinic	monoclinic	monoclinic	triclinic	triclinic
space group	P $\bar{1}$	P2 ₁ /c	P2 ₁ /c	P $\bar{1}$	P $\bar{1}$
<i>a</i> (Å)	10.6585(3)	11.5369(5)	12.9011(7)	11.4262(10)	10.7814(2)
<i>b</i> (Å)	1.7628(4)	38.7027(14)	14.0250(7)	12.1111(11)	10.8562(2)
<i>c</i> (Å)	17.3425(6)	11.8500(4)	25.5191(14)	17.7291(16)	20.1873(4)
α (°)	90.3090(10)	90	90	76.8410(10)	78.2730(10)
β (°)	91.0120(10)	112.211(2)	94.979(2)	81.2330(10)	79.6030(10)
γ (°)	112.4100(10)	90	90	68.2440(10)	78.3390(10)
V(Å ³)	2009.60(11)	4898.5(3)	4599.9(4)	2212.5(3)	2241.69(7)
Z	2	4	4	2	2
D _{calcd} (g cm ⁻³)	1.391	1.367	1.433	1.460	1.517
λ (Å), μ (mm ⁻¹)	0.71073, 2.605	1.54178, 5.066	0.71073, 2.681	0.71073, 2.787	1.54178, 5.936
T	123(2)	123(2)	123(2)	173(2)	123(2)
θ (°)	2.197 – 30.536	4.139 – 74.647	2.245 – 43.109	1.183 – 27.250	4.222 – 74.588
relns collected	37888	43324	124210	25794	33217
unique relfns	10582	7815	24284	8608	8162
data/restraint/ parameters	12243/0/427	9883/0/536	34226/18/535	9816/0/481	9120/25/589
R ₁ , wR ₂ (I>2 σ (I))	0.0289, 0.0488	0.0334, 0.0665	0.0345, 0.0602	0.0282, 0.0555	0.0283, 0.0618

Table S2. Selected Literature Heterobimetallic d-f Complexes with Short Intermetal Distances

Complex	M-M Distance (Å)	Sum of Covalent Radii ²⁹	<i>r</i> ^a	ref.
3	2.4644	2.72	0.91	<i>This work</i>
3-THF	2.5989	2.72	0.96	<i>This work</i>
4	2.9771	2.72	1.09	<i>This work</i>
FU(OC ₆ H ₂ -6-But-4-Me-2-PPh ₂ -κ ₂ O ,P) ₃ Ni	2.520	2.80	0.90	³⁰
[U(Cl) ₂ {C(PPh ₂ NSiMe ₃)(PPh[C ₆ H ₄]-NSiMe ₃)} {Rh(CH(SiMe ₃)(PPh ₂)}]	2.5835	2.95	0.88	³¹
[Lu{Ni(ArO) ₃ tacn ₂ }[ClO ₄]	2.918, 2.925	2.72	1.07, 1.08	³²
C ₆ H ₄ {N=CHC ₆ H ₄ -2-(O-)} ₂ Ni Lu(CF ₃ COCH ₂ COCF ₃) ₃	3.151	2.72	1.16	³³
(C ₅ Me ₄ SiMe ₂ CH ₂ PPh ₂)Lu(μ-CH ₂ SiMe ₂ CH ₂)(OC ₄ H ₈)PtMe ₂	2.7668	2.85	0.97	³⁴
[(Ph ₂ PNHPh)Pd{μ-(Ph ₂ PNPh)} ₃ Lu(μ-Cl)Li(THF) ₃]	2.9031	2.82	1.03	³⁵
[(Ph ₂ PNHPh)Pt{μ-(Ph ₂ PNPh)} ₃ Lu(μ-Cl)Li(THF) ₃]	2.9523	2.85	1.04	³⁶
[Cp ₂ Lu-ReCp ₂]	2.8958	2.93	0.99	³⁷
(C ₄ H ₈ O)(C ₅ H ₅) ₂ Lu-Ru(CO) ₂ (C ₅ H ₅)	2.995	2.87	1.04	³⁸
[2,6-(CH ₂ C ₅ H ₃) ₂ C ₅ H ₃ N] ₂ Dy-FeCp(CO) ₂	2.884	2.83	1.02	³⁹
[Nd(Bu ^t NCH ₂ CH ₂ {C(NCSiMe ₃ CHNBu ^t)}- (N(SiMe ₃) ₂)} {FeCp(CO) ₂ }]	2.9942	2.90	1.03	⁴⁰
Me-PdNd{O[Si(CH ₃) ₂ NH-(4-CH ₃ C ₅ H ₃ N) ₂]} ₂	3.0345	2.94	1.03	⁴¹

^a *r* is the ratio of their metal-metal bond distance to the corresponding sum of the metals' covalent single-bond radii²⁹

NMR Spectroscopy

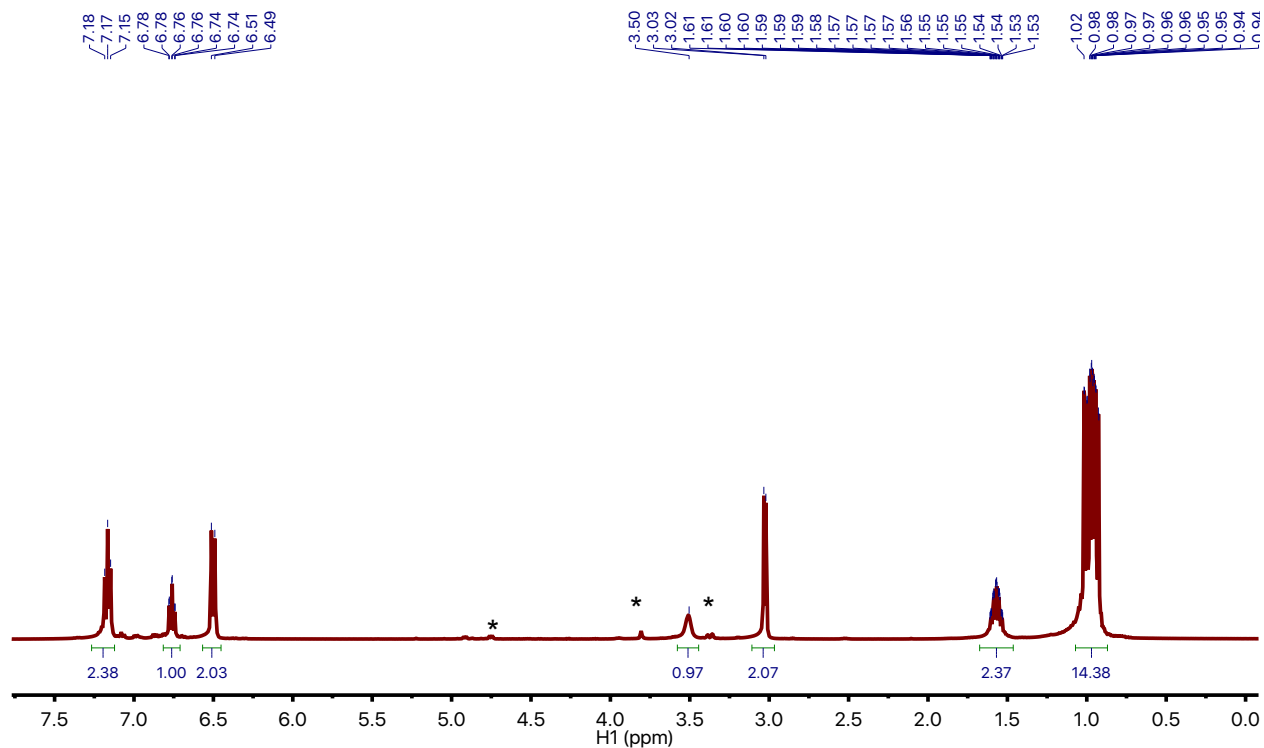


Figure S1. ¹H NMR (400 MHz, C₆D₆) spectrum of *i*Pr₂PCH₂NHPh. Residual impurity peaks are indicated by *.

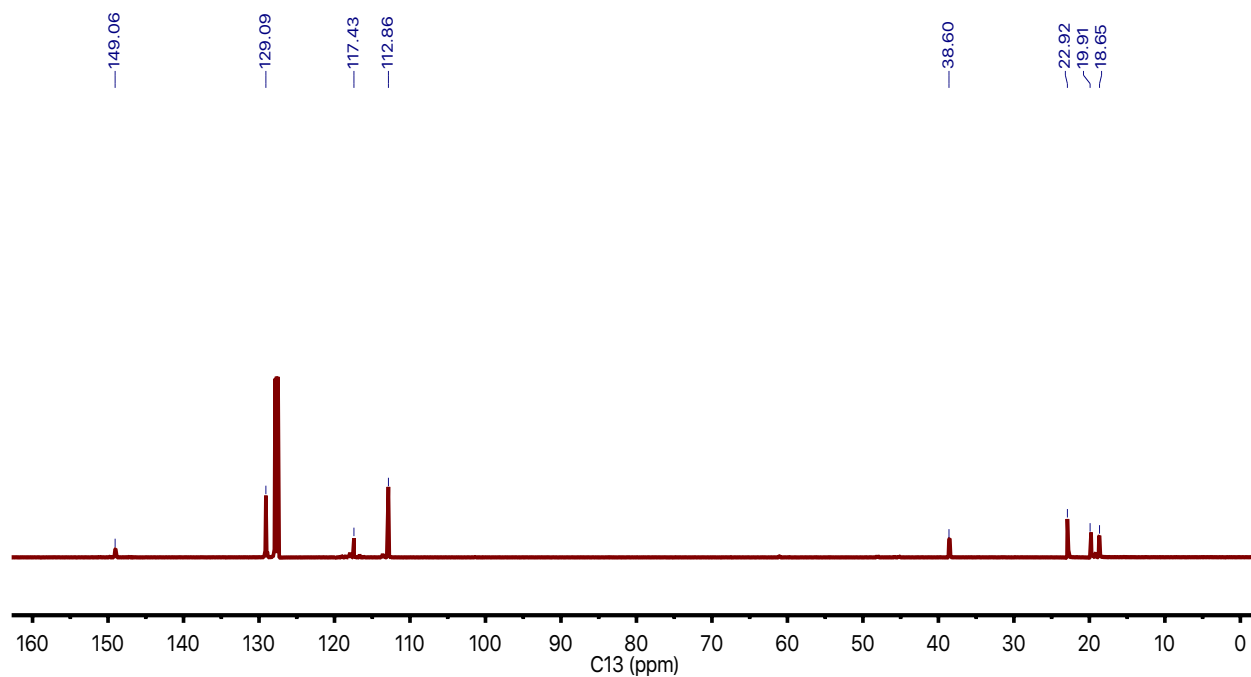


Figure S2. ¹³C NMR (126 MHz, C₆D₆) spectrum of *i*Pr₂PCH₂NHPh.

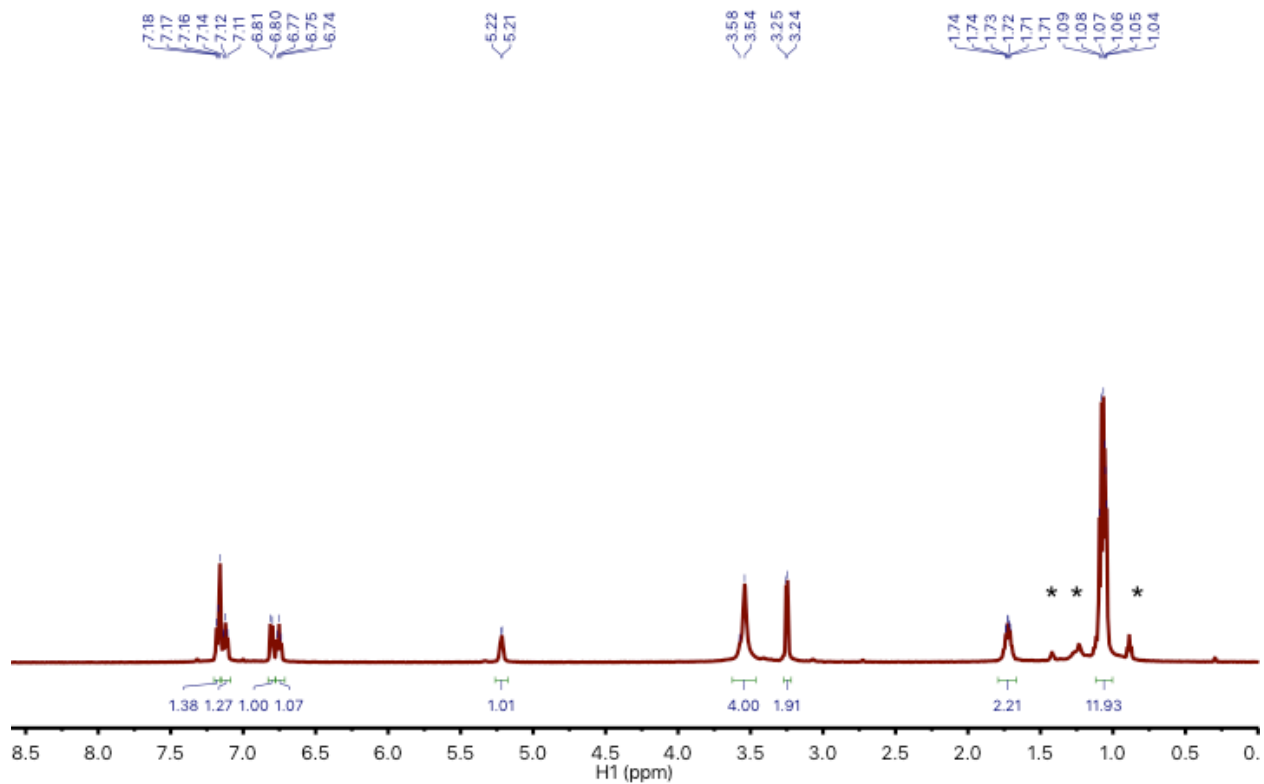


Figure S3. ^1H NMR (400 MHz, C_6D_6) spectrum of $(i\text{Pr}_2\text{PCH}_2\text{NHPAr})_3\text{tacn}$. Residual solvent peaks (hexanes) are indicated by *.

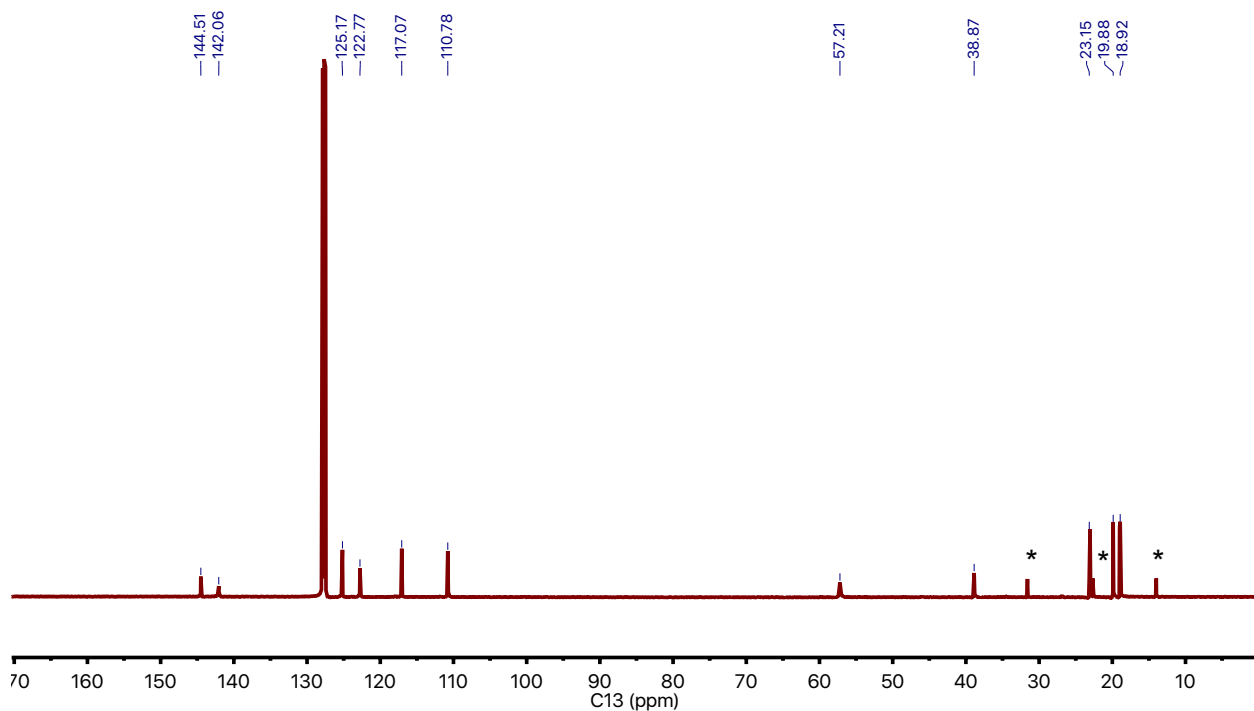


Figure S4. Proton ^{13}C NMR (126 MHz, C_6D_6) spectrum of $(i\text{Pr}_2\text{PCH}_2\text{NHPAr})_3\text{tacn}$. Residual solvent peaks (hexanes) are indicated by *.

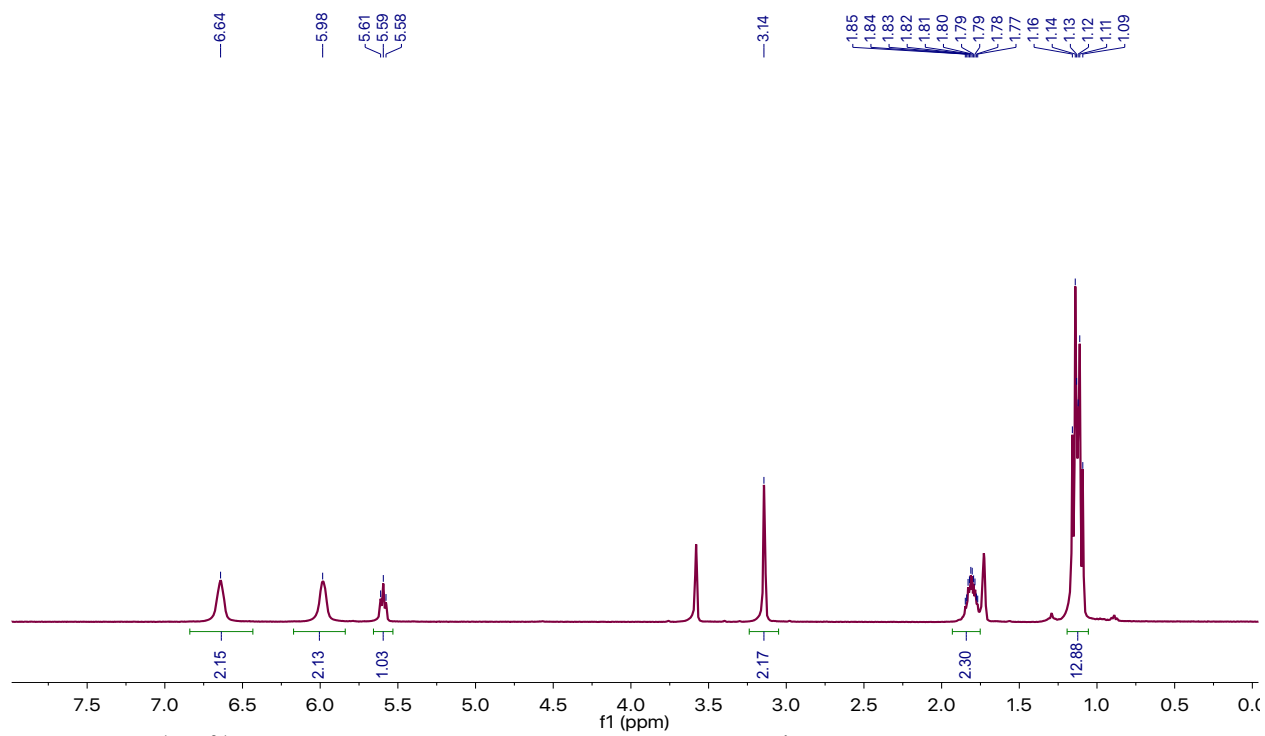


Figure S5. $^1\text{H}\{^{31}\text{P}\}$ NMR (400 MHz, $\text{THF}-d_8$) spectrum of $i\text{Pr}_2\text{PCH}_2\text{NKPh}$.

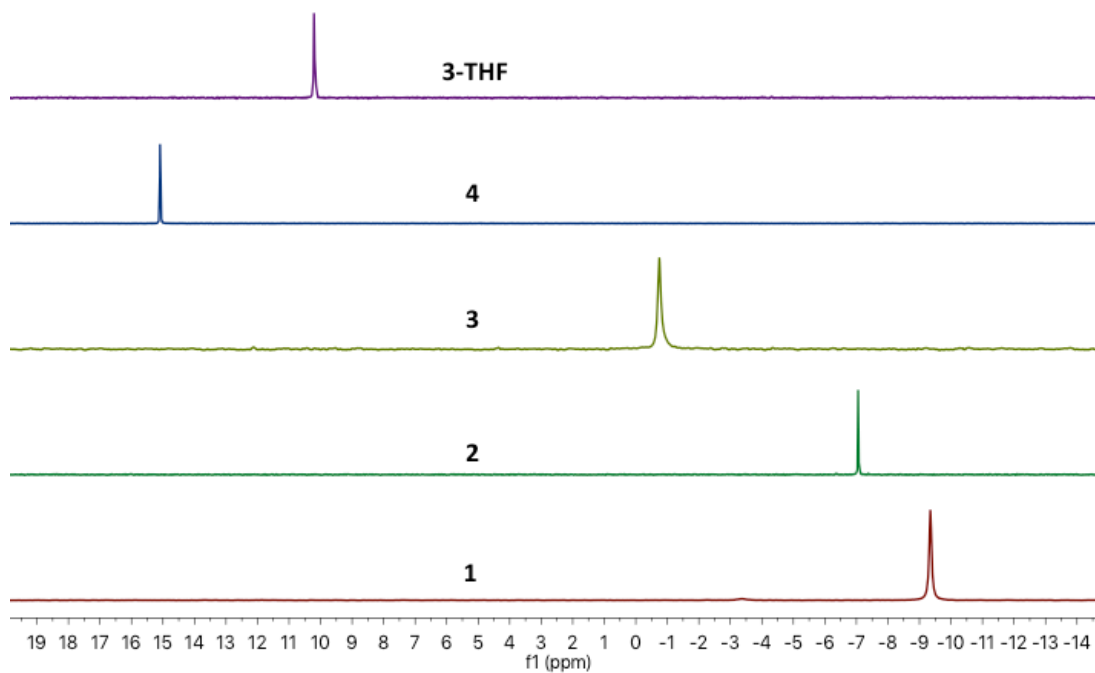


Figure S6. ^{31}P NMR (282 MHz) spectra overlay of all reported complexes: **1**, **2**, **3**, **4** (in C_6D_6), and **3-THF** (in $\text{THF}-d_8$).

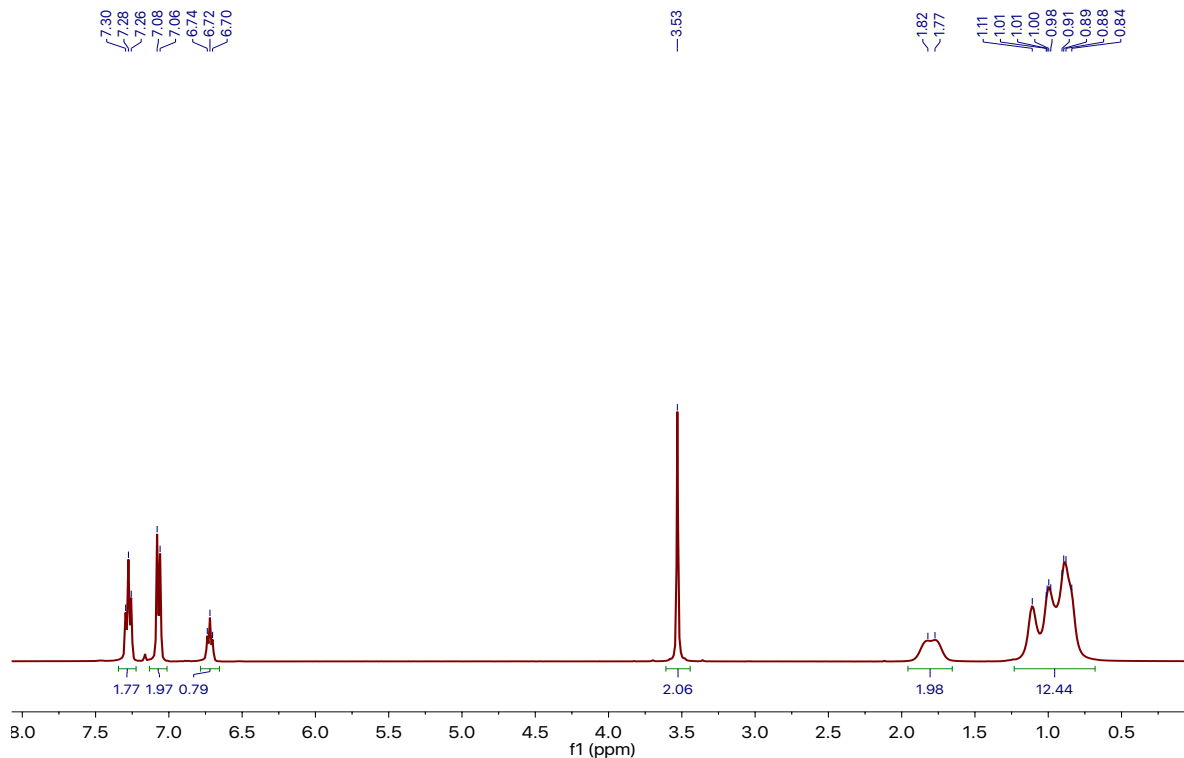


Figure S7. $^1\text{H}\{^{31}\text{P}\}$ NMR (400 MHz, C_6D_6) spectrum of **1**.

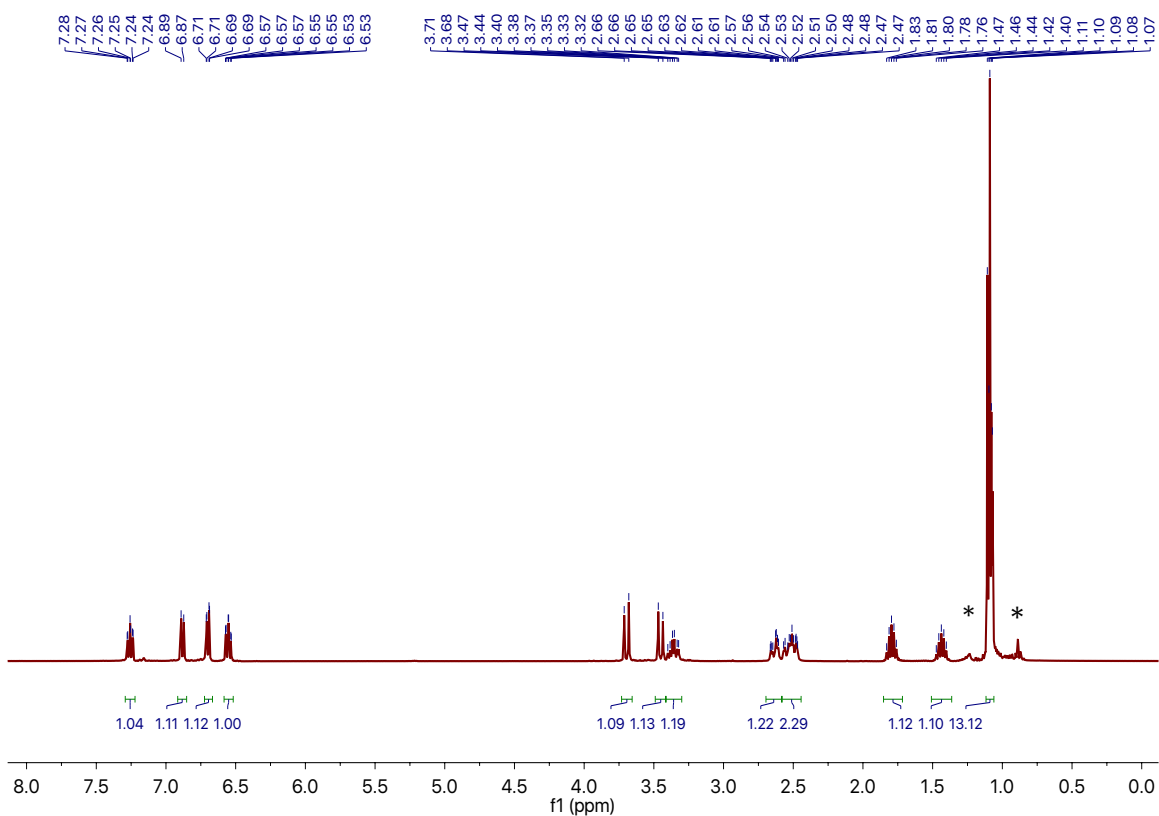


Figure S8. $^1\text{H}\{^{31}\text{P}\}$ NMR (400 MHz, C_6D_6) spectrum of **2**. Residual solvent peaks (hexanes) are indicated by *.

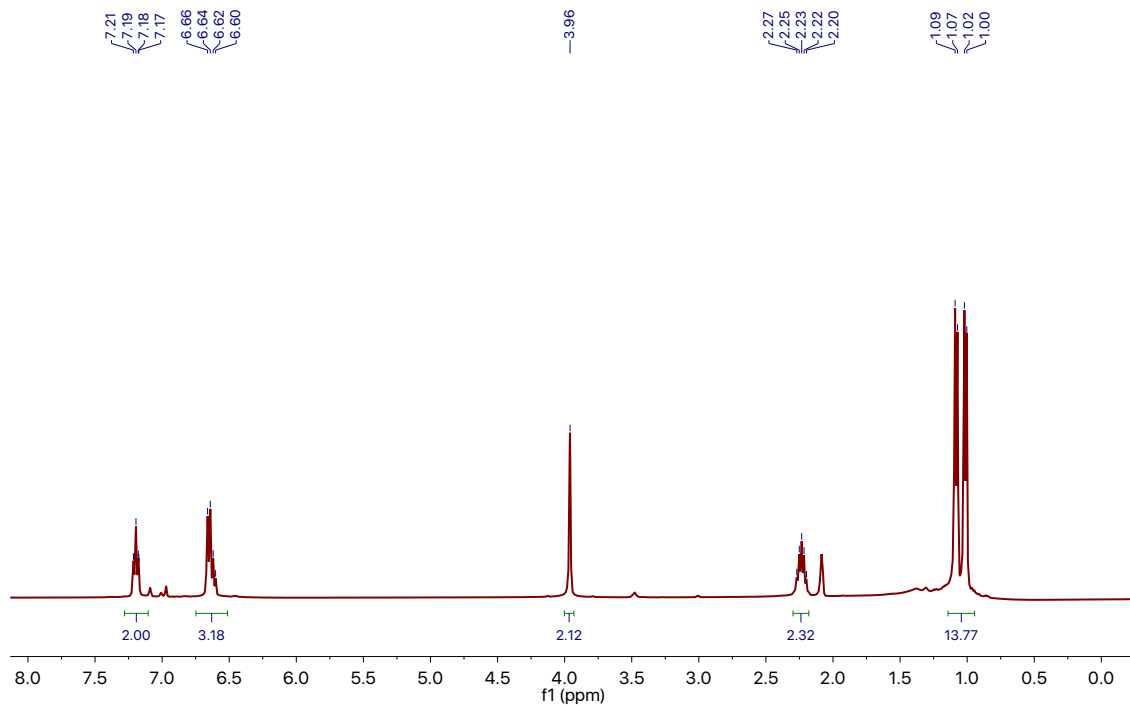


Figure S9. $^1\text{H}\{^{31}\text{P}\}$ NMR (400 MHz, toluene- d_8) spectrum of **3**.

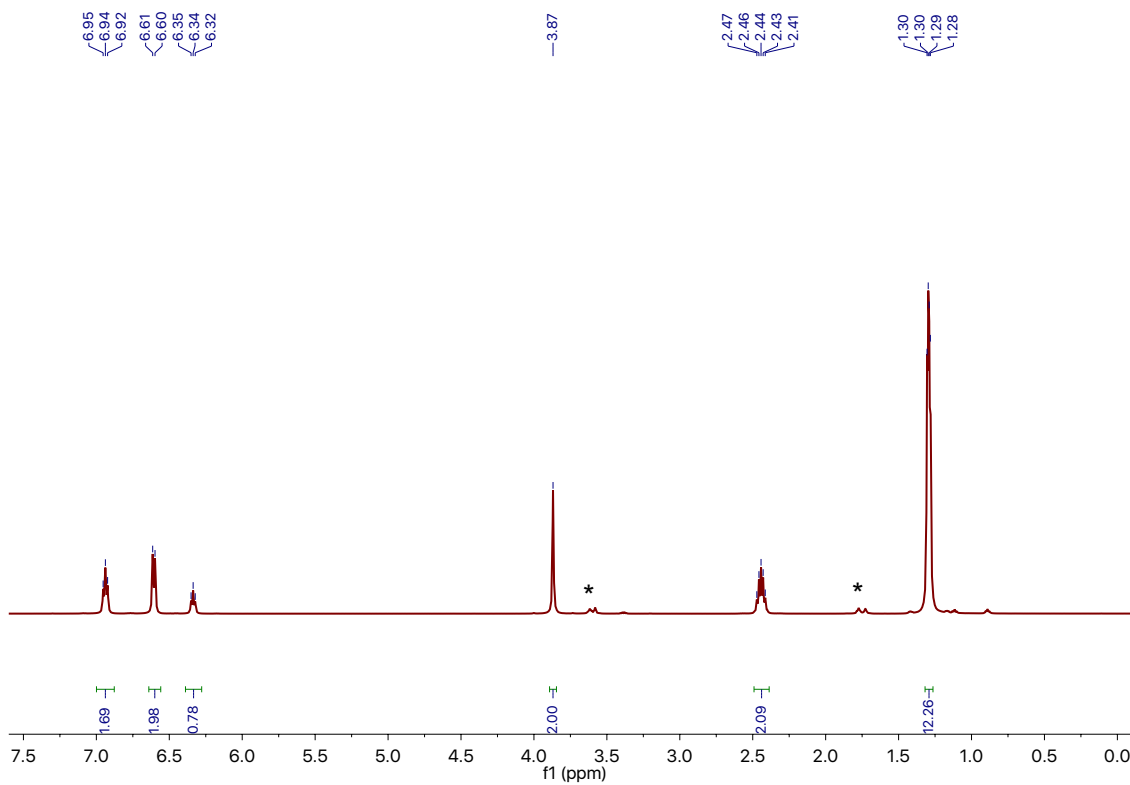


Figure S10. $^1\text{H}\{^{31}\text{P}\}$ NMR (400 MHz, THF- d_8) spectrum of **3**-THF. Residual solvent peaks (THF) are indicated by *.

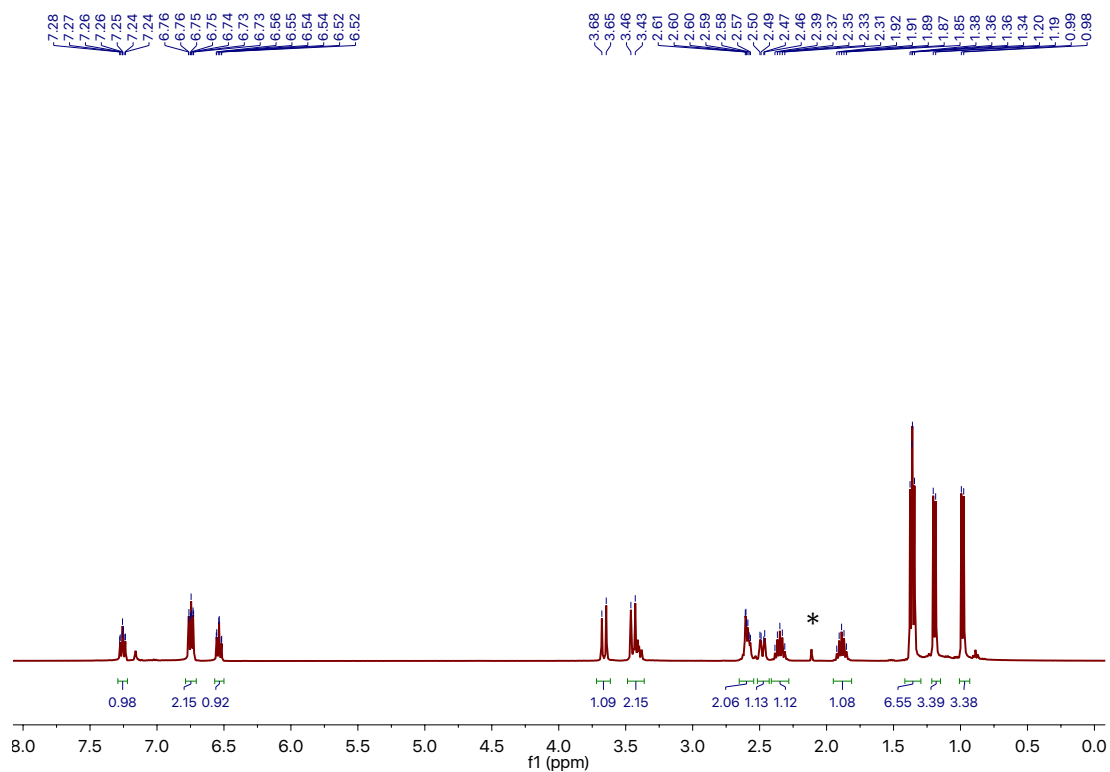


Figure S11. $^1\text{H}\{^{31}\text{P}\}$ NMR (400 MHz, C_6D_6) spectrum of **4**. Residual solvent peaks (toluene) are indicated by *.

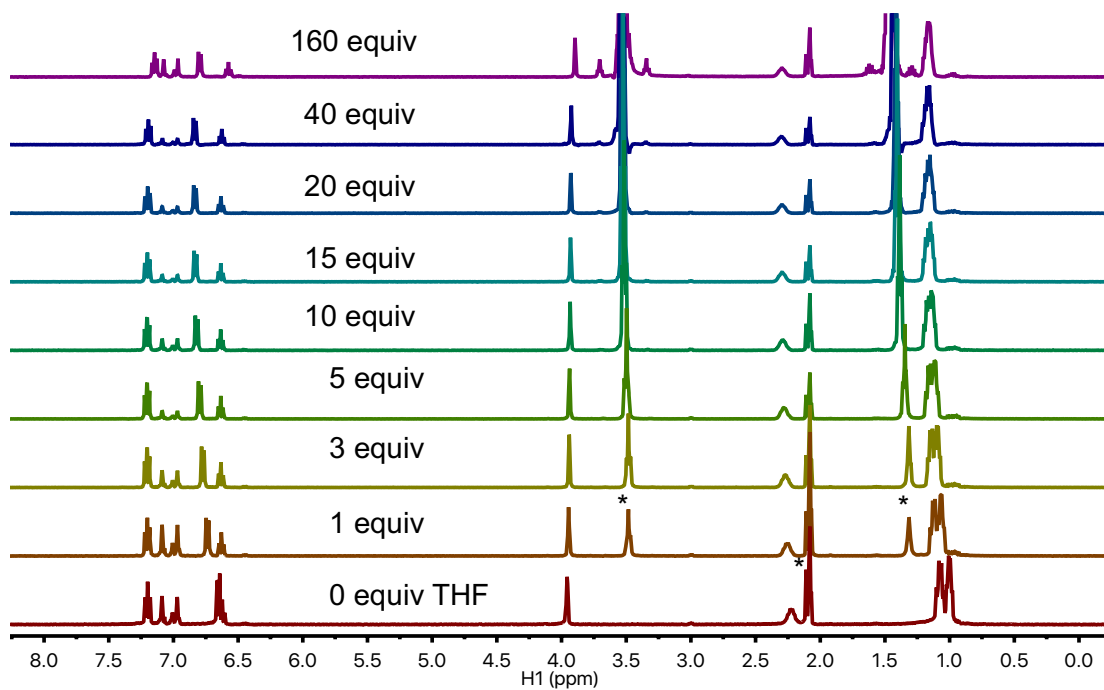


Figure S12. $^1\text{H}\{^{31}\text{P}\}$ NMR (400 MHz, toluene- d_8) spectrum of **3** titrated with varying equivalents of THF. Residual solvent peaks (toluene and THF) are indicated by *.

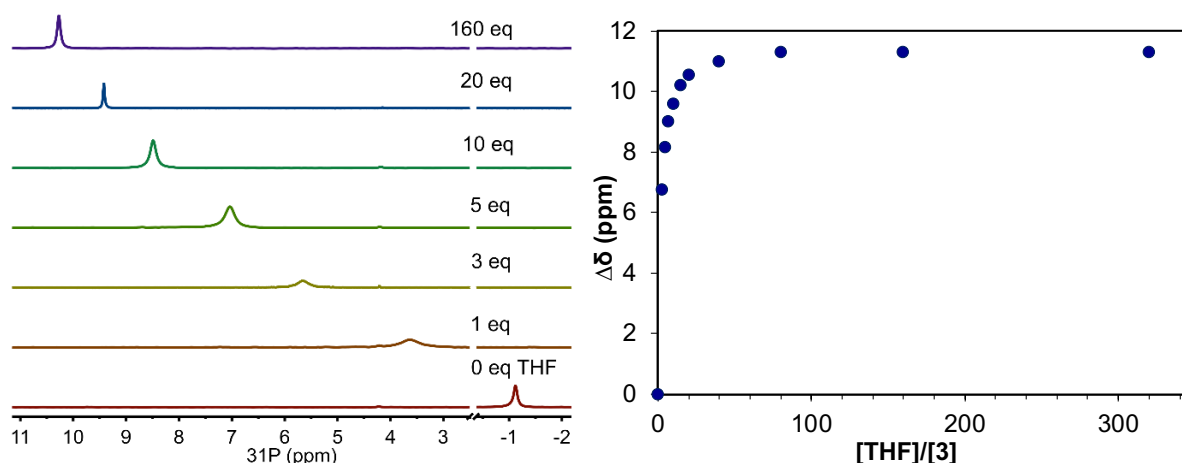


Figure S13. (Left) ^{31}P NMR spectra from titration of 10 mM **3** with THF in d_8 -toluene (Right). Solvent binding isotherm data for the titration of 10 mM **3** with THF (blue circles) at 25 ± 1 °C in d_8 -toluene.

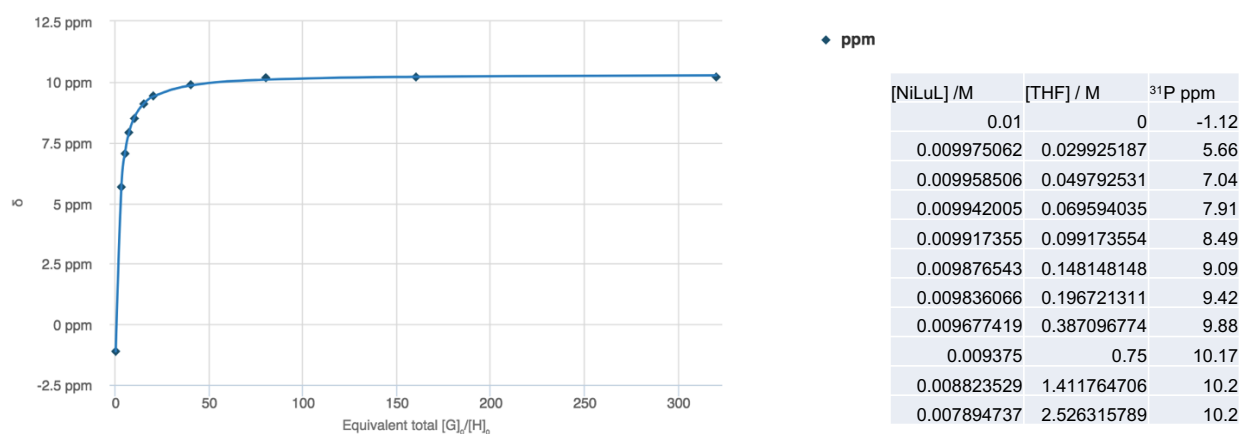


Figure S14. (Left) A fitted plot of the δ versus equivalents of $[\text{THF}]_0/[\mathbf{3}]_0$ (guest (G) = THF; host (H) = **3**) at 25 ± 1 °C in d_8 -toluene, where δ is the ^{31}P chemical shift. Data was modeled using *bindfit* fitting software, available through supramolecular.org,¹ using a simple 1:1 binding model between **3** and THF.^{2,3} From the non-linear regression, $K_a = 59(2) \text{ M}^{-1}$. Lower equivalent addition data point (1 eq) was excluded due to issues in solubility of **3** at lower equiv additions of THF. (Right) Raw titration data used for non-linear and linear regression (Figure S15) plots.

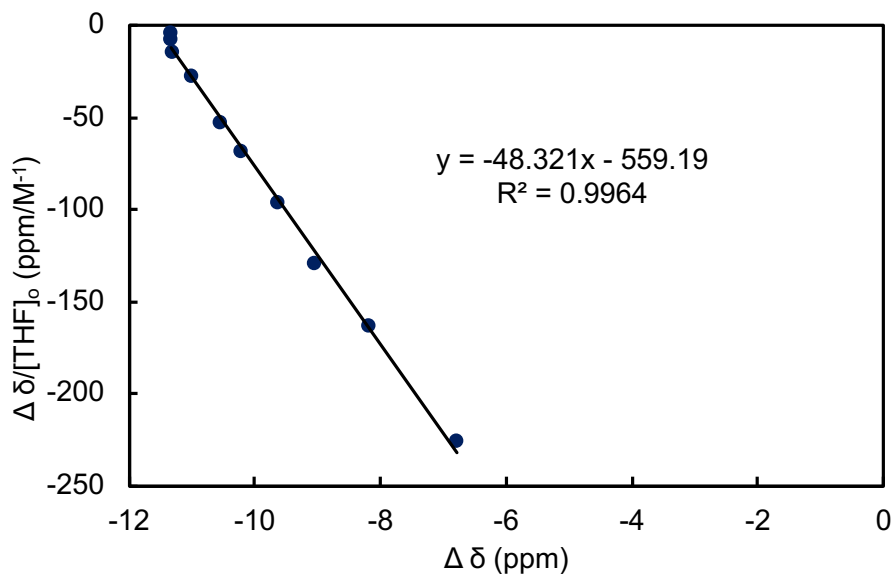


Figure S15. A Scatchard plot of the $\Delta\delta$ versus $\Delta\delta/[\text{THF}]_0$, where $\Delta\delta$ is the measured change in ^{31}P chemical shift (upon addition of THF) referenced to that of the un-complexed **3**.^{2, 42} From the plot, $K_a = 48.32 \text{ M}^{-1}$ which is in close agreement to the K_a value obtained by non-linear regression.

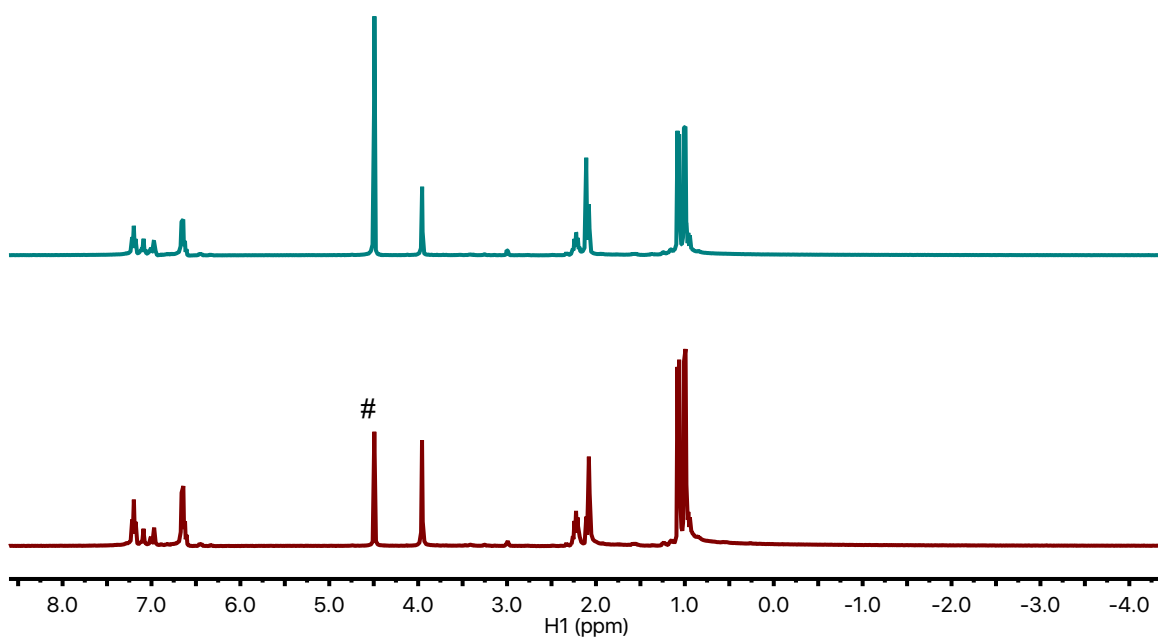


Figure S16. $^1\text{H}\{^{31}\text{P}\}$ NMR spectrum of **3** under 1 atm and 4 atm H_2 at room temperature (400 MHz, toluene- d_8). At 1 atm and 4 atm H_2 , a non-perturbed ^1H resonance (indicated by #) for free H_2 is observed at 4.5 ppm (free H_2 is 4.50 ppm in toluene- d_8)⁴³. A bound H_2 resonance is not observed at either pressure.

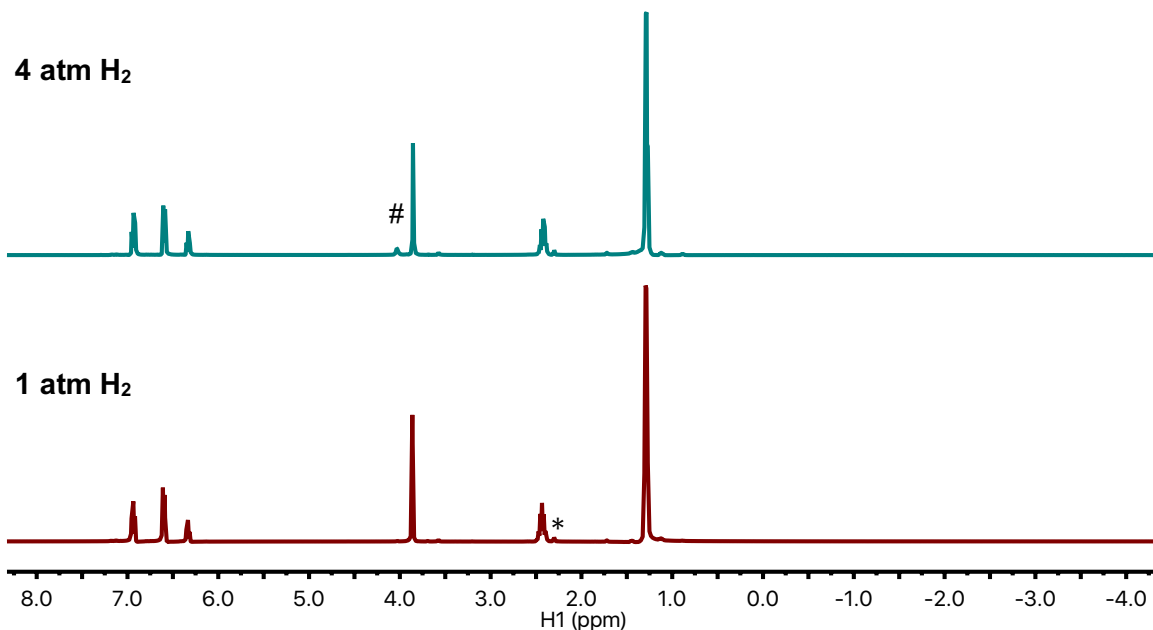


Figure S17. $^1\text{H}\{^{31}\text{P}\}$ NMR spectrum of **3**-THF under 1 atm and 4 atm H_2 at room temperature (400 MHz, $\text{THF}-d_8$). Residual solvent peaks (toluene) are indicated by *. At 1 atm, the ^1H resonance for free H_2 is not observed, whereas a perturbed ^1H resonance for free H_2 (indicated by #) is observed at 4.0 ppm under 4 atm H_2 (free H_2 is 4.55 ppm in $\text{THF}-d_8$)⁴³. A bound H_2 resonance is not observed at either pressure.

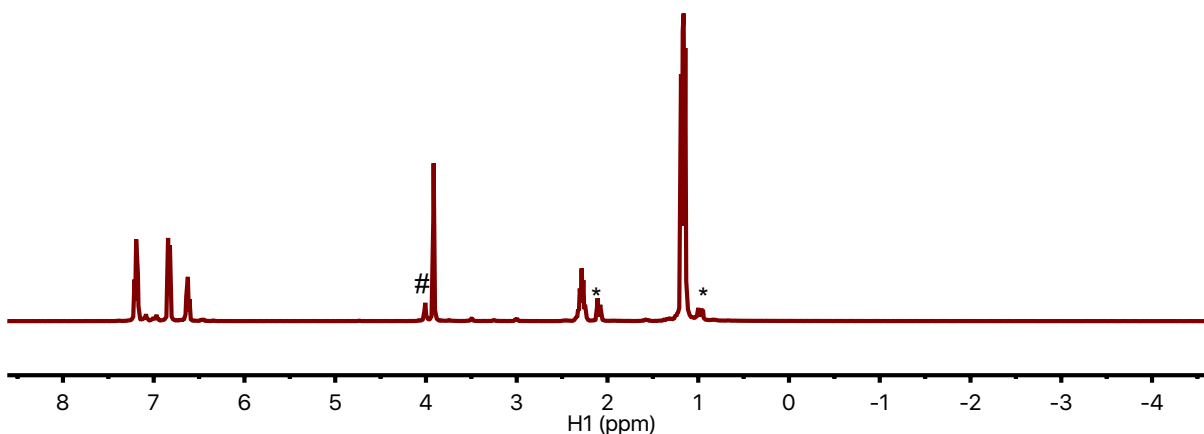


Figure S18. $^1\text{H}\{^{31}\text{P}\}$ NMR spectrum of **3** + 15 eq THF under 4 atm H_2 at room temperature (400 MHz, toluene- d_8). Residual solvent peaks (toluene and hexanes) are indicated by *. At 4 atm H_2 , a perturbed ^1H resonance (indicated by #) for free H_2 is observed at 4.0 ppm (free H_2 is 4.50 ppm in toluene- d_8)⁴³. A bound H_2 resonance is not observed under these conditions.

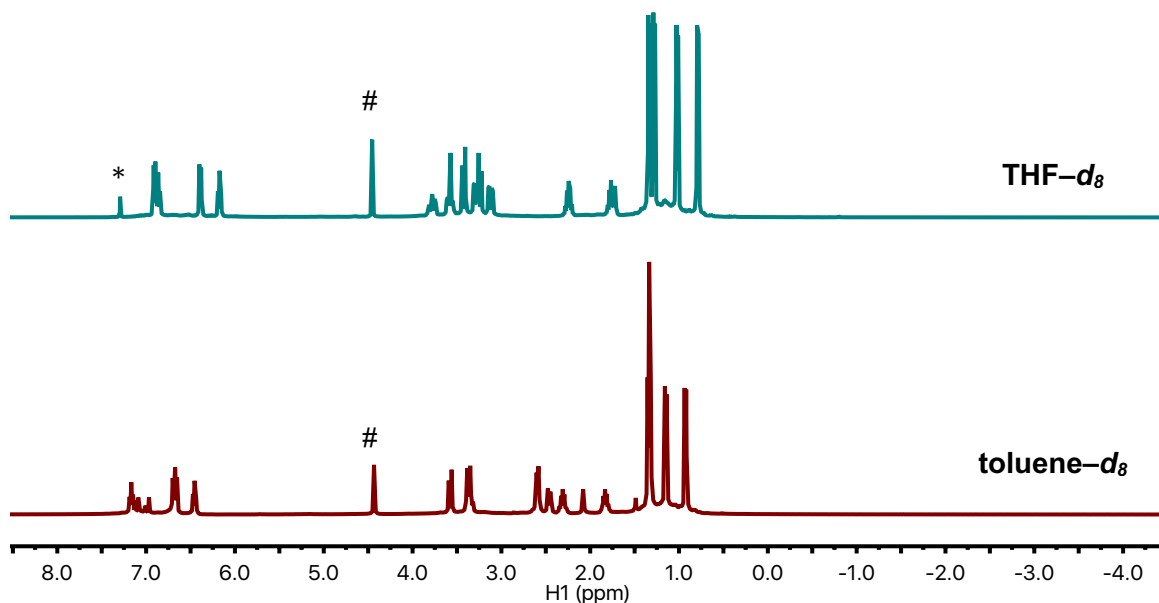


Figure S19. $^1\text{H}\{^{31}\text{P}\}$ NMR spectrum of **4** under 4 atm H_2 at room temperature in (top) $\text{THF-}d_8$ and (bottom) $\text{toluene-}d_8$ (400 MHz). Residual solvent peaks (benzene) are indicated by *. At 4 atm, a perturbed ^1H resonance for free H_2 (indicated by #) is observed at 4.45 ppm in $\text{THF-}d_8$ and at 4.43 ppm in $\text{toluene-}d_8$ (free H_2 is 4.55 ppm in $\text{THF-}d$ and 4.50 ppm in $\text{toluene-}d_8$). A bound H_2 resonance is not observed at either pressure.

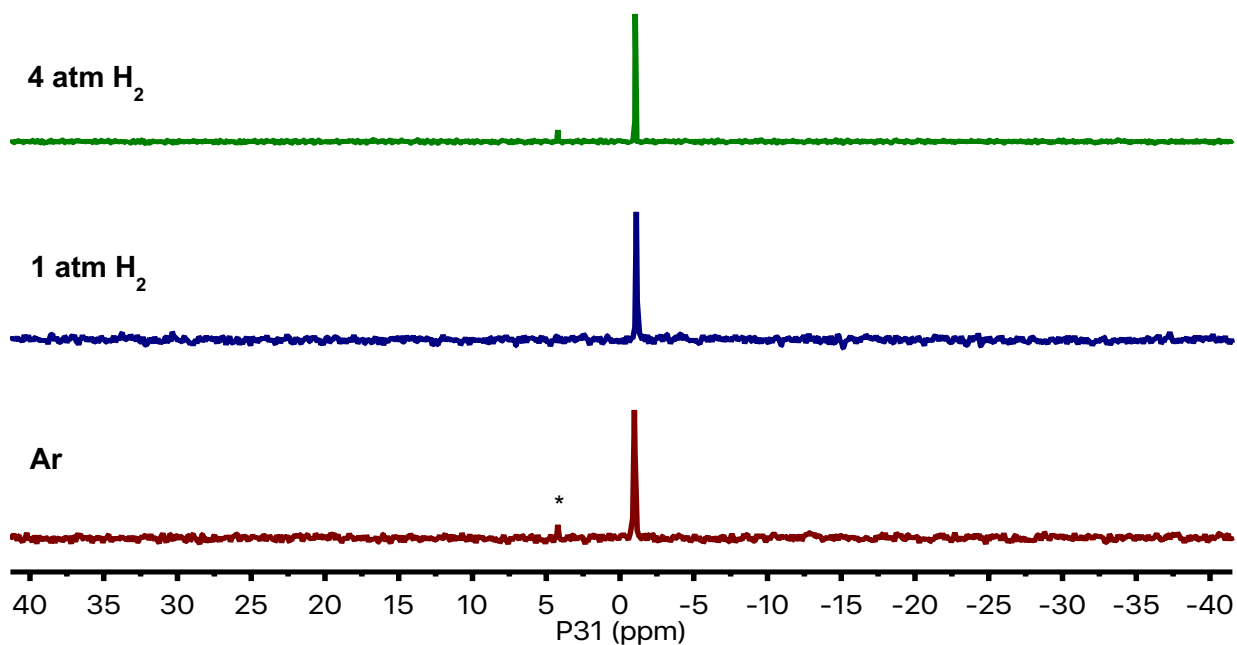


Figure S20. ^{31}P NMR overlay of **3** under Ar, 1 atm H_2 and 4 atm H_2 at 298 K (400 MHz, $\text{toluene-}d_8$). Residual water in d_8 -toluene and H_2 gas results in the formation of a small amount of $\text{Pr}_2\text{PCH}_2\text{NHPH}$ which can be seen at 4.22 ppm.

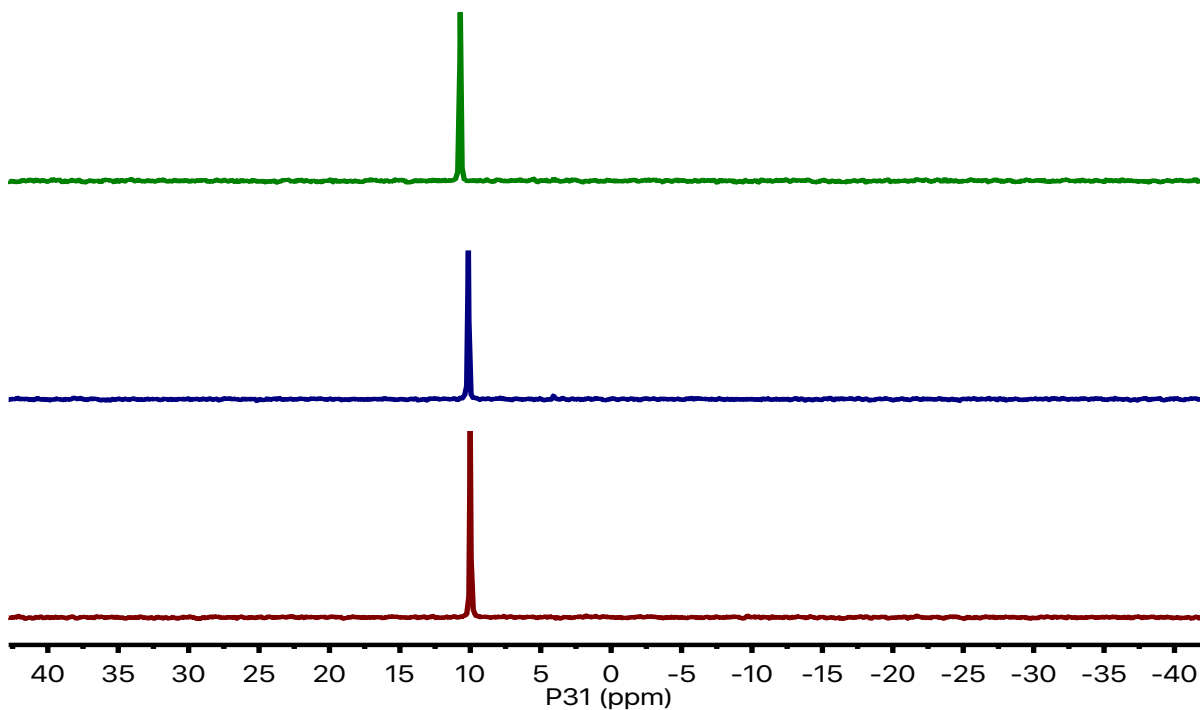


Figure S21. ^{31}P NMR overlay of **3**-THF (**3** + 15 eq THF- d_8) under Ar, 1 atm H_2 and 4 atm H_2 at 298 K (400 MHz, toluene- d_8).

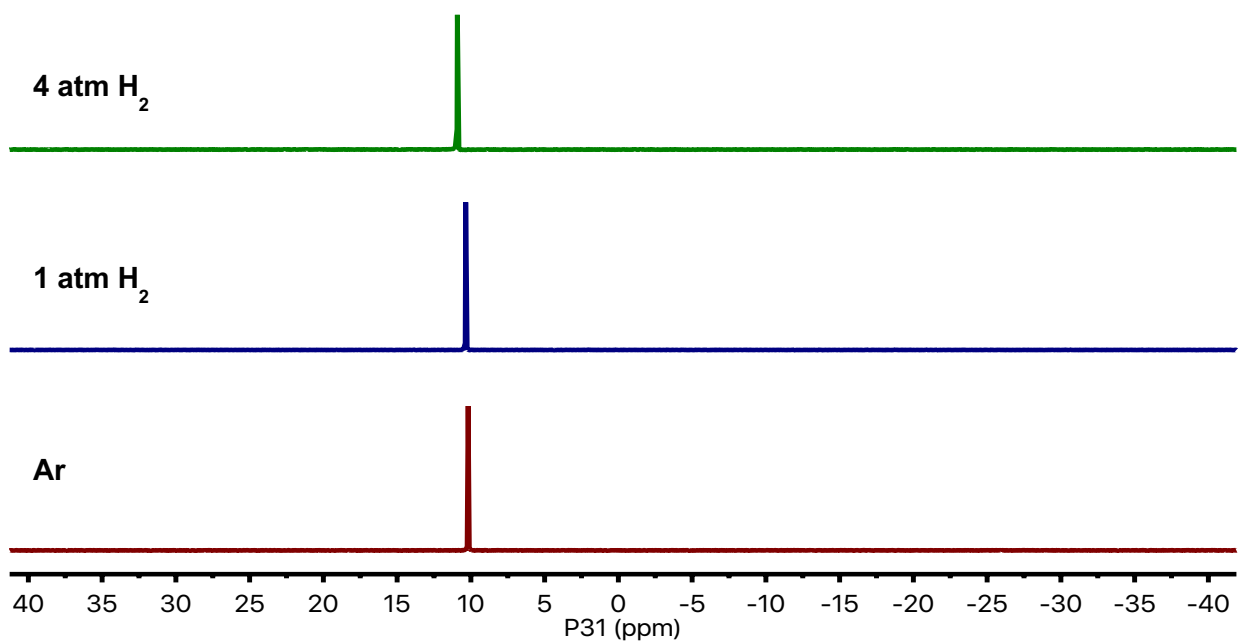


Figure S22. ^{31}P NMR overlay of **3**-THF under Ar, 1 atm H_2 and 4 atm H_2 at 298 K (400 MHz, THF- d_8).

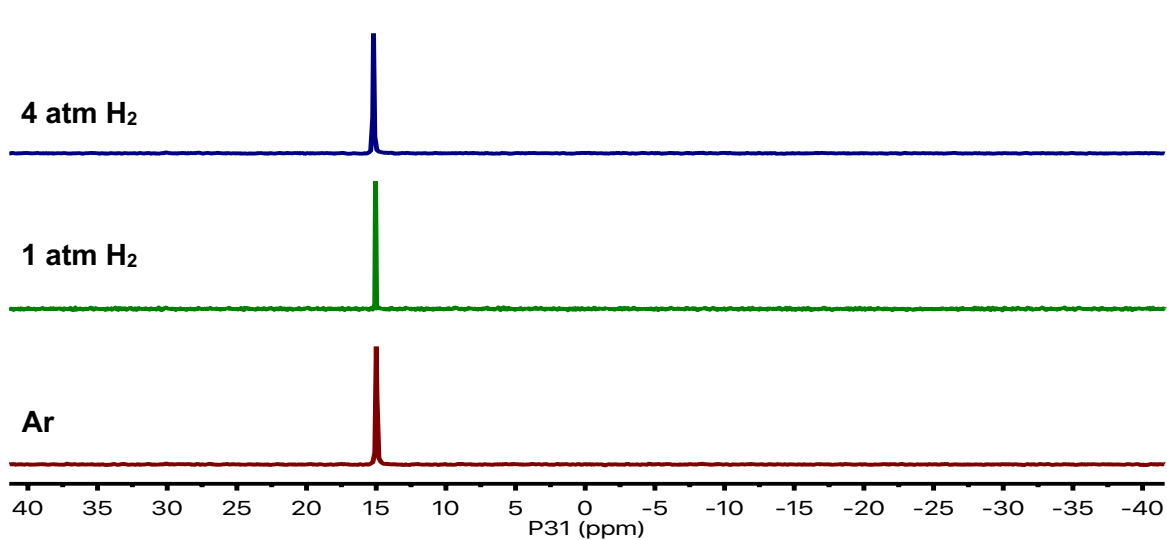


Figure S23. ^{31}P NMR overlay of **4** under Ar, 1 atm H_2 and 4 atm H_2 at 298 K (400 MHz, toluene- d_8).

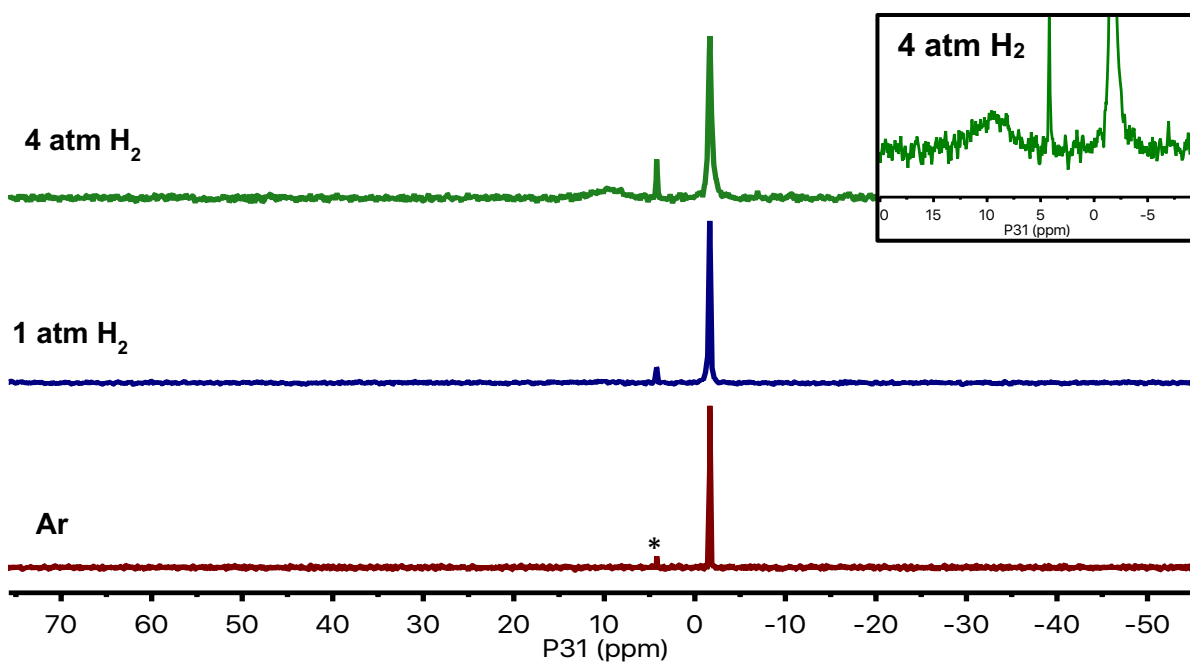


Figure S24. ^{31}P NMR overlay of **3** under Ar, 1 atm H_2 , and 4 atm H_2 (at rt) cooled to 190 K (400 MHz, toluene- d_8). Reported H_2 pressures are with respect to their initial pressures at room temperature. Residual water in d_8 -toluene and H_2 gas results in the formation of a small amount of $\text{Pr}_2\text{PCH}_2\text{NHPH}$ denoted by an asterisk (*).

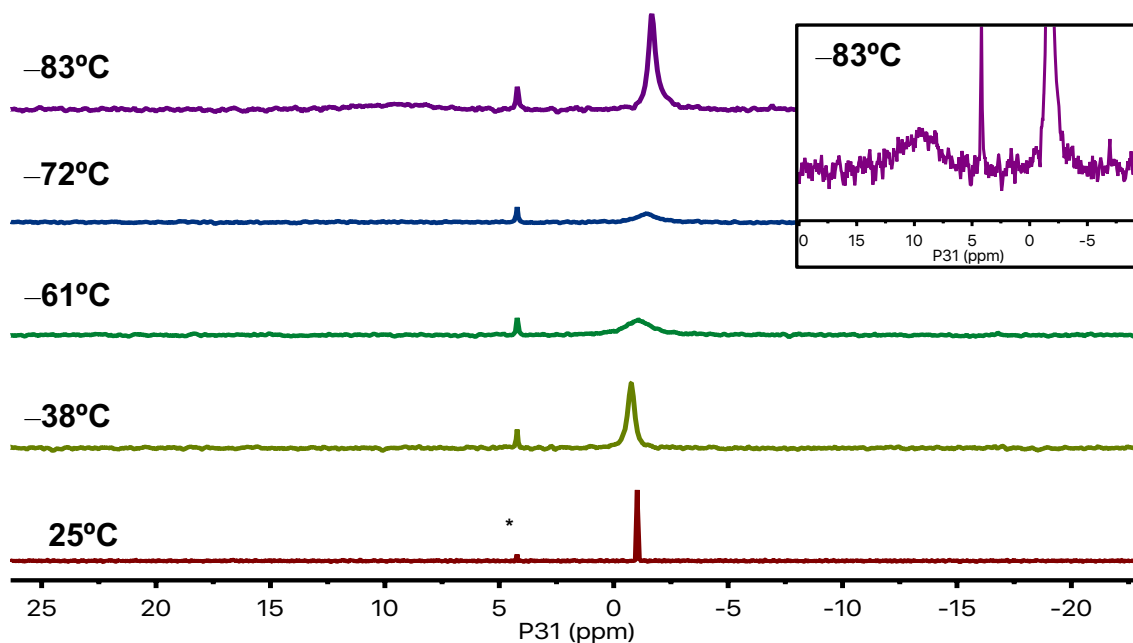


Figure S25. Variable temperature ^{31}P NMR of **3** under 4 atm H_2 at rt (400 MHz, toluene- d_8). Initially, the phosphorus resonance generally broadens upon cooling. At -83°C , the exchange becomes slower such that a slow exchange regime is achieved in which both **3** and **3**-(H_2) can be observed. In turn, a discrete bound **3**-(H_2) phosphorus resonance (9.6 ppm) appears at -83°C . Residual water in H_2 gas results in the formation of a small amount of $\text{Pr}_2\text{PCH}_2\text{NHPh}$ denoted by an asterisk (*).

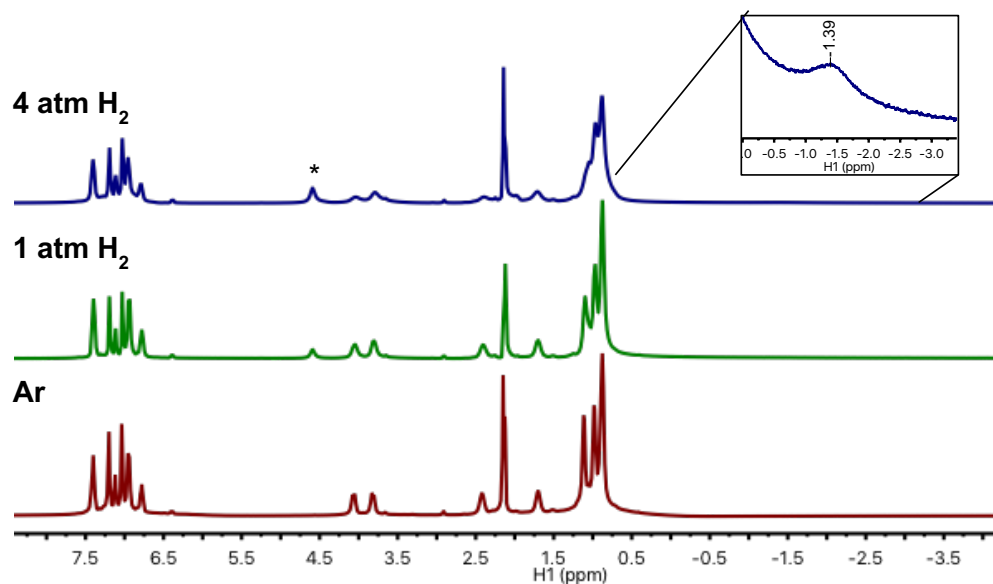


Figure S26. $^1\text{H}\{^{31}\text{P}\}$ NMR overlay of **3** under Ar, 1 atm H_2 , and 4 atm H_2 (at rt) cooled to 190 K (400 MHz, toluene- d_8). Reported H_2 pressures are with respect to their initial pressures at room temperature. Free H_2 is marked by an asterisk (*). A zoomed inset of **3** under 4 atm H_2 (at rt) cooled to 190 K between 0 and -3.0 ppm shows the bound H_2 resonance of the **3**-(H_2) species. Reliable T_1 values could not be obtained due to the broadness of the bound H_2 resonance at 190 K.

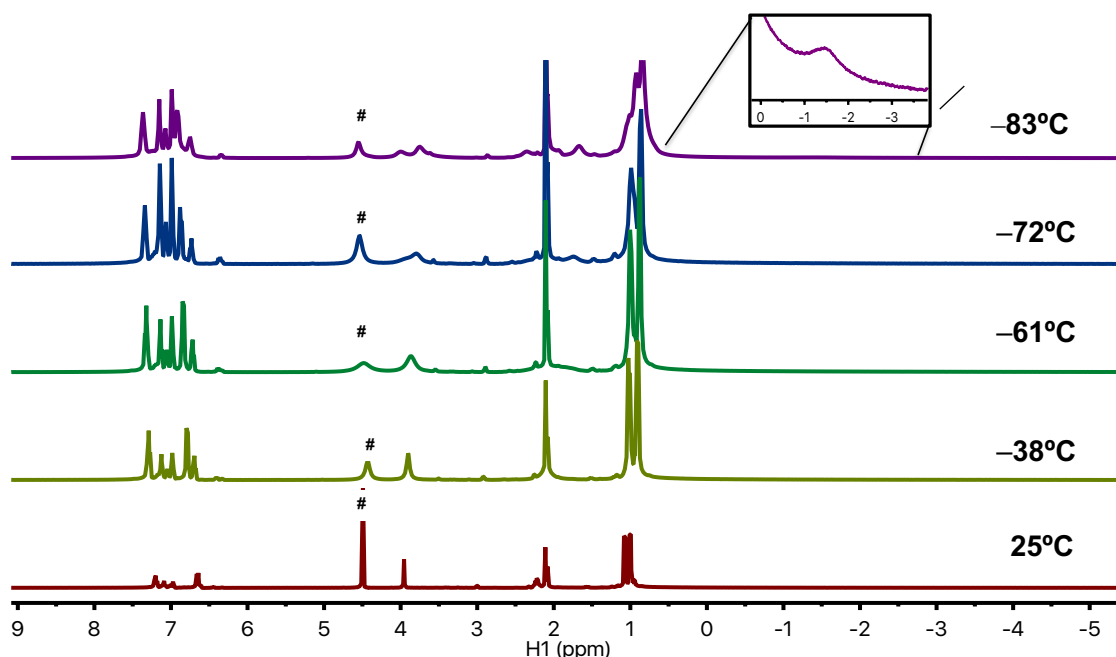


Figure S27. Variable temperature proton NMR of **3** under 4 atm H₂ at rt (400 MHz, toluene-*d*₈). Though the bound H₂ resonance is not visible at rt, it appears at -83°C. The resonance of free H₂ (at 4.50 ppm) generally broadens and shifts slightly upfield upon cooling to -61°C. At -72°C, the resonance shifts back downfield to that of free H₂ (4.50 ppm).

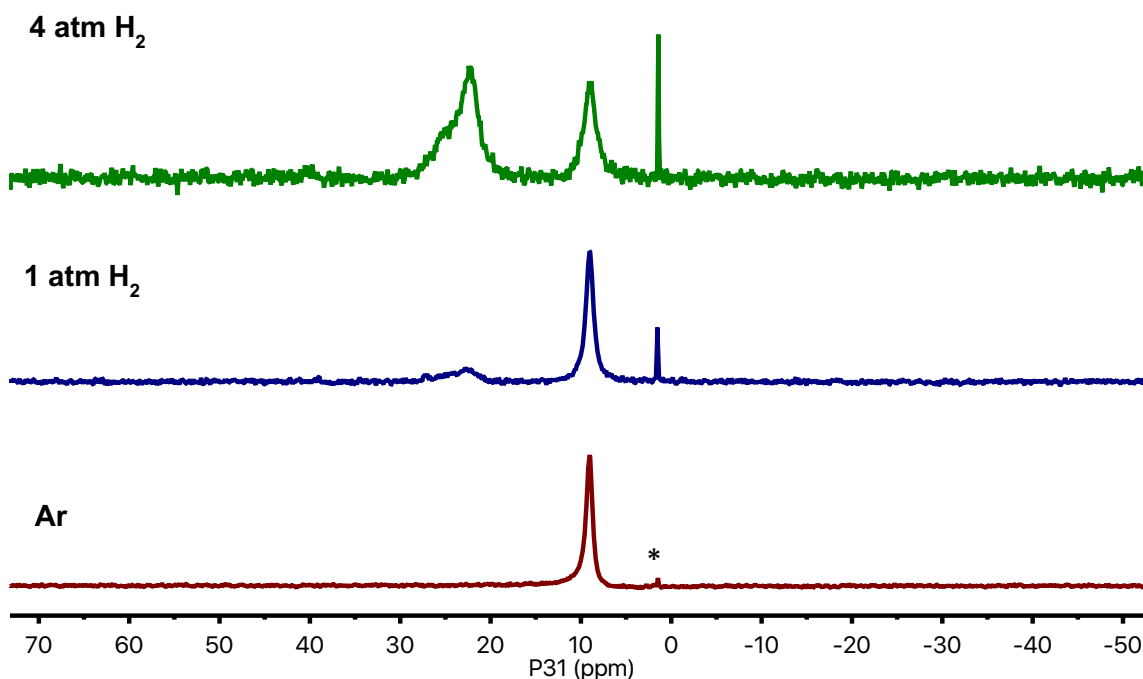


Figure S28. ³¹P NMR overlay of **3**-THF (**3** + 15 eq THF-*d*₈) under Ar, 1 atm H₂, and 4 atm H₂ cooled to 190 K (400 MHz, toluene-*d*₈). Reported H₂ pressures are with respect to their initial pressures at room temperature. Residual water in THF-*d*₈ and H₂ gas results in the formation of a small amount of Pr₂PCH₂NHPh denoted by an asterisk (*). Overall, behavior of H₂ binding is similar to that of **3** in bulk THF-*d*₈ (Figure S29).

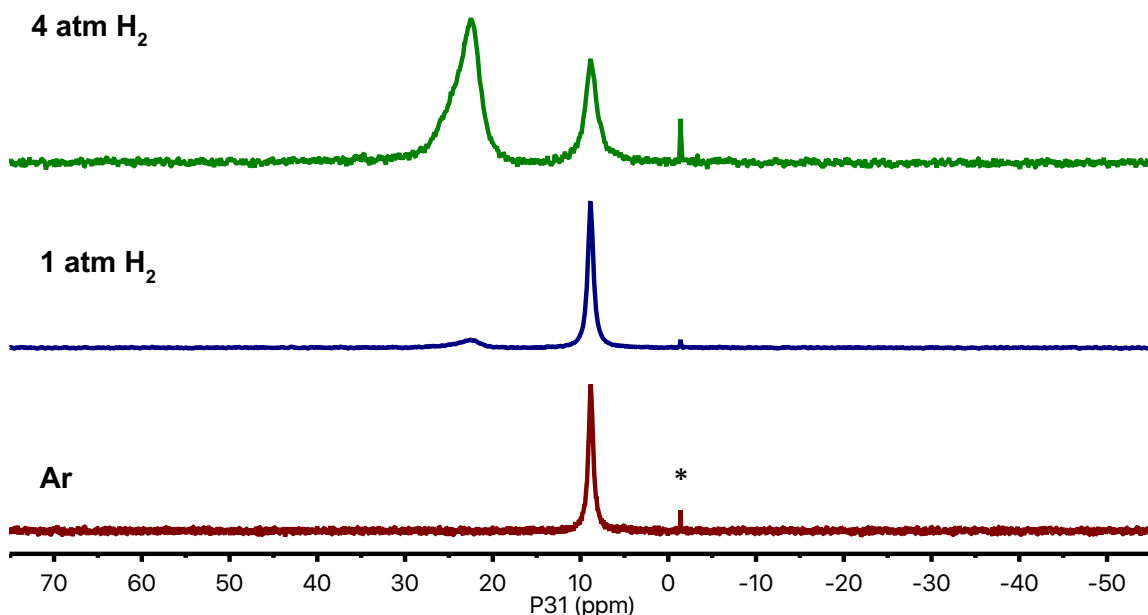


Figure S29. ^{31}P NMR overlay of **3**-THF under Ar, 1 atm H_2 , and 4 atm H_2 cooled to 190 K (400 MHz, $\text{THF}-d_8$). Reported H_2 pressures are with respect to their initial pressures at room temperature. Residual water in d_8 -THF and H_2 gas results in the formation of a small amount of $\text{Pr}_2\text{PCH}_2\text{NHPH}$ denoted by an asterisk (*).

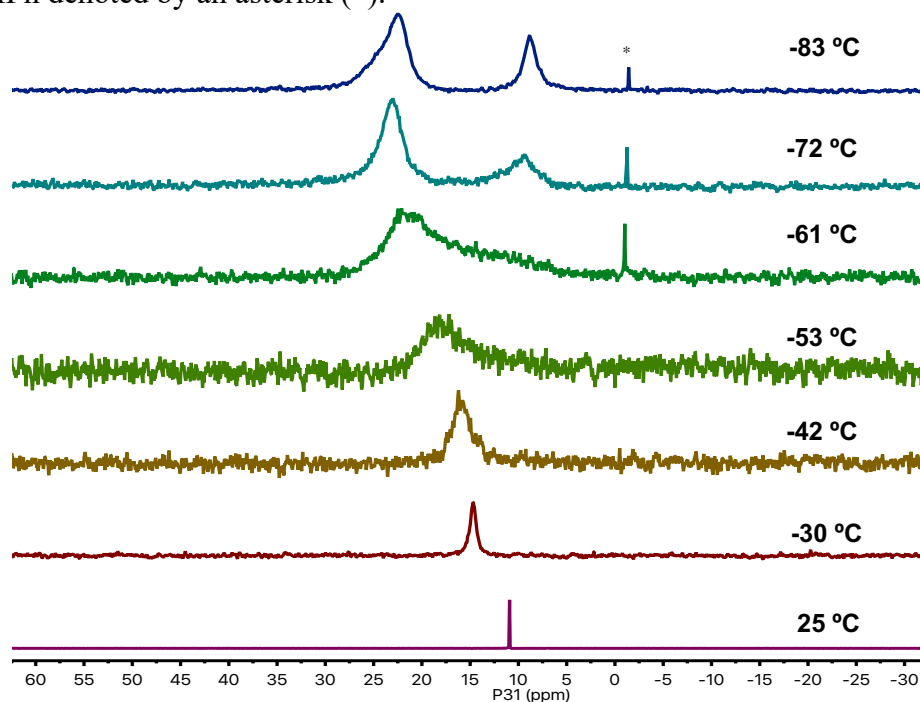


Figure S30. Variable temperature ^{31}P NMR of **3**-THF under 4 atm H_2 at rt (400 MHz, $\text{THF}-d_8$). Initially, the phosphorus resonance generally broadens upon cooling indicating an intermediate exchange regime between **3**-THF and **3**- $(\text{H}_2)\text{THF}$. At -61°C , the exchange becomes slower such that a slow exchange regime is achieved.⁴⁴ In turn, a discrete bound H_2 -**3**-THF phosphorus resonance appears at -72°C . Residual water in H_2 gas results in the formation of a small amount of $\text{Pr}_2\text{PCH}_2\text{NHPH}$, denoted by *, which can be seen at -1.4 ppm.

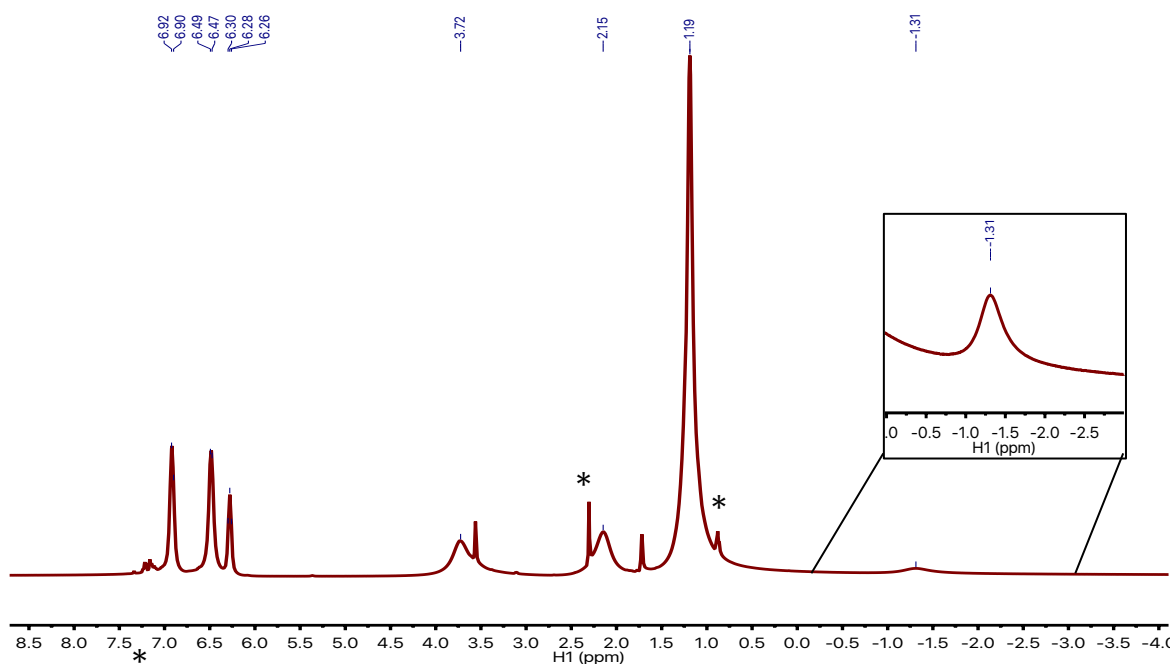


Figure S31. Proton $^1\text{H}\{^{31}\text{P}\}$ NMR spectrum of **3**-THF under 4 atm H_2 (at rt) cooled to 190 K (400 MHz, $\text{THF}-d_8$). At this temperature, a slow exchange regime is achieved between H_2 -**3**-THF and **3**-THF, thus the NMR is a combination of H_2 -**3**-THF and **3**-THF. Residual solvent peaks (toluene, hexanes) are indicated by *.

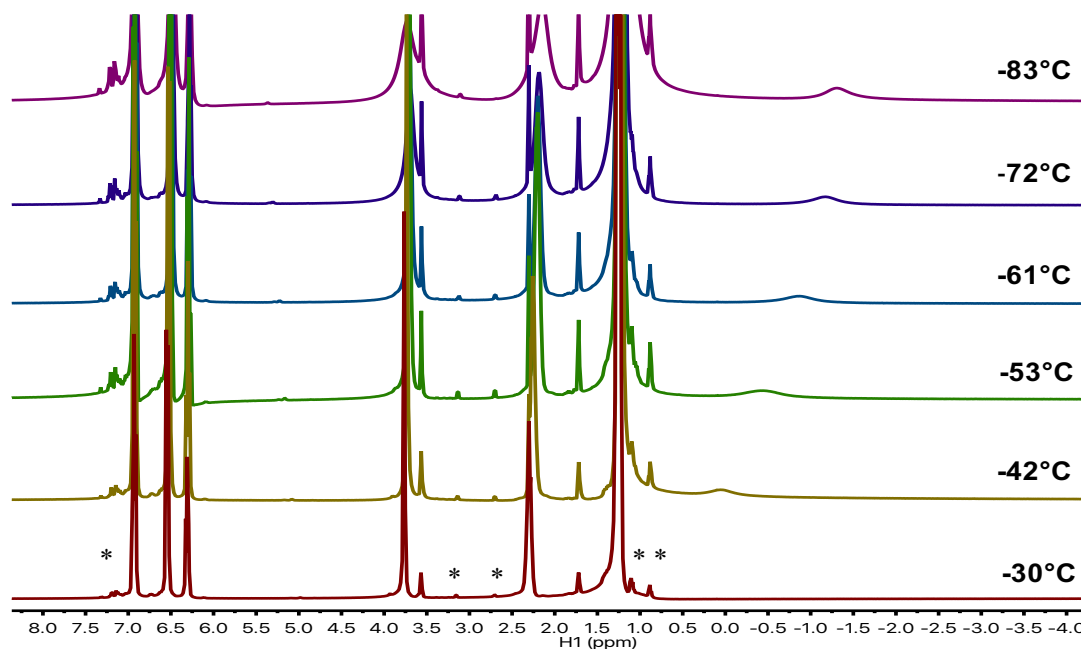


Figure S32. Variable temperature proton NMR of **3**-THF under 4 atm H_2 at rt (400 MHz, $\text{THF}-d_8$). Though the bound H_2 resonance is not visible at rt, appearing at -42°C , the bound H_2 resonance generally sharpens and shifts upfield upon cooling. Residual solvent peaks in spectra for toluene and THF are denoted with * in -30°C spectrum.

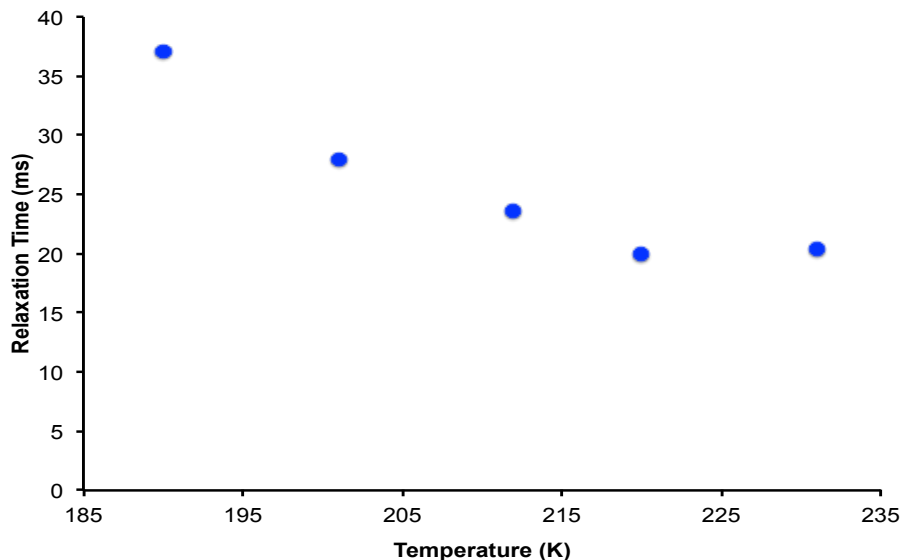


Figure S33. Plot of T_1 relaxation time of bound H_2 resonances of **3**-(H_2)THF at various temperatures from 243 K to 210 K (400 MHz, THF- d_8). T_1 values for **3**-(H_2)THF above 243 K could not be reliably obtained due to the broadness of the bound H_2 resonance at those temperatures.

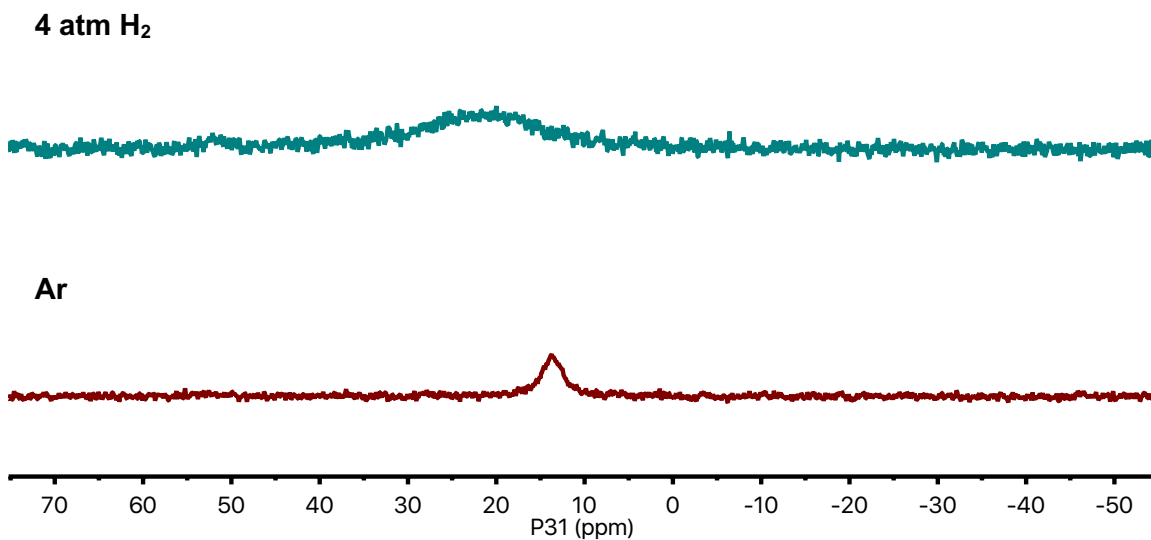


Figure S34. ^{31}P NMR overlay of **4** under Ar and 4 atm H_2 (at rt) cooled to 190 K (400 MHz, toluene- d_8). A bound H_2 ^{31}P resonance is not visible even at 190 K, though the broadness of the ^{31}P resonance at 4 atm indicates the binding of H_2 to **4** is very fluxional in this case.

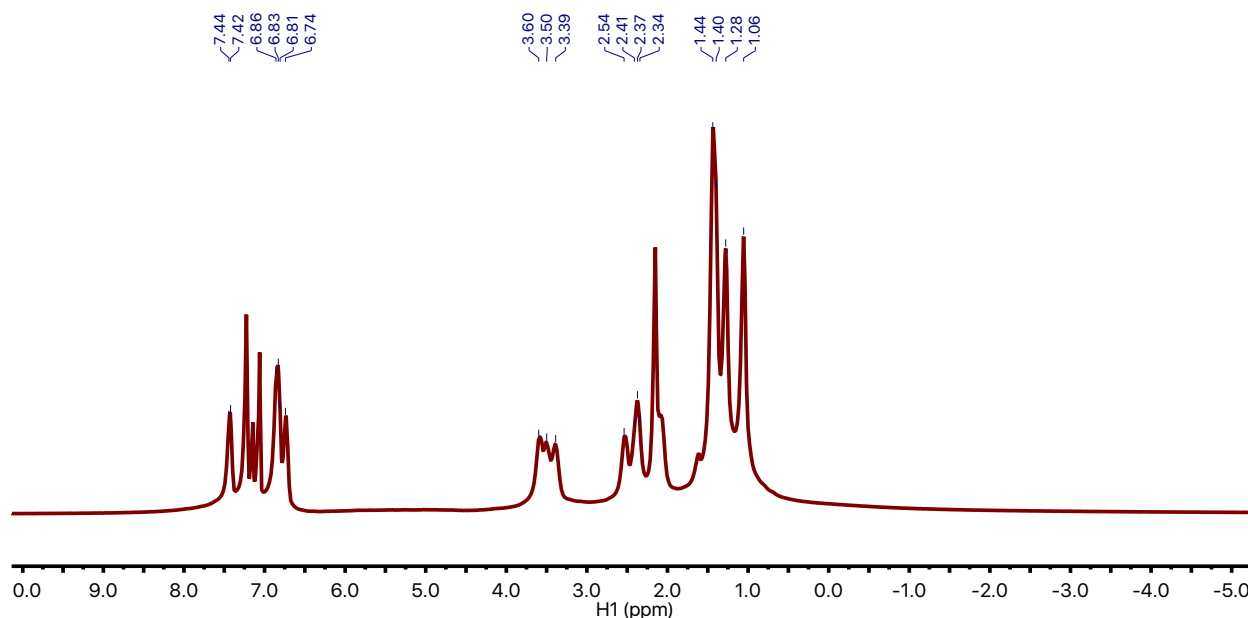


Figure S35. Proton $^1\text{H}\{^{31}\text{P}\}$ NMR spectrum of **4** under 4 atm H_2 (at rt) cooled to 190 K (400 MHz, toluene- d_8). Residual solvent peaks (benzene) are indicated by *. A bound H_2 resonance is not visible even at 190 K, though the absence of a free H_2 resonance indicates the binding of H_2 is very fluxional in this case. T_1 values could not be obtained due to the inability to observe a bound H_2 resonance at low temperatures.

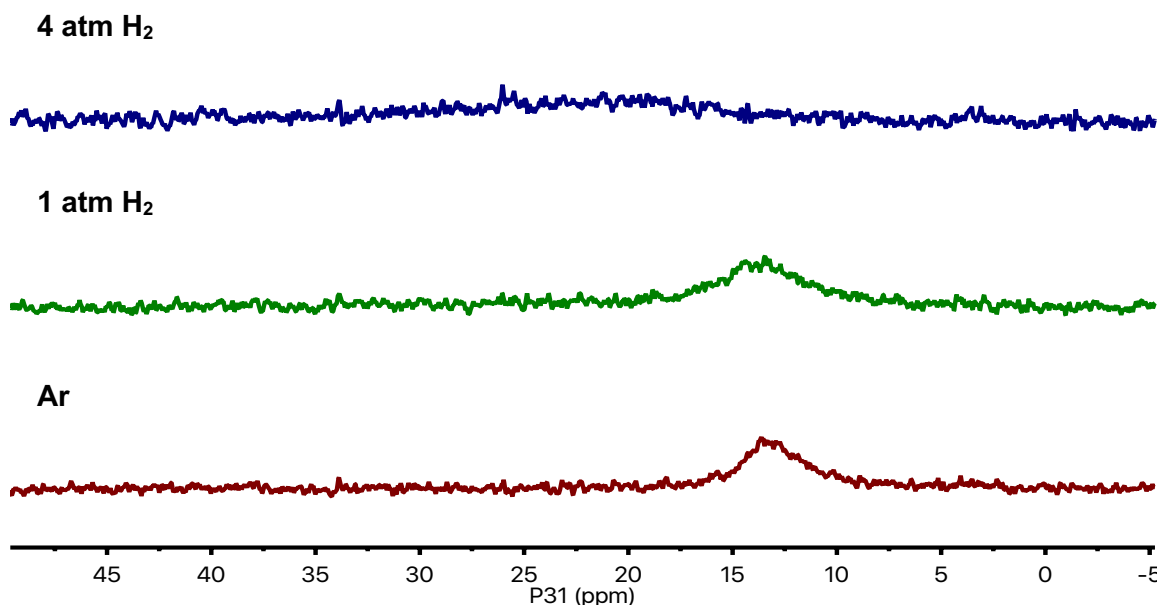


Figure S36. ^{31}P NMR overlay of **4** under Ar, 1 atm H_2 and 4 atm H_2 (at rt) cooled to 190 K (400 MHz, THF- d_8). A bound H_2 ^{31}P resonance is not visible even at 190 K, though the broadness of the ^{31}P resonance at 4 atm indicates the binding of H_2 to **4** is very fluxional in this case.

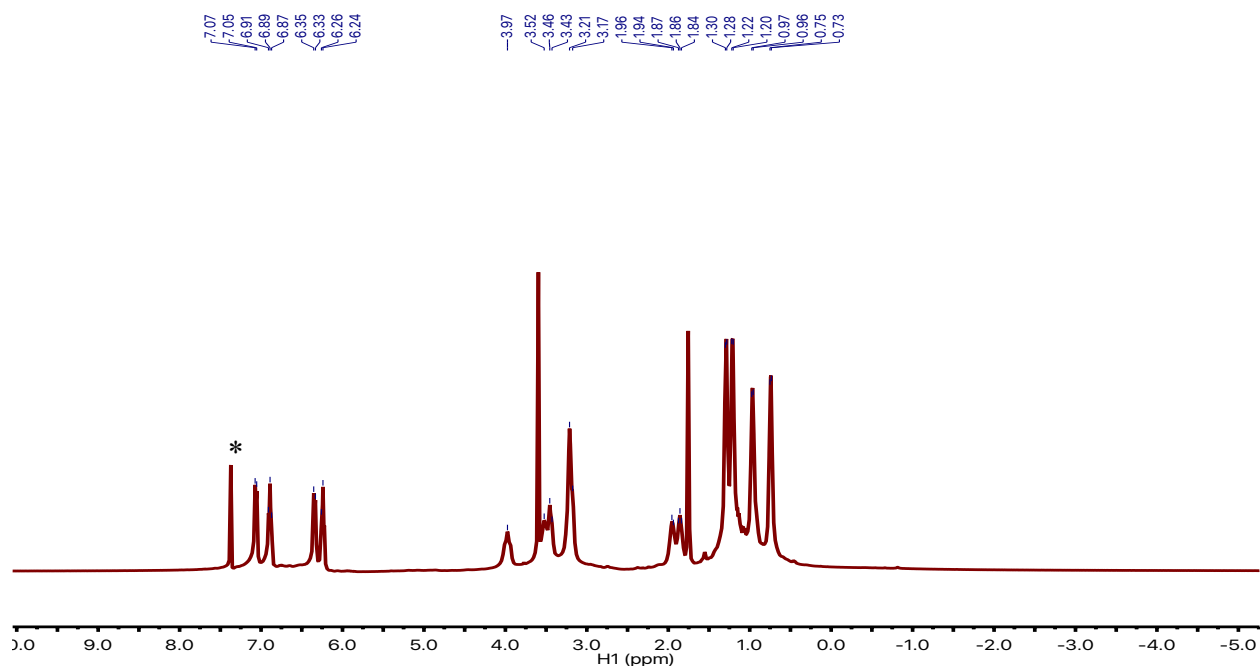


Figure S37. Proton $^1\text{H}\{^{31}\text{P}\}$ NMR spectrum of **4** under 4 atm H_2 (at rt) cooled to 190 K (400 MHz, $\text{THF}-d_8$). Residual solvent peaks (benzene) are indicated by *. A bound H_2 resonance is not visible even at 190 K, though the absence of a free H_2 resonance indicates the binding of H_2 is very fluxional in this case. T_1 values could not be obtained due to the inability to observe a bound H_2 resonance at low temperatures.

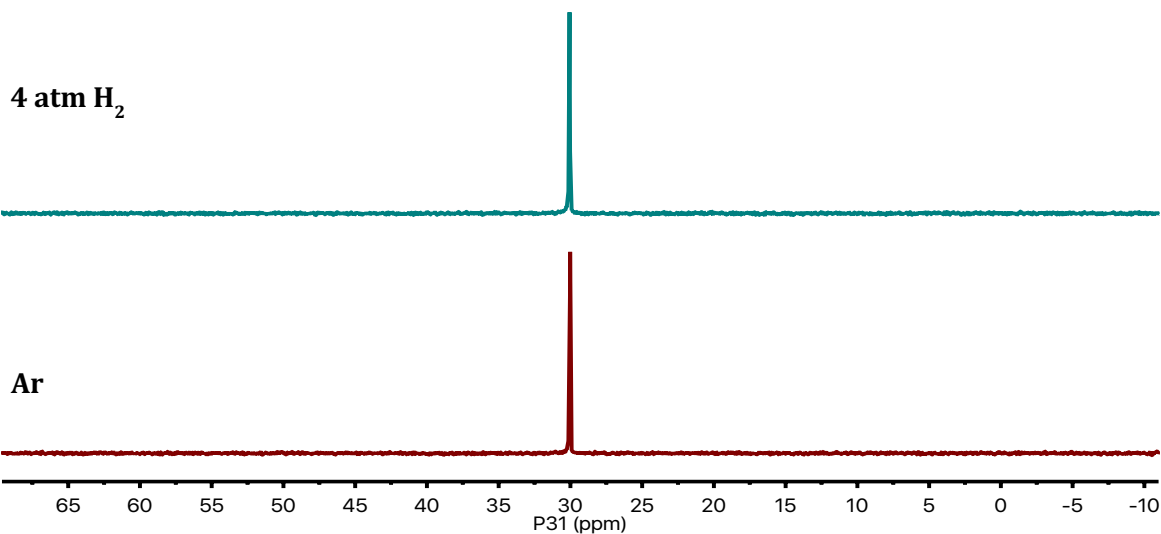


Figure S38. ^{31}P NMR overlay of $\text{Ni}(\text{N}(o\text{-(NHCH}_2\text{P}^i\text{Pr}_2)\text{C}_6\text{H}_4)_3)$ under Ar and 4 atm H_2 (at rt) cooled to 190 K (400 MHz, $\text{THF}-d_8$). With no change in the chemical shift upon cooling, a related trigonal monometallic $\text{Ni}(0)$ species $\text{Ni}(\text{N}(o\text{-(NHCH}_2\text{P}^i\text{Pr}_2)\text{C}_6\text{H}_4)_3)$ shows no indication of H_2 binding. This experiment highlights the importance of the presence of a supporting Lu^{III} ion in promoting the binding of H_2 at a $\text{Ni}(0)$ metal center in **3**, **3-THF** and **4**.

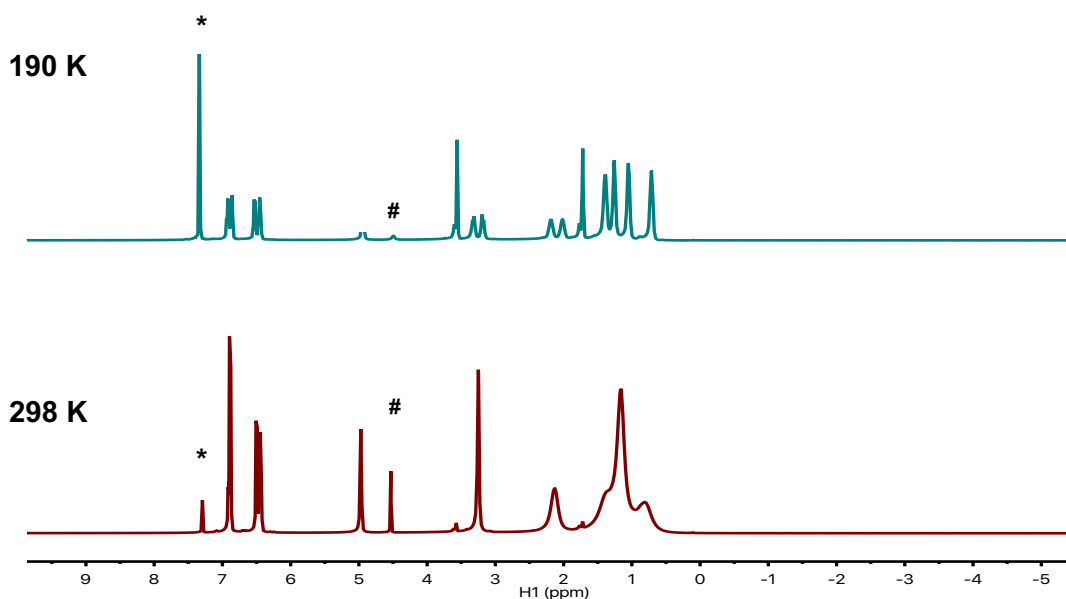


Figure S39. Proton $^1\text{H}\{^{31}\text{P}\}$ NMR spectrum of $\text{Ni}(\text{N}(o\text{-(NHCH}_2\text{P}^i\text{Pr}_2)\text{C}_6\text{H}_4)_3)$ under 4 atm H_2 at rt and cooled to 190 K (400 MHz, $\text{THF-}d_8$). Residual solvent peaks (benzene) are indicated by *. Free H_2 resonance indicated by #.⁴³ With no change in the chemical shift upon cooling, the a related trigonal monometallic $\text{Ni}(0)$ species $\text{Ni}(\text{N}(o\text{-(NHCH}_2\text{P}^i\text{Pr}_2)\text{C}_6\text{H}_4)_3)$ shows no indication of H_2 interaction. This experiment highlights the importance of the presence of a supporting Lu^{III} ion in promoting the binding of H_2 at a $\text{Ni}(0)$ metal center in **3**, **3-THF** and **4**.

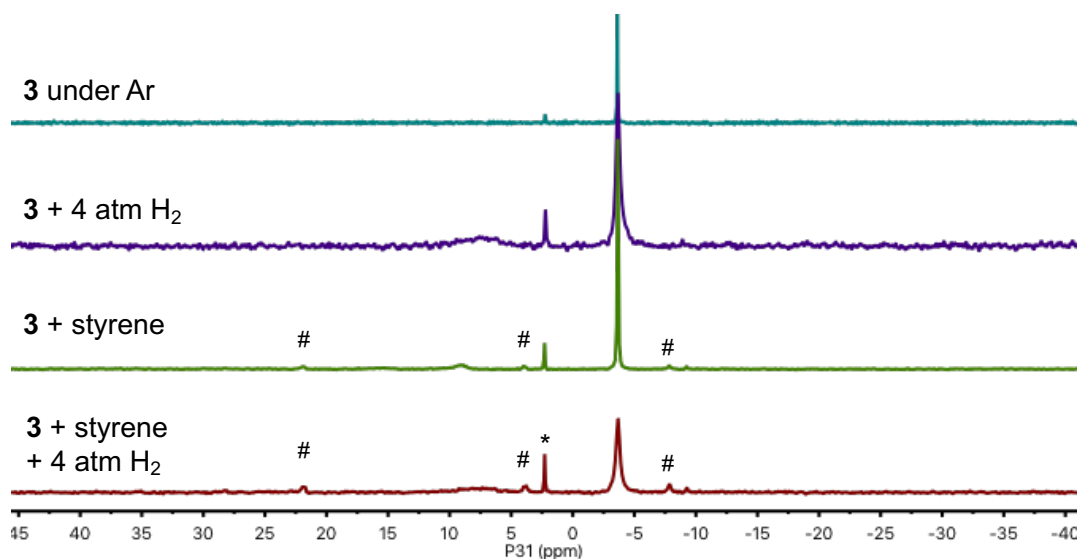


Figure S40. ^{31}P NMR overlay of **3** in presence of (red trace) 0.37 M styrene and (blue trace) 0.37 M styrene and 4 atm H_2 (at rt) cooled to 190 K (400 MHz, toluene- d_8). At these low temperatures, there is evidence for substrate binding between styrene and **3** as shown by new ^{31}P peaks being present in the catalytic mixture (denoted by #) which share similarities with that of **3** with only styrene in the mixture. Residual water in H_2 gas results in the formation of a small amount of $\text{Pr}_2\text{PCH}_2\text{NPh}$, denoted by *.

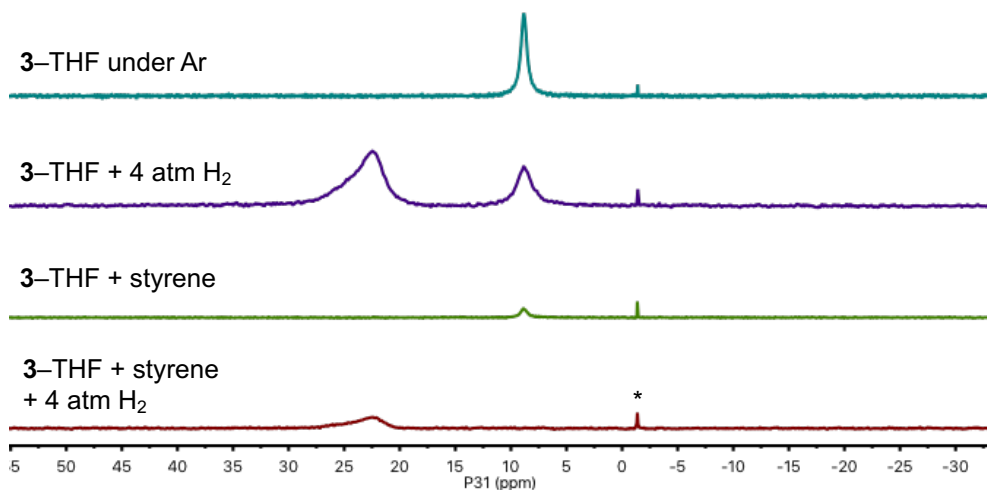


Figure S41. ^{31}P NMR overlay of **3**-THF in presence of (red trace) 0.37 M styrene and (blue trace) 0.37 M styrene and 4 atm H_2 (at rt) cooled to 190 K (400 MHz, $\text{THF-}d_8$). At these low temperatures, H_2 binding seems favored with no observable styrene binding. Residual water in H_2 gas results in the formation of a small amount of $\text{Pr}_2\text{PCH}_2\text{NHPh}$, denoted by *.

Electrochemical Studies

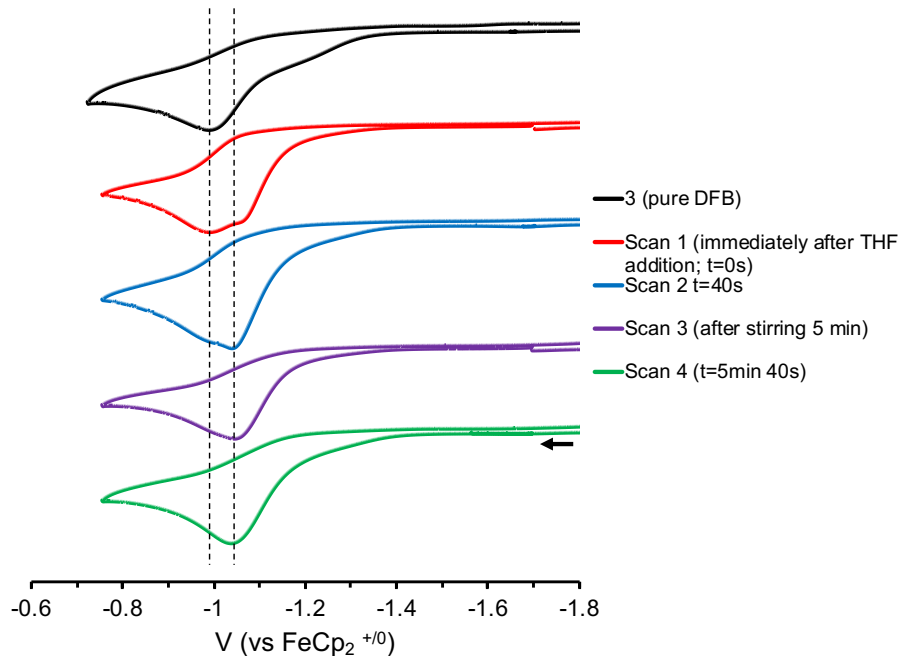


Figure S42. Stacked cyclic voltammograms of the *in situ* generation of **3**-THF prepared by the addition of 320 equiv THF to a solution of **3** in 0.1M [ⁿPr₄N][BAR^F₄] in difluorobenzene with FeCp₂ as an internal reference. The dotted lines represent the E_{pa} values for **3** (-1.00 V) and **3**-THF (-1.05 V). (scan rate of 100 mV/s; collected under Ar)

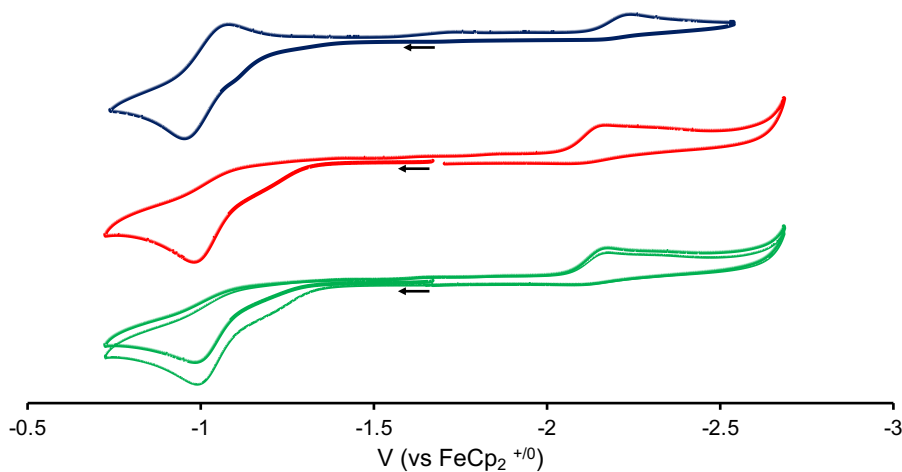


Figure S43. Overlay of cyclic voltammograms of **3** under varying electrolyte conditions (blue: 0.1 M [ⁿPr₄N][BAR^F₄] in THF; blue and green: 0.1 M [ⁿPr₄N][BAR^F₄] in difluorobenzene). Of note, when the applied voltage does exceed ca. -0.75 V, then the oxidative process for **3** is stable over multiple scans (green trace). (scan rate of 100 or 250 mV/s; collected under Ar)

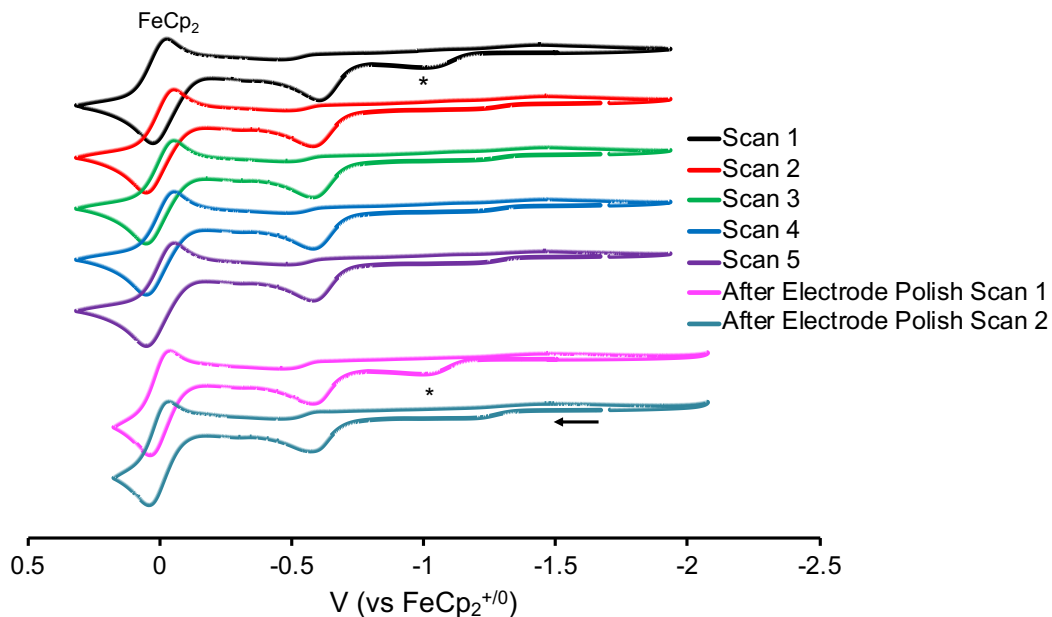


Figure S44. Stacked CVs of **3** in 0.1 M [$n\text{Pr}_4\text{N}$][BAr^{F_4}] in DFB with FeCp_2 as an internal reference. In the experiment, 5 continuous scans were performed, and then the electrode was polished and the original sample of **3** was remeasured in two consecutive scans. The asterisk marks the first oxidative process. (scan rate of 100 mV/s; collected under Ar)

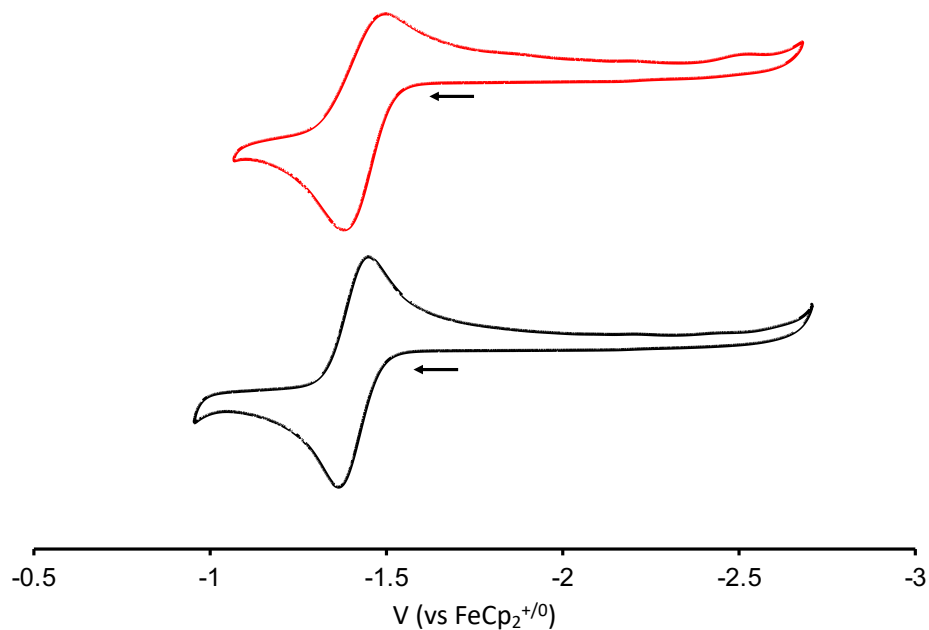


Figure S45. Overlay of cyclic voltammograms of **4** under varying electrolyte conditions (red: 0.1 M [Pr_4N][BAr^{F_4}] in THF; black: 0.1 M [$n\text{Pr}_4\text{N}$][BAr^{F_4}] in difluorobenzene). (scan rate of 100 mV/s; collected under Ar)

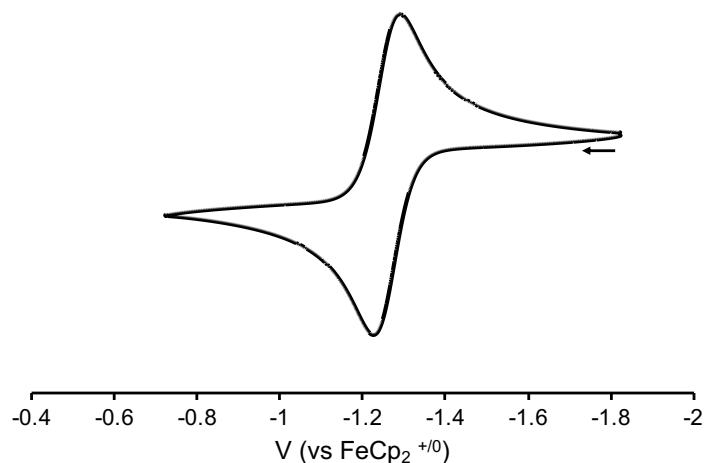


Figure S46. Cyclic voltammogram of $\text{Ni}\{\text{N}(o\text{-(NCH}_2\text{P}^i\text{Pr}_2)\text{C}_6\text{H}_4)_3\}$ in 0.1 M $[\text{nPr}_4\text{N}][\text{BAr}^{\text{F}}_4]$ in difluorobenzene. (scan rate of 100 mV/s; collected under Ar)

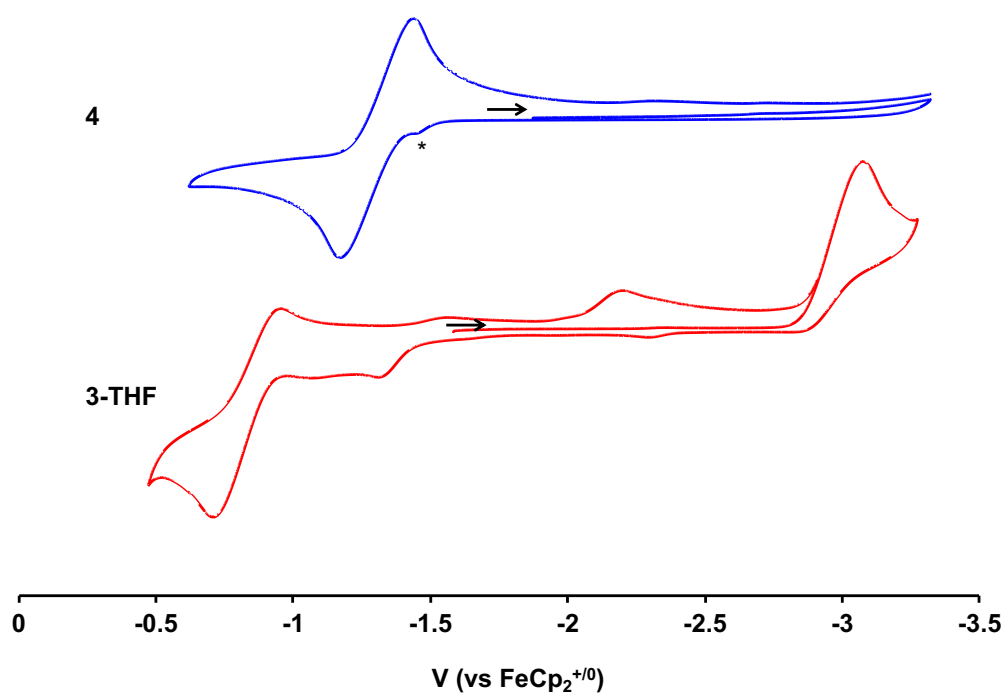


Figure S47. Comparative cyclic voltammograms of **3**-THF and **4** with 0.1 M $[\text{nBu}_4\text{N}][\text{PF}_6]$ electrolyte in THF (scan rate of 250 mV/s; collected under Ar). With a widened reduction window, complex **3**-THF shows the presence of a reduction event at $E_{\text{pc}} \sim -3$ V. In contrast, no such event can be observed in **4**.

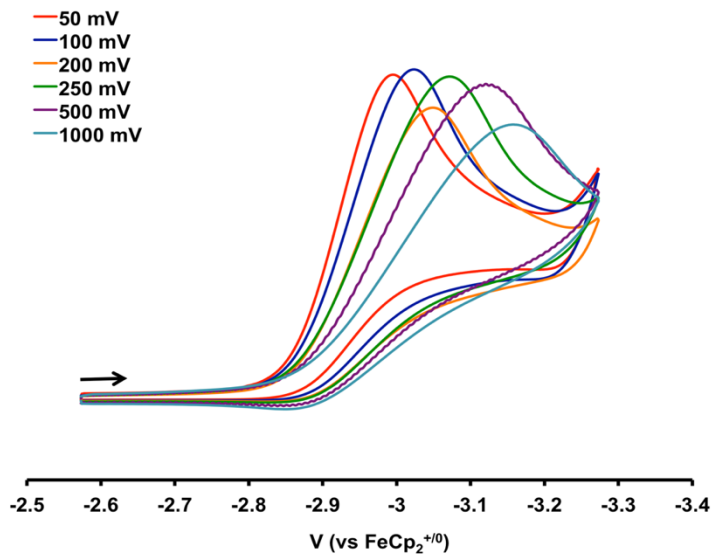


Figure S48. Cyclic voltammogram study of **3**-THF showing there is no scan rate dependence between 50 – 1000 mV/s (0.1 M [ⁿBu₄N][PF₆] in THF). The current values were normalized by dividing the measured current by the square root of the scan speed. (collected under Ar)

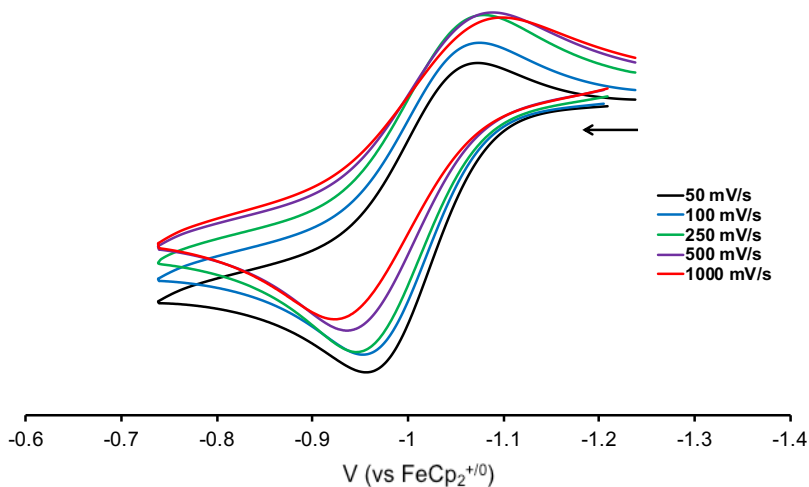


Figure S49. Cyclic voltammogram study of **3**-THF demonstrating a scan rate dependence between 50 – 1000 mV/s (0.1 M [ⁿPr₄N][BAr^F₄] in THF). The current values were normalized by dividing the measured current by the square root of the scan speed. (collected under Ar)

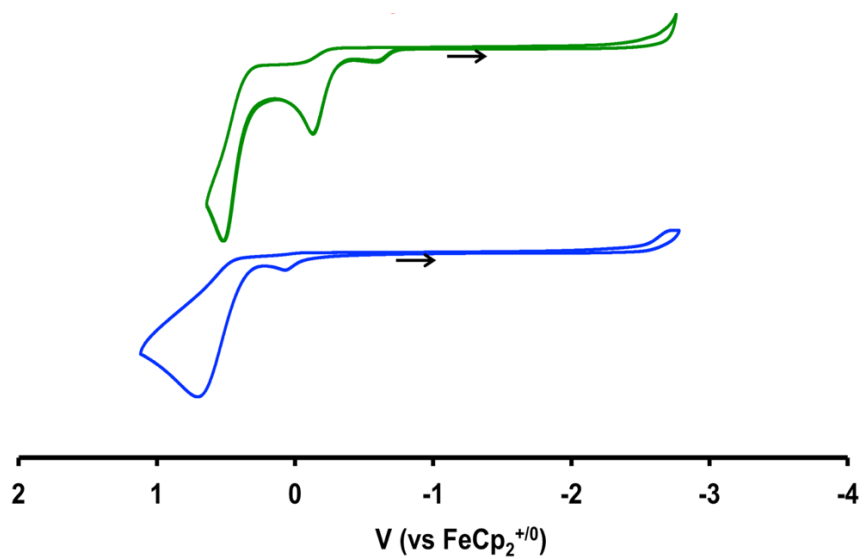


Figure S50. Cyclic voltammograms of $i\text{Pr}_2\text{PCH}_2\text{NKPh}$ (blue) and **1** (green) in 0.1 M $[\text{nPr}_4\text{N}][\text{BARF}_4]$ in THF. (scan rate of 100 mV/s; collected under Ar)

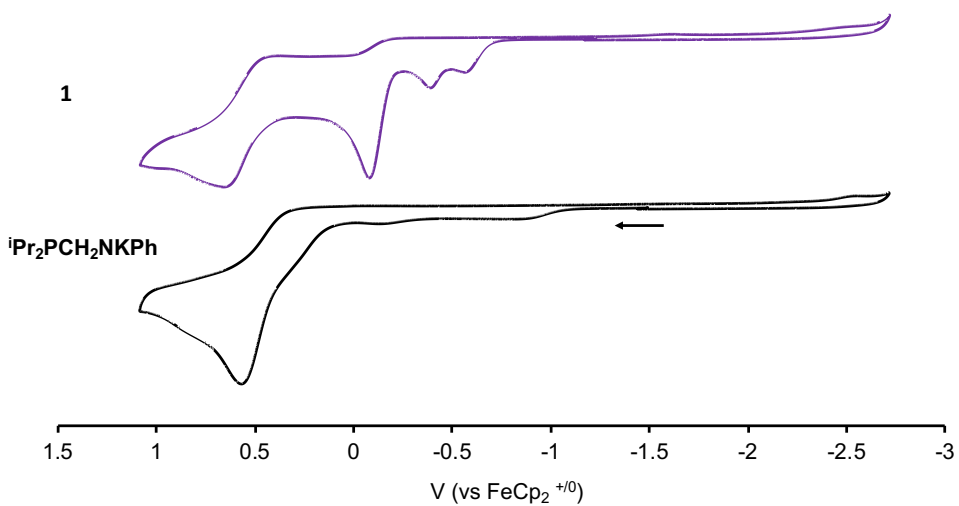


Figure S51. Full window cyclic voltammograms of $i\text{Pr}_2\text{PCH}_2\text{NKPh}$ (black), and **1** (purple), in 0.1 M $[\text{nPr}_4\text{N}][\text{BARF}_4]$ in difluorobenzene. (scan rate of 100 mV/s; collected under Ar)

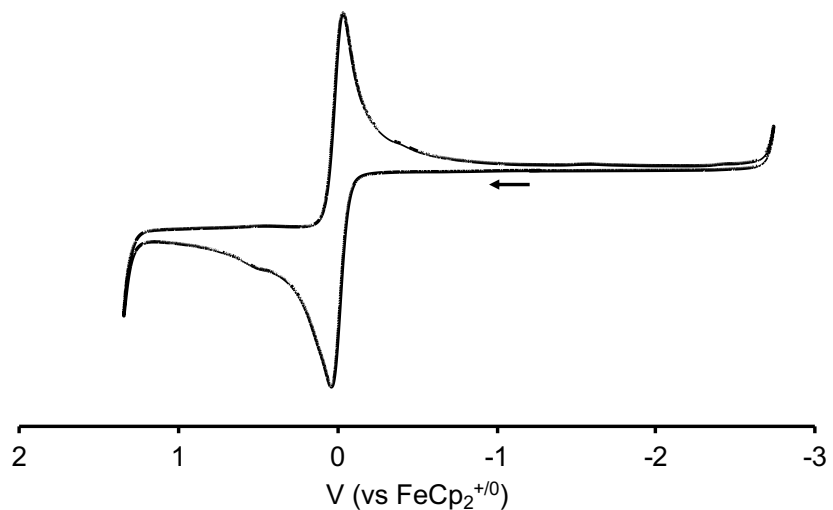


Figure S52. Cyclic voltammogram of difluorobenzene solvent window (1.3 to -2.8 V) with 0.1 M $[\text{Pr}_4\text{N}][\text{BAr}^{\text{F}}_4]$ electrolyte with reference to the internal standard $\text{FeCp}_2^{+/0}$. (scan rate of 100 mV/s; collected under Ar) Of note, a literature value of +2.0 V to -2.2 V vs SSCE for the solvent window of difluorobenzene have been previously reported by Sullivan and Meyer employing a Pt electrode in 0.1 M solutions of tetraalkylammonium salts of the anions ClO_4^- , BF_4^- , and PF_6^- .⁴⁵

UV-Visible Spectroscopy

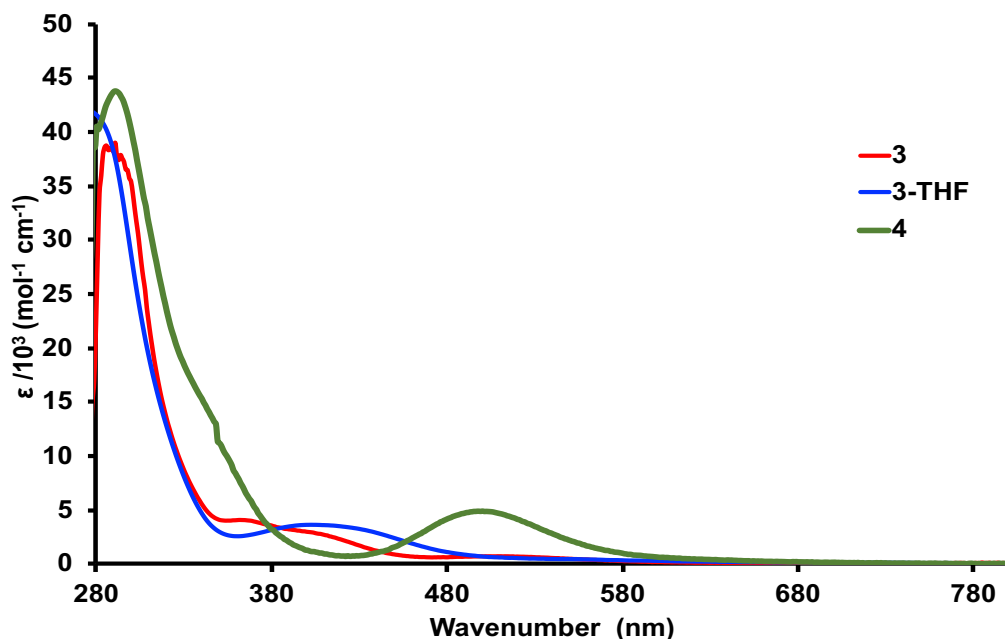


Figure S48. Expanded UV-Vis spectra of complexes **3** (red) and **4** (green) in DFB and **3**-THF (blue) in THF at 298 K.

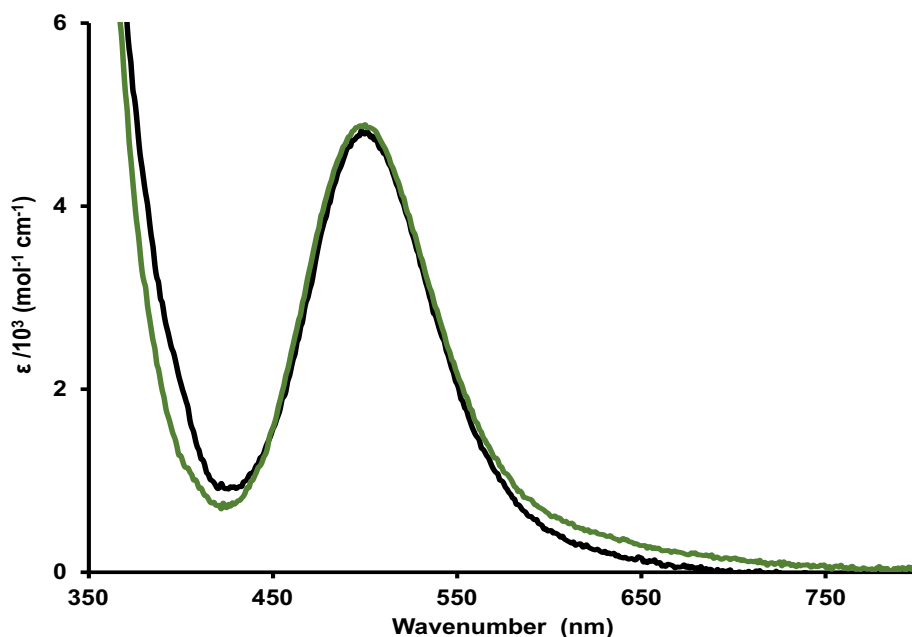


Figure S49. UV-Visible spectra of **4** in DFB (green) and in THF (black) at 298 K (0.019 mM). The spectra serve as a control for possible solvent effects resulting from dielectric constant differences between difluorobenzene and THF on the resulting UV-Visible spectrum. Any possible solvent effects resulting from dielectric constant differences are minimal and do not impact the wavenumber of a transition observed if there is no solvent binding in the complex.

Table S3. UV-Vis Model Parameters
0.025 mM UV-VIS MODEL PARAMETERS

PEAK	Energy (cm ⁻¹)	nm	ϵ (M ⁻¹ cm ⁻¹)	eV	Amplitude
1	18908	528.9		2.3443	0.01753
2	33703	296.7		4.1786	0.1189
3	35319	283.1		4.379	1.022
4	24651	405.7		3.0563	0.08322
5	22196	450.5		2.7519	0.04327
0.103 mM UV-VIS MODEL PARAMETERS					
0.103 mM	Energy (cm ⁻¹)	nm	ϵ (M ⁻¹ cm ⁻¹)	eV	Amplitude
1	18242	548.19	345.34	2.2617	0.03557
2	22425	450.54	707.48	2.7519	0.07287
3	24558	407.2	3312.62	3.0448	0.3412

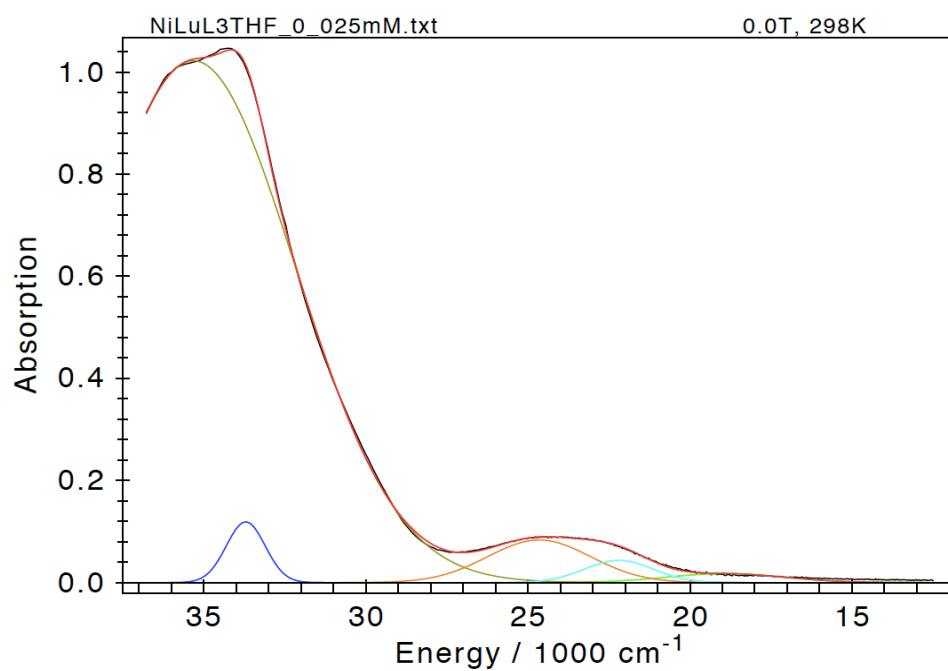


Figure S50. UV–Visible spectrum of **3**–THF (black trace) and the modeled spectrum (red trace) (0.025mM in THF).

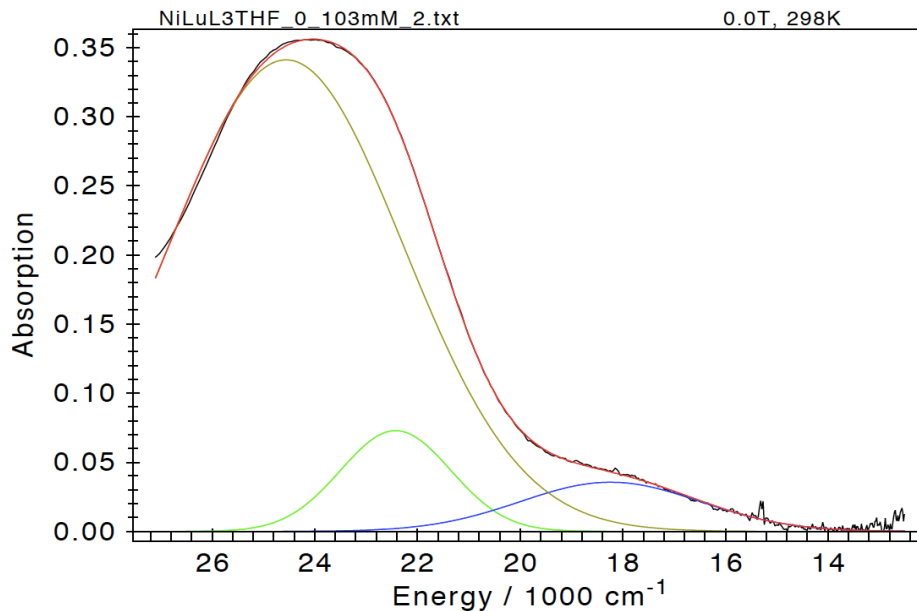


Figure S51. UV–Visible spectrum of **3**–THF (black trace) and the modeled spectrum (red trace) (0.103 mM in THF).

Catalysis Tables

Table S4. Hydrogenation of Styrene to Ethylbenzene Mediated by 1–4^a

entry	catalyst	T (°C)	% conversion	overall rate (h ⁻¹)
1	1	100	<1 ^c	0
2	2	100	<1 ^c	0
3	3	100	94(4) ^c	18.8(9)
4	4	100	24(3) ^c	4.7(2)
5	3	63	>99 ^d	4.1(1)
6 ^b	3 –THF	63	35(2) ^d	1.4(1)

^aCatalytic conditions: 2.5 mol % catalyst, 0.37 M olefin in ca. 600 μ L of *d*₈-toluene, 4 atm H₂. Conversion are based on triplicate runs using ¹H NMR integration. ^bIn ca. 600 μ L of *d*₈-THF. ^c*t* = 2 h. ^d*t* = 10 h.

Table S5. Substrate Scope for Olefin Hydrogenation for 3^a

entry	substrate	conversion (%) ^b	time to >90% conversion (h) ^b
1	styrene	>99	2 h
2	1-octene	>99	<1 h
3	<i>cis</i> -cyclooctene	>99	1.5 h
4	allylbenzene	>99	2 h
5	<i>trans</i> -2-octene	68 ^c	-
6	<i>trans</i> -4-octene	<1	-
7	<i>cis</i> -stilbene	>99 (93:7 <i>trans</i> :bibenzyl)	6 h
8	<i>trans</i> -stilbene	2 (bibenzyl product only)	-

^aSee Table 2 for catalytic conditions. ^b if >90% conversion not reached reaction was stopped at 24 h. ^cTrace isomerization products were observed.

Table S6. Optimization Conditions for 3^a

Entry	Loading (mol %)	Solvent	T (°C)	P H ₂ (atm) ^b	Time to >90% Conversion (h)	Conversion (%)	Overall rate (h ⁻¹)
1	10	THF	20	1	-	-	-
2	10	toluene	63	1	7	>99	1.4
3	2.5	toluene	100	4	2	94	18.8
4	2.5	toluene	63	4	10	>99	4.1
5	5	toluene	63	4	5.75	>99	3.5
6	5	toluene	100	4	1.5	99	13.3

^aConversion are based on single runs using ¹H NMR integration. ^bPressure at room temperature

Computational Details

Table S7. Calculated bond lengths (Å) and angles for **4** with different functionals and mean unsigned error(MUE) with respect the crystal structure.

	Exp.	PBE	PBE-D3	PBE0	PBE0D3	B3LYP-D3	B97-D3	M06L	B3P86	B3PW91
Lu-Ni	2.977	3.03	2.97	3.03	2.97	2.96	2.96	2.94	3.05	3.07
Ni-P1	2.156	2.18	2.17	2.17	2.16	2.16	2.16	2.17	2.17	2.18
Ni-P2	2.158	2.19	2.18	2.18	2.17	2.18	2.18	2.18	2.18	2.19
Ni-P3	2.163	2.22	2.21	2.21	2.20	2.20	2.21	2.21	2.21	2.22
Avg Lu-tacn	2.562	2.60	2.59	2.57	2.58	2.58	2.58	2.58	2.57	2.59
Avg Lu-amide	2.309	2.30	2.29	2.28	2.28	2.29	2.29	2.29	2.28	2.29
Total angle-N	348.7	349.0	350.5	348.8	350.3	350.5	350.7	351.3	348.1	347.8
Total angle-P	358.9	359.9	360.0	359.8	359.9	359.9	359.9	359.9	359.9	359.9
FSR	1.10	1.12	1.10	1.12	1.10	1.09	1.09	1.09	1.13	1.13
MUE (M-L)		0.03	0.02	0.03	0.02	0.02	0.02	0.02	0.02	0.03
MUE (MM)		0.06	0.00	0.05	0.00	0.02	0.01	0.04	0.07	0.09
MUE (Total)		0.03	0.02	0.03	0.02	0.02	0.02	0.02	0.03	0.04

Note: MUE (Total) is mean unsigned error over M-L and MM

Table S8. Calculated charges at the metal centers of the ground spin state.

3	Lu		Ni	
	Mulliken	LoProp	Mulliken	LoProp
CASSCF	2.45	1.00	-0.18	0.22
DFT	1.14	N/A	-0.22	N/A
3-THF	Lu		Ni	
	Mulliken	LoProp	Mulliken	LoProp
CASSCF	2.64	1.06	-0.16	0.20
DFT	1.05	N/A	-0.25	N/A
4	Lu		Ni	
	Mulliken	LoProp	Mulliken	LoProp
CASSCF	2.54	1.03	-0.22	0.19
DFT	1.27	N/A	-0.14	N/A

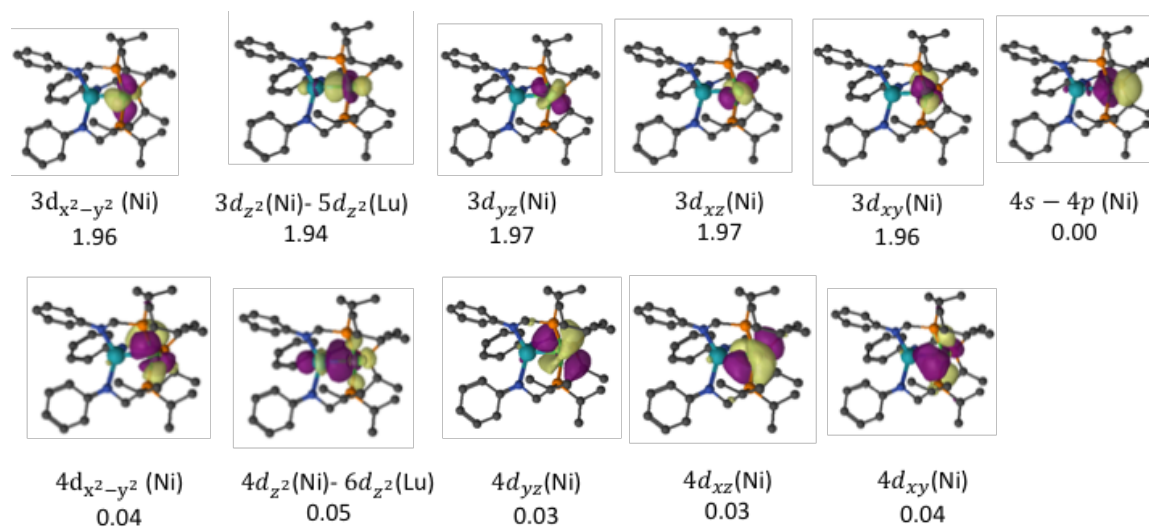


Figure S52. Figure showing the natural orbitals for **3** resulting from CASSCF calculations. The complete active space of 10 electrons in 11 orbitals is shown, with the occupancies of the MOs.

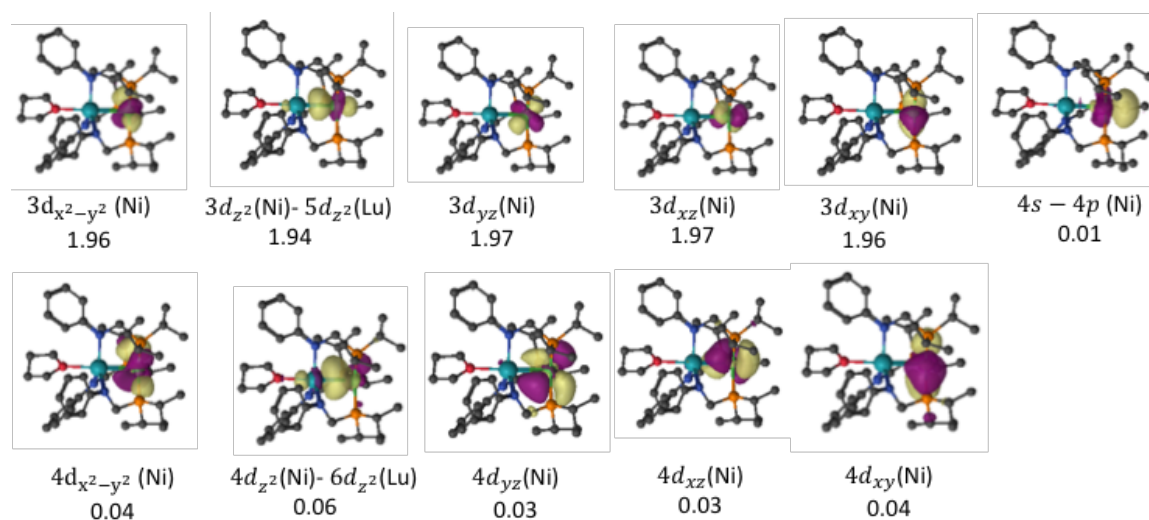


Figure S53. Figure showing the natural orbitals for **3-THF** resulting from CASSCF calculations. The complete active space of 10 electrons in 11 orbitals is shown, with the occupancies of the MOs.

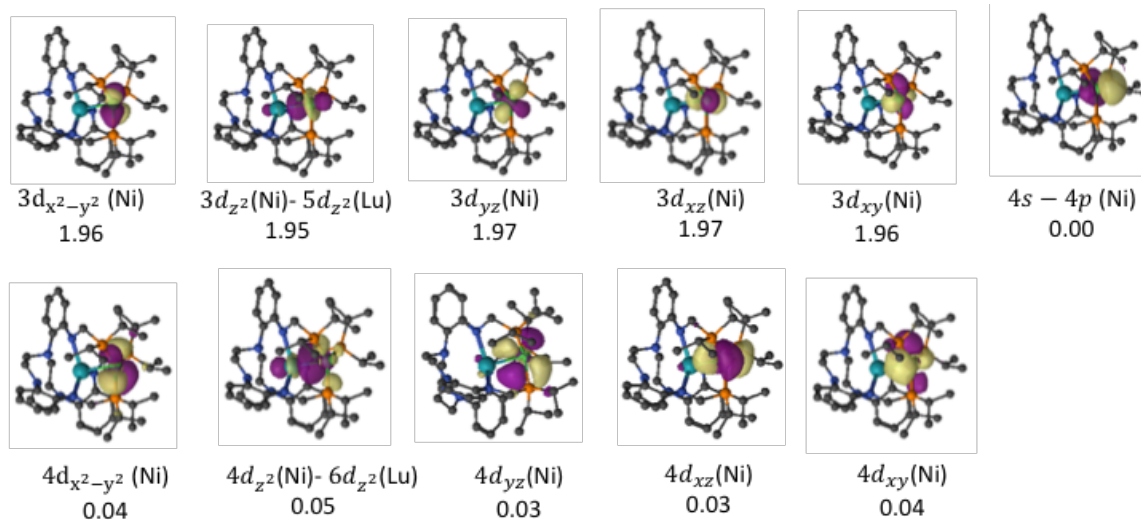


Figure S54. Figure showing the natural orbitals for **4** resulting from CASSCF calculations. The complete active space of 10 electrons in 11 orbitals is shown, with the occupancies of the MOs.

Table S9. Percentage of Metal Character (% Lu and %Ni) in Ni-Lu Bonding Orbitals From CASSCF Calculations at DFT-Optimized Geometries (PBE-D3)

Complex	Orbital	% Ni	% Lu	total electrons	Electron Ni	Electron Lu
3	$3d_{z^2}(\text{Ni})-5d_{z^2}(\text{Lu})$	90.66	9.33	1.94	1.76	0.18
	$4d_{z^2}(\text{Ni})-6d_{z^2}(\text{Lu})$	43.60	32.76	0.06	0.03	0.02
3-THF	$3d_{z^2}(\text{Ni})-5d_{z^2}(\text{Lu})$	90.36	8.50	1.94	1.75	0.17
	$4d_{z^2}(\text{Ni})-6d_{z^2}(\text{Lu})$	42.38	31.38	0.06	0.03	0.02
4	$3d_{z^2}(\text{Ni})-5d_{z^2}(\text{Lu})$	94.05	5.95	1.95	1.83	0.12
	$4d_{z^2}(\text{Ni})-6d_{z^2}(\text{Lu})$	52.42	26.17	0.05	0.03	0.01

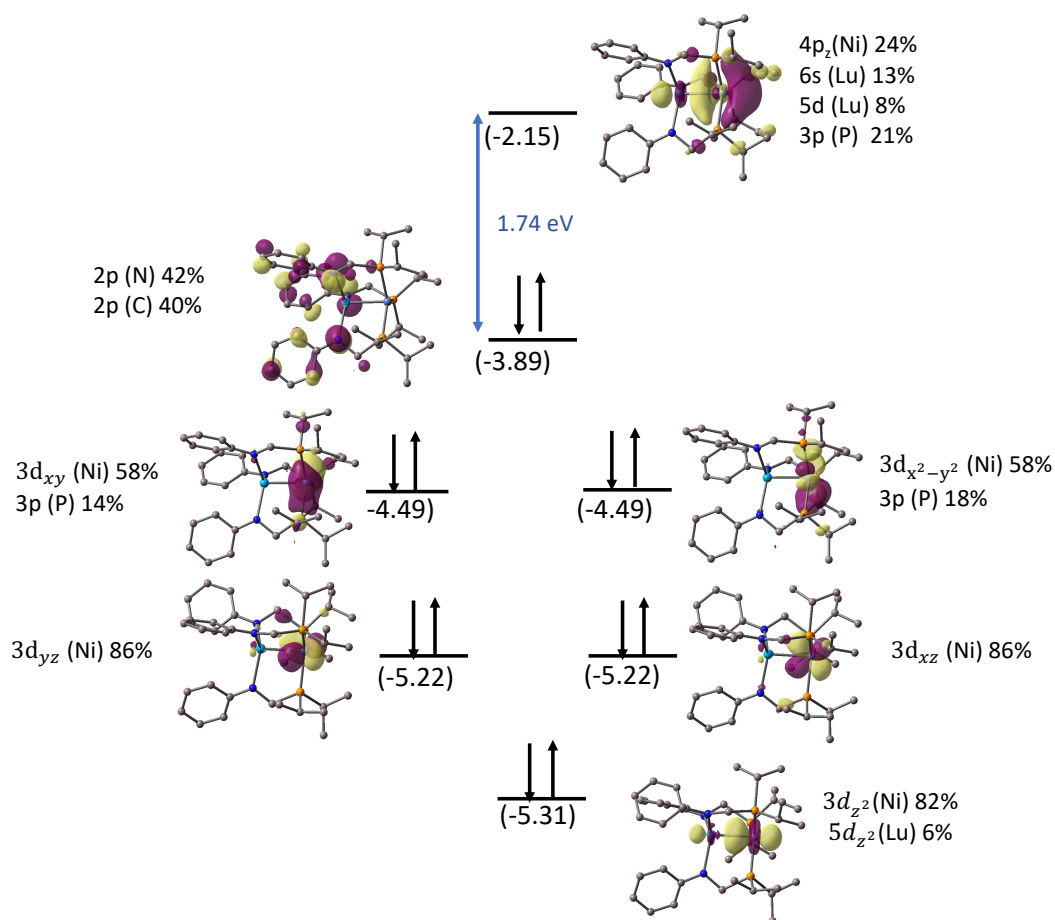


Figure S55. 3d orbital splitting (Ni) for **3** as predicted by DFT calculations.

Table S10. Frontier molecular orbitals and the orbital energies for **3** calculated using DFT calculations.

Orbital	Orbital Character	Energy (eV)
LUMO	Ligand*	-2.15
HOMO	Ligand	-3.89
HOMO-3	$3d_{xy}$ (Ni), $3d_{x^2-y^2}$ (Ni)	-4.49
HOMO-5	$3d_{xz}$ (Ni), $3d_{yz}$ (Ni)	-5.22
HOMO-7	$3d_{z^2}$ (Ni)	-5.31

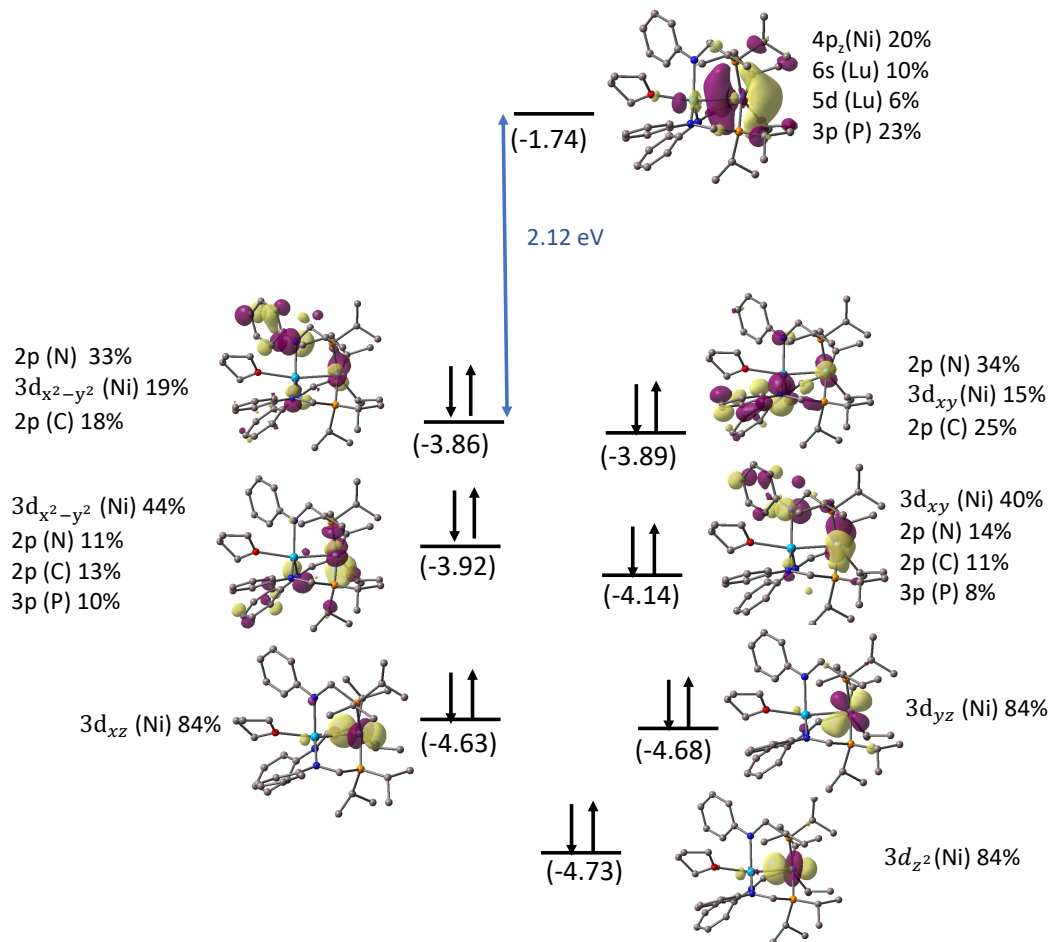


Figure S56. 3d orbital splitting of Ni for 3-THF as predicted by DFT calculations.

Table S11. Frontier molecular orbitals and the orbital energies for 3-THF calculated using DFT calculations.

Orbital	Orbital Character	Energy (eV)
LUMO	Ligand*	-1.74
HOMO	Ligand-Ni	-3.86
HOMO-2	Ligand-Ni	-3.89
HOMO-3	3d _{x²-y²} (Ni)	-3.92
HOMO-4	3d _{xy} (Ni)	-4.14
HOMO-5	3d _{xz} (Ni)	-4.63
HOMO-6	3d _{yz} (Ni)	-4.68
HOMO-7	3d _{z²} (Ni)	-4.73

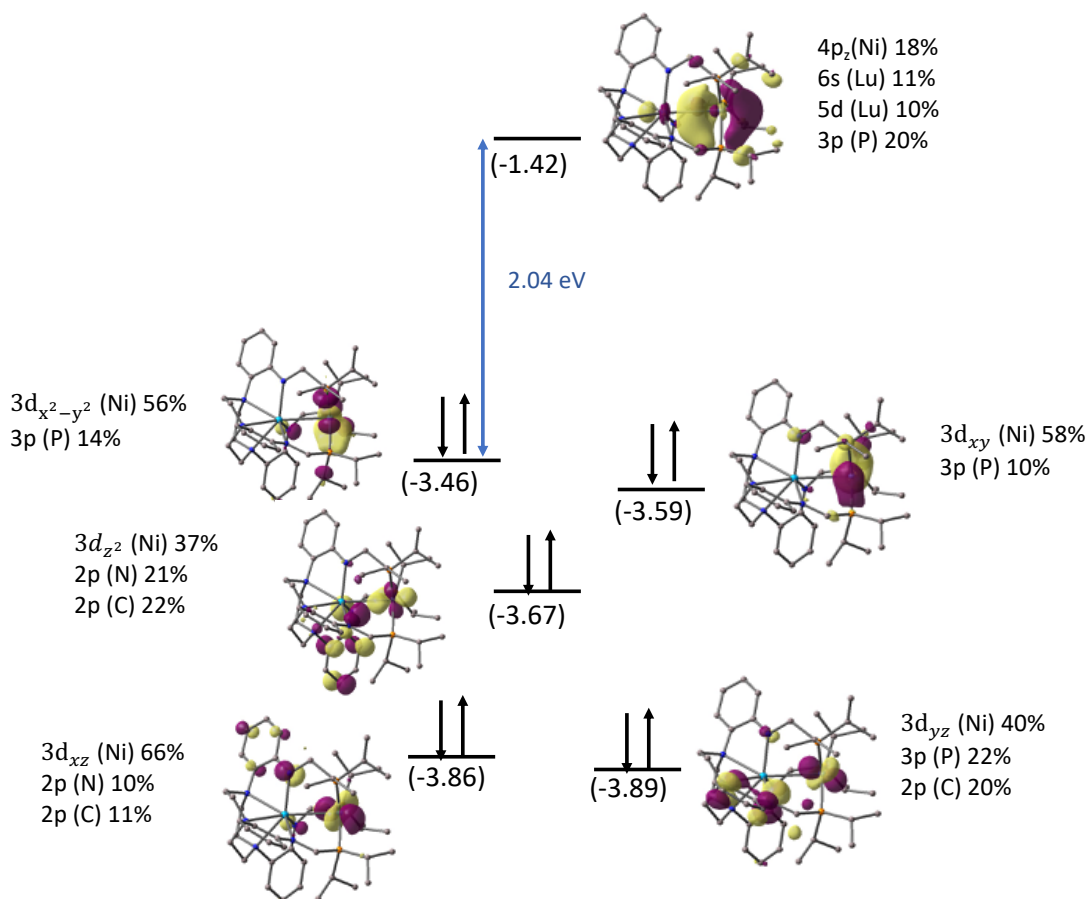


Figure S57. 3d orbital splitting of Ni for **4** as predicted by DFT calculations.

Table S12. Frontier molecular orbitals and the orbital energies for **4** calculated using DFT calculations.

Orbital	Orbital Character	Energy (eV)
LUMO	Ligand*	-1.42
HOMO	$3d_{x^2-y^2}$ (Ni)	-3.46
HOMO-1	$3d_{xy}$ (Ni)	-3.59
HOMO-2	$3d_{z^2}$ (Ni)	-3.67
HOMO-3	$3d_{xz}$ (Ni)	-3.86
HOMO-4	$3d_{yz}$ (Ni)	-3.89

Table S13. Compositions of LUMO from the DFT calculations

Complex	Ni	Lu	three P
3	24 % (4pz)	21 % (6s 13%, 5d 8%)	21 % (3p)
3-THF	20 % (4pz)	16% (6s 10%, 5d 6%)	23 % (3p)
4	18 % (4pz)	21 % (6s 11%, 5d 10%)	20 % (3p)

Table S14. Absolute DFT and CASSCF energies in atomic units

Complex	DFT	CASSCF
3	-5453.747075	-18768.445718
3–THF	-5685.852714	-19000.678130
4	-5851.494687	-19165.433623

Cartesian coordinates of the optimized geometries of bimetallic systems **3**, **3–THF**, and **4**.

➤ Cartesian coordinate of **3** species. Units are presented in Å.

○ Singlet, charge=0

Lu	0.71058000	0.06993000	0.06672600	H	-1.94102000	1.13186000	-5.04080400
Ni	-1.74735500	0.09284800	-0.17076800	H	-3.17926600	1.63095100	-3.85019500
P	-1.83336400	0.15059600	2.06604500	H	-2.23220000	0.13948500	-3.57727700
P	-1.40713300	1.96030700	-1.35553200	C	0.31572800	1.44846800	-3.53427100
P	-1.42379300	-1.93782400	-1.06499500	H	0.45493000	0.39769400	-3.21682200
N	0.69877100	-0.91613400	2.04580400	H	1.11375600	2.03577700	-3.03977200
N	1.04021500	2.24191100	-0.17667500	H	0.49285700	1.49705800	-4.62842200
N	1.17469300	-1.28203100	-1.61468500	C	-0.00397100	3.05335600	-0.77108600
C	-3.35834900	-0.74294700	2.71875900	H	0.34656500	3.66304100	-1.64019400
H	-3.08004100	-1.79715400	2.51020200	H	-0.43933800	3.78462600	-0.04180400
C	-4.60685000	-0.42832000	1.88585900	C	2.15870000	2.89573500	0.31331600
H	-5.45426200	-1.07912100	2.18805000	C	3.11718100	2.14421900	1.06066200
H	-4.41766500	-0.60128100	0.80671400	H	2.93682000	1.07481700	1.28719400
H	-4.93870200	0.62263300	2.00407500	C	4.28097600	2.72782700	1.56497300
C	-3.60506600	-0.61718500	4.22650300	H	4.98956800	2.10549900	2.13369200
H	-3.93060900	0.40333500	4.51264500	C	4.53831800	4.09814600	1.36508100
H	-2.70496100	-0.86756100	4.82315800	H	5.45281500	4.56064200	1.76475400
H	-4.41189400	-1.31361900	4.53852100	C	3.59702400	4.86146900	0.65826100
C	-0.46981400	-0.83152700	2.89808200	H	3.77341600	5.93775400	0.50015600
H	-0.26347000	-0.35387100	3.88753400	C	2.42638200	4.28278900	0.14246500
H	-0.88936900	-1.84338100	3.13336700	H	1.71691500	4.91519600	-0.40962100
C	1.78760800	-1.62298300	2.53864400	C	0.07206800	-2.03758100	-2.17493500
C	1.89982000	-2.10937700	3.87132300	H	0.31850300	-3.10969600	-2.35271600
H	1.08347500	-1.94603600	4.58879000	H	-0.25941200	-1.63262800	-3.16634600
C	3.05364700	-2.78682300	4.29730400	C	2.37394900	-1.30645600	-2.31318400
H	3.10788300	-3.14323800	5.33873900	C	3.44235000	-0.46683800	-1.87558000
C	4.13042800	-3.01272800	3.42671200	H	3.30068600	0.21279700	-1.01496800
H	5.03078900	-3.54282300	3.77087600	C	4.67770900	-0.44776300	-2.52587700
C	4.02697700	-2.56128200	2.09672100	H	5.46942700	0.21924300	-2.15016800
H	4.84324000	-2.74542300	1.38058400	C	4.90635400	-1.25860400	-3.65440800
C	2.87990500	-1.89522800	1.65969800	H	5.87870200	-1.24311300	-4.16855300
H	2.80991600	-1.62476300	0.59001000	C	3.86326400	-2.07566800	-4.11466000
C	-1.75609900	1.72442300	3.09082000	H	4.01578400	-2.71058500	-5.00240400
H	-1.85667600	1.38133900	4.14335200	C	2.61761100	-2.10251500	-3.46730000
C	-0.39074400	2.40423900	2.93805700	H	1.82719700	-2.75543700	-3.86313400
H	-0.21258300	2.73369100	1.89655000	C	-2.75860900	-2.45080500	-2.28644700
H	0.45256900	1.73790700	3.20815900	H	-2.52642700	-1.75922100	-3.12630100
H	-0.33181500	3.29791600	3.59291800	C	-4.16460100	-2.08986400	-1.79114700
C	-2.90680700	2.68355400	2.77601000	H	-4.91271800	-2.25132400	-2.59552700
H	-2.80871600	3.61560000	3.37075900	H	-4.21674200	-1.02275200	-1.49081400
H	-3.90112200	2.24973200	2.99917700	H	-4.47564100	-2.70232500	-0.92214500
H	-2.90082700	2.97101300	1.70538900	C	-2.66195100	-3.88312600	-2.82667400
C	-2.89640000	3.08980300	-1.13789400	H	-2.89743200	-4.63677500	-2.04993000
H	-2.72072600	3.46246000	-0.10561200	H	-1.65559700	-4.11374700	-3.22754500
C	-4.20263300	2.28513100	-1.11690900	H	-3.38944900	-4.02752100	-3.65344600
H	-5.05820500	2.92793000	-0.82115800	C	-1.13345800	-3.33381800	0.17514200
H	-4.14063900	1.45011800	-0.38756500	H	-0.60352400	-2.77313400	0.97495000
H	-4.44148200	1.84852700	-2.10726700	C	-0.20381300	-4.47600800	-0.25094800
C	-2.95949200	4.30295400	-2.07142500	H	-0.08306400	-5.18423700	0.59582600
H	-3.17541400	4.01012900	-3.11904600	H	0.80936800	-4.10916300	-0.50674400
H	-2.01663400	4.88607100	-2.06794600	H	-0.59807000	-5.05430500	-1.11062800
H	-3.77350000	4.98762500	-1.75222200	C	-2.45579600	-3.85232400	0.75607300
C	-1.09117700	1.96356300	-3.20709700	H	-2.97409200	-4.53937400	0.05730300
H	-1.14548100	3.03220300	-3.50773000	H	-3.15856500	-3.02949300	0.99360100
C	-2.17271700	1.18049600	-3.95649900	H	-2.27041000	-4.41720100	1.69310700

➤ Cartesian coordinate of 3-THF species. Units are presented in Å.

○ Singlet, charge=0

Lu	0.63520400	-0.02595300	-0.04632000	H	0.09022200	-1.72761800	-4.49598100
Ni	-1.98937500	-0.03872600	-0.10043600	C	-0.44850900	1.90472100	-2.45017200
P	-1.98078800	1.50495500	1.51608300	H	-0.00815800	1.75060600	-3.46622900
P	-1.79802200	0.64066800	-2.18441700	H	-0.93563000	2.91011400	-2.49105500
P	-1.80146300	-2.17949700	0.42574400	C	1.40877600	2.87341900	-1.28476600
O	2.92591300	0.17502800	-0.49734400	C	2.11689700	3.09916300	-0.06388000
N	0.54899900	0.58557500	2.06561700	H	1.90331300	2.45314000	0.80277000
N	0.51200900	1.82142700	-1.36575900	C	3.05066700	4.12956900	0.07102000
N	0.78516900	-2.26938400	-0.41324400	H	3.56556500	4.26081700	1.03657300
C	-3.02662500	0.97485400	2.99479500	C	3.31983500	5.00334400	-1.00096000
H	-2.41497400	0.11895400	3.35641700	H	4.05016000	5.81892300	-0.89340400
C	-4.38876500	0.42183500	2.55766200	C	2.61556500	4.82111900	-2.20145600
H	-4.87294900	-0.14249100	3.38270900	H	2.79901800	5.49850000	-3.05134800
H	-4.27814700	-0.26297200	1.69375000	C	1.67683600	3.78763300	-2.34794600
H	-5.08946800	1.22603200	2.25861800	H	1.15777700	3.67669900	-3.31042500
C	-3.16340500	1.98336200	4.14121700	C	-0.47625000	-2.97350900	-0.59971900
H	-3.80532500	2.84375400	3.86263700	H	-0.37912700	-4.05286500	-0.33936700
H	-2.18680600	2.38498600	4.47882600	H	-0.87772500	-2.94695500	-1.64363700
H	-3.63674800	1.49864200	5.02126600	C	1.89551500	-2.98280200	-0.87434600
C	-0.31103300	1.72115500	2.34908500	C	3.16719900	-2.80162800	-0.25948500
H	0.09899900	2.70039100	2.00629500	H	3.23086200	-2.14796600	0.62010700
H	-0.48621500	1.83391500	3.44446600	C	4.31035700	-3.46074700	-0.72419200
C	1.65023300	0.38612400	2.88422300	H	5.27134800	-3.29587400	-0.20967700
C	2.23320100	1.38953100	3.71182800	C	4.23811600	-4.34921000	-1.81348500
H	1.78461400	2.39276100	3.75437600	H	5.13649600	-4.87127300	-2.17534100
C	3.39960100	1.12468100	4.44653200	C	2.98672500	-4.57633500	-2.40838500
H	3.83335200	1.92530100	5.06741000	H	2.90049100	-5.28059900	-3.25175100
C	4.02348800	-0.13323900	4.39600400	C	1.83558800	-3.91909900	-1.94844500
H	4.93765900	-0.32934500	4.97573800	H	0.87641900	-4.11611900	-2.44879100
C	3.44186300	-1.14432100	3.60690200	C	-3.26014300	-3.24699000	-0.11533500
H	3.89482800	-2.14824200	3.57132100	H	-3.15744100	-3.16402700	-1.22024200
C	2.27538200	-0.89715700	2.87680200	C	-4.61677900	-2.63340200	0.25034500
H	1.80235000	-1.70505300	2.29483700	H	-5.44154300	-3.20629800	-0.22418400
C	-2.45621700	3.31479900	1.29085300	H	-4.68971800	-1.58422300	-0.09984300
H	-2.27660800	3.78699100	2.28218600	H	-4.79740100	-2.64038400	1.34342300
C	-1.57240500	4.01958600	0.25704200	C	-3.18054000	-4.73606100	0.24752500
H	-1.73285600	3.59909900	-0.75379300	H	-3.30410200	-4.90285400	1.33560600
H	-0.48950400	3.93786800	0.46811900	H	-2.22146300	-5.19734700	-0.05812300
H	-1.82542200	5.09956300	0.21540300	H	-3.99405300	-5.29490700	-0.26247800
C	-3.93894500	3.47588200	0.92984600	C	-1.29744200	-2.64752400	2.18669800
H	-4.16663700	4.53772000	0.69896200	H	-0.70435600	-1.74673200	2.46159600
H	-4.61768400	3.16403700	1.74586400	C	-0.38456300	-3.87019900	2.34036800
H	-4.19944700	2.87762300	0.03238400	H	-0.07681500	-3.96922400	3.40310400
C	-3.35389200	1.60757400	-2.62744700	H	0.53931700	-3.77376100	1.73769000
H	-3.20077800	2.52645700	-2.02093700	H	-0.88953300	-4.81497500	2.05555600
C	-4.60600800	0.90779400	-2.08035500	C	-2.49814500	-2.71632700	3.14029500
H	-5.50013200	1.55814700	-2.18432000	H	-3.08133800	-3.64904600	3.00297100
H	-4.48453000	0.66846400	-1.00178100	H	-3.19335700	-1.86745000	3.00743800
H	-4.82166700	-0.04227600	-2.60878300	H	-2.15024600	-2.70265700	4.19424700
C	-3.49522000	2.02318200	-4.09471100	C	3.31699300	0.10329900	-1.91234500
H	-3.68639300	1.15384300	-4.75655600	H	2.81829100	0.94892600	-2.43008700
H	-2.59147800	2.54453400	-4.47039200	H	2.95247000	-0.86288300	-2.31468000
H	-4.35291600	2.71828300	-4.21735200	C	4.83729000	0.23022300	-1.91519400
C	-1.49924300	-0.46262400	-3.68279700	H	5.21006100	0.69727500	-2.84726900
H	-1.58909700	0.20155800	-4.56983500	H	5.30299300	-0.77166000	-1.81454800
C	-2.54928100	-1.57164300	-3.79336900	C	5.09976100	1.07976300	-0.66308400
H	-2.31120000	-2.25918200	-4.63181700	H	4.87246300	2.14866000	-0.85612900
H	-3.56752500	-1.17272500	-3.96917100	H	6.13952000	0.99993700	-0.29031700
H	-2.58732600	-2.17591500	-2.86382900	C	4.09447700	0.50346900	0.32214300
C	-0.06899700	-1.02026500	-3.65605700	H	4.45873800	-0.43100600	0.79826200
H	0.15168600	-1.57001000	-2.71837100	H	3.76798400	1.19914500	1.11667200
H	0.69165200	-0.22117600	-3.75310500				

Cartesian coordinate of 4 species. Units are presented in Å.

○ Singlet, charge=0

Lu	-1.06930400	0.12180500	-0.19302600	Ni	1.79153800	-0.06625400	0.59542300
----	-------------	------------	-------------	----	------------	-------------	------------

P	2.53221800	1.20079700	-1.05420900	H	0.54933700	1.18045800	4.73934900
P	1.19285600	0.95035800	2.41768900	C	-0.01112400	-2.75893800	1.19961200
P	1.57153100	-2.22747900	0.39528900	H	-0.20918300	-3.83691300	0.99630100
N	-2.27581000	-0.86245000	-2.24573400	H	0.23685400	-2.69796400	2.28830700
N	0.06430900	0.45036900	-2.12870500	C	3.79794900	0.33579900	-2.15940300
N	-1.15973600	-1.92698800	0.88793600	H	3.18446500	-0.52749100	-2.49501300
N	-0.89214800	2.09272200	0.95818100	C	-0.96452700	-0.10428700	3.91401400
N	-2.74465400	1.83963300	-1.13988500	H	-1.59951400	0.69620100	3.48458700
N	-3.50954600	-0.56015200	0.38402200	H	-1.39037900	-0.37104800	4.90365300
C	-3.43880500	-1.43000500	1.55643200	H	-1.07263700	-0.98943000	3.26487700
C	3.19884100	2.97648400	-1.03034200	C	4.96541500	-0.23781100	-1.34665500
H	3.28585700	3.25471000	-2.10436500	H	5.68286900	0.54343000	-1.02759800
C	-2.25203500	3.16639200	-0.75531100	H	5.53573900	-0.98139800	-1.94336300
C	-4.16491900	0.74195200	0.64201000	H	4.59471700	-0.74501100	-0.43533500
H	-3.62700300	1.21053400	1.48955100	C	-4.16481800	-1.33838600	-0.71753700
H	-5.23307100	0.62986000	0.94326000	H	-4.89729000	-0.68842000	-1.23302600
C	0.96873000	-0.82596300	-4.08490100	H	-4.75296300	-2.17060800	-0.28233300
H	1.86367900	-0.19826200	-4.17806400	C	-4.49360300	-2.52283100	3.46907900
C	-2.71428500	1.62647400	-2.60915500	H	-5.34101600	-2.61512400	4.16367100
H	-1.70101100	1.89940400	-2.94926800	C	4.28293000	1.09419100	-3.39974600
H	-3.44487100	2.28429600	-3.13649500	H	3.45243400	1.52612900	-3.99476700
C	-0.27507500	-2.79729700	-4.82501200	H	4.84506100	0.41176200	-4.07259000
H	-0.36334300	-3.68841300	-5.46288000	H	4.96957200	1.92473800	-3.13718800
C	-4.12148300	1.65441400	-0.57711700	C	2.74158000	-3.19938900	1.52413000
H	-4.78405300	1.26106300	-1.37289100	C	2.39330500	-2.83537200	2.51552200
H	-4.54259000	2.63947000	-0.29375300	H	2.71748800	1.91385800	2.99816200
C	1.08256500	1.47462400	-2.21395200	H	2.80531700	2.65886000	2.17990900
H	0.64158100	2.43825400	-1.88239600	C	2.60323100	2.67632400	4.32176400
H	1.44760700	1.64744800	-3.25096300	H	3.48685400	3.33513100	4.46307900
C	-2.68794400	4.31234900	-1.43214700	H	2.56803400	1.99380800	5.19559300
H	-3.33817400	4.20262600	-2.31351200	H	1.70173200	3.32140800	4.35954600
C	-3.03375900	0.18697600	-3.00566700	C	1.52607500	-3.10094900	-1.27974300
H	-4.11714700	-0.00657900	-2.88389300	H	1.08201900	-2.30486400	-1.90899000
H	-2.82869700	0.07238400	-4.08931300	C	2.24033700	3.97273600	-0.36790300
C	-2.25131200	-2.21920600	1.68147100	H	2.20037100	3.82210700	0.72885100
C	-0.00542100	-0.52440600	-3.08576700	H	1.19875600	3.91480200	-0.73672500
C	-3.17001800	-1.91332900	-1.72058800	H	2.59207500	5.01191500	-0.53813900
H	-2.52991300	-2.66861500	-1.22731100	C	0.62017700	-4.33101400	-1.41490200
H	-3.74980300	-2.42098200	-2.52838100	H	-0.43266300	-4.09894600	-1.16035600
C	-2.28652700	-3.22826100	2.69725200	H	0.94912500	-5.18105100	-0.78412900
H	-1.43084100	-3.90217000	2.82650700	H	0.62345000	-4.67203900	-2.47157100
C	0.83490100	-1.94359100	-4.92094500	C	4.20535300	-2.76506400	1.39126800
H	1.62929300	-2.15737000	-5.65385000	H	4.82146400	-3.23994600	2.18443300
C	-1.12425100	4.57594300	0.85702600	H	4.30542400	-1.66724400	1.49878400
H	-0.53983600	4.72078600	1.77386500	H	4.64434000	-3.05338600	0.41619300
C	-2.33394100	5.60069900	-0.99785500	C	2.59419400	-4.72689100	1.50811100
H	-2.67392000	6.49035800	-1.54735100	H	3.21075600	-5.17721500	2.31566600
C	0.00139400	2.34109200	2.08591900	H	2.94281000	-5.16480600	0.55190600
H	-0.55199500	2.61565200	3.01679600	H	1.54922300	-5.05634500	1.66943000
H	0.67293800	3.19999500	1.86915600	C	2.92866900	-3.36754000	-1.84131500
C	-4.51788800	-1.56965700	2.43452600	H	2.86469400	-3.58087300	-2.92861700
H	-5.40960100	-0.93753700	2.30564100	H	3.41225700	-4.24083900	-1.35816600
C	-3.37667300	-3.36424000	3.56713000	H	3.60113400	-2.49900400	-1.71254800
H	-3.34245500	-4.14367700	4.34511600	C	3.97505900	1.03677400	2.92958300
C	4.58964600	3.07702500	-0.38805800	H	4.89088500	1.64394300	3.09420100
H	4.90299900	4.13975500	-0.30789500	H	3.97171100	0.23031600	3.68990200
H	5.36958800	2.54908100	-0.96789400	H	4.05878200	0.55548800	1.93161500
H	4.59315800	2.65274300	0.63709800	C	1.34965900	-0.82431000	4.63242400
C	-1.56640200	5.71290700	0.17042700	H	2.38448100	-0.50674100	4.86717100
C	-1.40143100	3.24744400	0.39565000	H	0.89832500	-1.21331100	5.56934300
C	-1.29958700	-2.46747400	-3.91470600	H	1.41584600	-1.67161900	3.91862300
H	-2.20723900	-3.08788400	-3.87558200	H	-1.30437100	6.70784600	0.56455200
C	-1.18297500	-1.35129200	-3.08350900				
C	0.50064500	0.30960900	4.05044700				

References

1. P. Thordarson, Supramolecular.org <http://supramolecular.org/> (accessed July 13, 2018).
2. P. Thordarson, *Chem. Soc. Rev.*, 2011, **40**, 1305-1323.
3. D. Brynn Hibbert and P. Thordarson, *Chem. Commun.*, 2016, **52**, 12792-12805.
4. E. Bill, BF, Max Plank Institute for Chemical Energy Conversion D-45470 Muelheim an der Ruhr, 2014.
5. I. A. Fallis, R. D. Farley, K. M. A. Malik, D. M. Murphy and H. J. Smith, *J. Chem. Soc., Dalton Trans.*, 2000, DOI: 10.1039/B005402J, 3632-3639.
6. P. A. Rudd, S. Liu, L. Gagliardi, V. G. Young and C. C. Lu, *J. Am. Chem. Soc.*, 2011, **133**, 20724-20727.
7. L. J. Clouston, R. B. Siedschlag, P. A. Rudd, N. Planas, S. Hu, A. D. Miller, L. Gagliardi and C. C. Lu, *J. Am. Chem. Soc.*, 2013, **135**, 13142-13148.
8. R. K. Thomson, B. L. Scott, D. E. Morris and J. L. Kiplinger, *Cr. Chim.*, 2010, **13**, 790-802.
9. J. P. Perdew, M. Ernzerhof and K. Burke, *J. Chem. Phys.*, 1996, **105**, 9982-9985.
10. S. Grimme, *J. Comput. Chem.*, 2006, **27**, 1787-1799.
11. S. Grimme, J. Antony, S. Ehrlich and H. Krieg, *J. Chem. Phys.*, 2010, **132**, 154104.
12. C. Adamo and V. Barone, *J. Chem. Phys.*, 1999, **110**, 6158-6170.
13. A. D. Becke, *J. Chem. Phys.*, 1993, **98**, 5648-5652.
14. C. Lee, W. Yang and R. G. Parr, *Phys. Rev. B*, 1988, **37**, 785.
15. S. H. Vosko, L. Wilk and M. Nusair, *Can. J. Phys.*, 1980, **58**, 1200-1211.
16. P. Stephens, F. Devlin, C. Chabalowski and M. J. Frisch, *J. Phys. Chem.*, 1994, **98**, 11623-11627.
17. A. D. Becke, *J. Chem. Phys.*, 1996, **104**, 1040-1046.
18. Y. Zhao and D. G. Truhlar, *J. Chem. Phys.*, 2006, **125**, 194101.
19. J. P. Perdew, *Phys. Rev. B*, 1986, **33**, 8822.
20. M. Frisch, G. Trucks, H. B. Schlegel, G. Scuseria, M. Robb, J. Cheeseman, G. Scalmani, V. Barone, B. Mennucci and G. Petersson, *Inc., Wallingford, CT*, 2009, **200**.
21. F. Weigend, *Phys. Chem. Chem. Phys.*, 2006, **8**, 1057-1065.
22. X. Cao and M. Dolg, *J. Chem. Phys.*, 2001, **115**, 7348-7355.
23. B. O. Roos, P. R. Taylor and P. E. M. Siegbahn, *Chem. Phys.*, 1980, **48**, 157-173.
24. F. Aquilante, L. De Vico, N. Ferré, G. Ghigo, P.-Å. Malmqvist, P. Neogrády, T. B. Pedersen, M. Pitoňák, M. Reiher, B. O. Roos, L. Serrano-Andrés, M. Urban, V. Veryazov and R. Lindh, *J. Comput. Chem.*, 2010, **31**, 224-247.
25. B. O. Roos, R. Lindh, P.-Å. Malmqvist, V. Veryazov and P.-O. Widmark, *J. Phys. Chem. A*, 2004, **108**, 2851-2858.
26. B. O. Roos, R. Lindh, P.-Å. Malmqvist, V. Veryazov and P.-O. Widmark, *J. Phys. Chem. A*, 2005, **109**, 6575-6579.
27. M. Douglas and N. M. Kroll, *Ann. Phys-New York*, 1974, **82**, 89-155.
28. G. t. Te Velde, F. M. Bickelhaupt, E. J. Baerends, C. Fonseca Guerra, S. J. van Gisbergen, J. G. Snijders and T. Ziegler, *J. Comput. Chem.*, 2001, **22**, 931-967.
29. P. Pyykkö, *J. Phys. Chem. A*, 2015, **119**, 2326-2337.
30. J. A. Hlina, J. R. Pankhurst, N. Kaltsoyannis and P. L. Arnold, *J. Am. Chem. Soc.*, 2016, **138**, 3333-3345.
31. E. Lu, A. J. Wooles, M. Gregson, P. J. Cobb and S. T. Liddle, *Angew. Chem. Int. Ed.*, 2018, **57**, 6587-6591.

32. P. Comba, M. Enders, M. Großhauser, M. Hiller, D. Müller and H. Wadepohl, *Dalton Trans.*, 2017, **46**, 138-149.
33. K. Nobuyuki, S. Yuko, K. Masato, S. Hiroshi, S. Masatomi, N. Yuzo, S. Yoshihiko, O. Masa-aki and O. Hisashi, *B. Chem. Soc. Jpn.*, 2003, **76**, 1007-1008.
34. Y. Nakajima and Z. Hou, *Organometallics*, 2009, **28**, 6861-6870.
35. F. Volcker, F. M. Muck, K. D. Vogiatzis, K. Fink and P. W. Roesky, *Chem. Commun.*, 2015, **51**, 11761-11764.
36. F. Volcker and P. W. Roesky, *Dalton Trans.*, 2016, **45**, 9429-9435.
37. M. V. Butovskii, B. Oelkers, T. Bauer, J. M. Bakker, V. Bezugly, F. R. Wagner and R. Kempe, *Chem. Eur. J.*, 2014, **20**, 2804-2811.
38. I. P. Beletskaya, A. Z. Voskoboynikov, E. B. Chuklanova, N. I. Kirillova, A. K. Shestakova, I. N. Parshina, A. I. Gusev and G. K. I. Magomedov, *J. Am. Chem. Soc.*, 1993, **115**, 3156-3166.
39. C. P. Burns, X. Yang, J. D. Wofford, N. S. Bhuvanesh, M. B. Hall and M. Nippe, *Angew. Chem. Int. Ed.*, 2018, **57**, 8144-8148.
40. P. L. Arnold, J. McMaster and S. T. Liddle, *Chem. Commun.*, 2009, 0, 818-820.
41. A. Spannenberg, M. Oberthür, H. Noss, A. Tillack, P. Arndt and R. Kempe, *Angew. Chem. Int. Ed.*, 1998, **37**, 2079-2082.
42. L. Fielding, *Tetrahedron*, 2000, **56**, 6151-6170.
43. G. R. Fulmer, A. J. M. Miller, N. H. Sherden, H. E. Gottlieb, A. Nudelman, B. M. Stoltz, J. E. Bercaw and K. I. Goldberg, *Organometallics*, 2010, **29**, 2176-2179.
44. I. R. Kleckner and M. P. Foster, *BBA-Proteins Proteom.*, 2011, **1814**, 942-968.
45. T. R. O'Toole, J. N. Younathan, B. P. Sullivan and T. J. Meyer, *Inorg. Chem.*, 1989, **28**, 3923-3926.